KOSARAJU, KARSHAK, Ph.D. Study of Toxicity and Uptake of Nanoparticles towards understanding Biotic-Abiotic Interactions. (2015)
Directed by Dr. Joseph M. Starobin. 143 pp

With the rapid growth in nanotechnology and tremendous applications the engineered nanomaterials (ENs) offer, there is increase in usage of ENs which increases their likelihood of coming in contact with biological systems which include complex beings like humans and other relatively simpler organism like bacteria and other microorganisms. The interaction between the nanomaterials (NMs) and biological systems includes the formation of protein coronas, particle wrapping, intracellular uptake and bio catalytic processes which could have biocompatible or bio adverse outcomes. Understanding these interactions allows the development of predictive relationships between structure and activity that are mainly determined by NM properties such as size, shape, surface chemistry, aggregation, and surface functionality among many others. This understanding will also provide insight towards the design and development of benign nanomaterials. The **overarching goal of this dissertation** is to understand the influence of the physicochemical characteristics of the NMs and their influence on their uptake and toxicity when they interact with the biological systems (cells and organs). For this purpose, thoroughly characterized NMs will be exposed to a cellular model, A549 cells (alveolar lung epithelial cells), and a mice model (CD-1 mice) through inhalational administration. The effects of NMs on the *in vitro* and *in vivo* models will be evaluated by bio- and immuno-chemical methods to understand toxicity, and a combination of analytical spectroscopic and microscopic tools to study uptake. *In vivo* toxicity assessment will also

be performed by using electrocardiogram (ECG) measurements as a tool to study the effects of inhalation of NMs on cardiac response in mice. Through *in vivo* studies, a novel non-invasive method, Reserve of Refractoriness (RoR), will be introduced as a tool to study cardiotoxicity.

STUDY OF TOXICITY AND UPTAKE OF NANOPARTICLES TOWARDS UNDERSTANDING BIOTIC-ABIOTIC INTERACTIONS

by

Karshak Kosaraju

A Dissertation Submitted to
the Faculty of the Graduate School at
The University of North Carolina at Greensboro
in Partial Fulfillment
of the Requirements for the Degree
Doctor of Philosophy

Greensboro
2015

Approved by

_____
Committee Chair

APPROVAL PAGE

This dissertation written by KARSHAK KOSARAJU has been approved by the following committee of the Faculty of The Graduate School at The University of North Carolina at Greensboro.

Committee Chair _____

Committee Members _____

_____

_____

_____

10-21-2015
Date of Acceptance by Committee

10-21-2015
Date of Final Oral Examination

TABLE OF CONTENTS

Page

LIST OF TABLES

Page

LIST OF FIGURES

Page

CHAPTER I

INTRODUCTION

There is an accelerating and non-uniform progress of innovations and discoveries leading to many technologies. Ramifications of these technologies budding mostly as a result of nanotechnology are enabling introduction of new and more efficient products in the market. The use of these products could lead to exposure of engineered nanomaterials (ENs) to the environment[1]. Figure 1.1 shows the pathways of exposure to EN, affected organs and associated diseases from epidemiological *in vivo* and *in vitro* studies. Since ancient times, humans have been exposed to nanoparticles from nature and other anthropogenic sources, but there is a heightened concern in the current times with development of nanotechnology. The effect of these products containing nanomaterials on humans and the environment are not completely understood. It therefore becomes extremely important to analyze the risks posed by EN on Environment, Health and Safety (EHS) in order to optimize design and/or control their production, distribution/use, storage and disposal and hence to control toxicity[1, 2].

The engineered nanomaterials on contact with biological systems can be absorbed via dermal, respiratory, intravenous and sub cutaneous routes[3]. Once absorbed they can be internalized and distributed throughout the body[4]. Biodistribution helps predict the plausible target system and the effects of ENs might have on the system as a whole. In order to understand EN toxicity, a systematic and focused approach is required to

understand many variables involved in their effects. Toxic effects can occur at different biological levels i.e. organism, organ, cells or nuclear level. In addition, there are different types of toxic effects, namely acute, chronic, cyto- and geno-toxicities, reproductive and developmental toxicities.

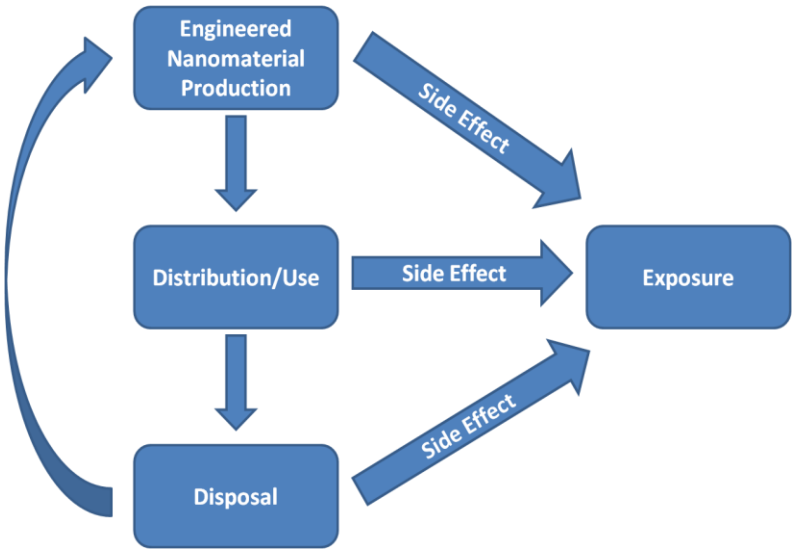

Figure 1.1. Schematic of EN Exposure[1]

Table 1.1. Diseases Associated with Various Systems on Exposure to Nanomaterials

Exposed systems	Associated diseases
Skin	Dermatitis, auto immune diseases
Nervous system	Neurological diseases: Alzheimer's and Parkinson's
Respiratory system	Bronchitis, asthma, emphysema, cancer
Circulatory system	Artheriosclerosis, vasoconstriction, arrrytmia, high BP
Lymphatic system	Podoconiosis, Kaposi's sarcoma
Digestive system	Crohn's disease, colon cancer
Other organs	Diseases of unknown origin in kidneys, liver

EN and their applications are aiding to revolutionize many sectors namely health care, information technology, energy, environmental science, homeland security, food safety, transportation and many others. Incorporation of ENs in existing products induces many desirable effects on their properties. Everyday products that use ENs include polymer composites, fabrics, thin film coatings, cosmetics, automotive, and household products to name a few[5]. The use of nanoscale transisitors, magnetic random access memory, organic light emitting diodes, and flash memory chips in electronics and information technology applications has helped manage and store larger amounts of information. In sustainable energy arena, scientists have developed nanostructured solar cells, efficient fuel production processes, nano-bioengineered enzymes and designed thin-film solar electric panels. In the environmental sector, products such as nanofabric paper towels that absorb 20 times its weight in oil, air filters having nanopores that allow finest mechanical filtration, nano sensors to detect and filter out chemical and biological agents have been developed[6, 7]. Potential applications in medical and health sectors include quantum dots for biological imaging and medical diagnostic, gold nanorods to detect Alzheimer's, multifunctional therapeutics for targeting and treating cancer using same EN, microfluidic chip based nanolabs for monitoring and manipulating individual cells, and use of nanofibers to cure spinal injuries along with regenerative medicine[8]. Apart from maintaining smarter, efficient and greener vehicles; cementitious materials are being engineered with nanoscale sensors for structural monitoring[9]. Along with this tremendous potential to revolutionize the world, it is evident that the use of EN at a larger scale could have potential impact on

environment, health, and safety. Therefore, understanding the EN's physicochemical characteristics, along with their fate and behavior is important.

With the rapid growth in nanotechnology and tremendous applications the nanomaterials offer, there is increase in usage of NMs which increases the likelihood of NMs coming in contact with biological systems which include complex beings like humans and other relatively simpler organism like bacteria and other microorganisms. This interaction between the NMs and the biological systems includes the formation of protein coronas, particle wrapping, intracellular uptake and bio catalytic processes which could have biocompatible or bio adverse outcomes[10]. From the biomolecules point of view, these interactions may induce phase transformations, changes in free energy and changes in the structure and surface. Understanding these interactions allows the development of predictive relationships between structure and activity that are mainly determined by NM properties such as size, shape, surface chemistry, roughness and surface functionality among many others. This will also provide insight on the design and development of benign nanomaterials.

I.1 Background and Significance

According to the 2013 ITRS roadmap, a number of ENs in the form of nanoparticles, nanotubes, nanowires, and thin sheets (graphene) are slated for introduction in front-end processing, interconnect, lithography, and assembly and packaging from now through 2028[11]. Therefore, there are growing concerns regarding not only of the possible exposure and toxic potential of unbound NPs to fab personnel and their release as discharges in air, water and waste streams, but also of other future materials including

bound ENs used/to be used in semiconductor packages. It is important to note that at this time, there are no US regulations in place for specific ENs or products that contain ENs, with a few exceptions. While it is likely that most ENs will be safe, the uncertainty about their novel physiochemical properties and how they may relate and interact with environmental and biological systems has generated considerable concern. Therefore, a comprehensive knowledge of their physicochemical properties (both before and after processing), toxicity (human and environmental), exposure during lifecycle stages - manufacturing, consumer use, and end-of life (disposal or recycling) and their associated risks will be extremely beneficial to the industry[12].

The nanoparticles that have been chosen for this dissertation are already being used in the real applications. For example, the highly dispersed slurries of silica, ceria and alumina have been used in the semiconductor industry for Chemical Mechanical Planarization (CMP) of the wafers. Even though the semiconductor industry believes that the chances of occupational exposure is very low, the dried particles after the CMP process could be air borne which increases the risk of occupational exposure. In terms of environmental exposure, the fact that the threshold levels of toxicity of these nanoparticles have not been reported yet makes it really important to study the uptake and toxicity of these nanomaterials. Carbon and metallic nanotubes have a great prospective for implementation in modern mechanics, electronics and medicine. However, the small size, large surface area and chemical reactivity of these nanostructures comprise a variety of essential environmental hazards. Recent experimental studies demonstrated that just a moderate pulmonary exposure to carbon nanotubes may trigger an oxidative vascular

damage which, in turn, may significantly accelerate the formation of atherosclerosis and atherosclerotic plaques[13]. As the exploration of NMs is occurring at a rapid pace, their increasing number and unique properties raise a question as to "How safe are NMs for living system"?[10] Clearly, as the nanomaterial applications increase, there will be greater and closer contact of these nanoparticles with environment and biotic system.

The **overarching goal of this dissertation** is to understand the influence of the physicochemical characteristics of the nanomaterials and their influence on their uptake and toxicity when they interact with the biological systems (cells and organs). This will need comprehensive characterization of the nanomaterials and relate the effects of the physicochemical properties (like size, surface area, aspect ratio and composition) on the toxicity and uptake in both *in vitro* (cell line) and *in vivo* (mice) systems.

I.2 Hypothesis

The central hypothesis of this dissertation is that the uptake, internalization and toxicity of nanomaterials is primarily due to changing physicochemical properties and that the uptake of nanomaterials by- 1) a cell may not necessarily lead to toxicity in a cell and 2) an organ may lead to change in the physiological behavior at a secondary site.

The two specific aims to test this hypothesis are

1) **Specific aim 1**: To study the effect of physicochemical properties on the toxicity and uptake of EN at the cellular level.

2) **Specific aim 2**: To study the uptake and accumulation of EN in an organ and the impact of this on physiological behavior of a secondary organ.

The hypothesis through the specific aims can be tested by following a sequence of experimental steps and it has been formulated to answer the following questions-

1) Does NP aggregation influence the cytotoxic activity?

2) What is the effect of composition, surface area, morphology, surface charge, chemistry, protein corona on toxicity?

3) Does nanoparticles uptake mean direct toxicity in an organ?

4) Can there be secondary effects due to which accumulation of nanoparticles in an organ (lungs or liver) may result in secondary effects in a different organ (heart)?

For the purpose of testing the hypothesis and to answer the above questions, the effects of NPs at the cellular level, *in vitro,* have been studied using an alveolar lung epithelial cell line (A549 cells). In order to understand the effect of physicochemical properties on cellular toxicity of silica, ceria and alumina NPs has been correlated with the changes in physicochemical properties such as size, surface area, charge and aggregation state. Since, it is not easy to perform *in vivo* studies, only CNTs and ceria will be used as a part of the specific aim 2 on a mice model. The objective of the experiments is to use inhalational as a route of exposure of carbon nanotubes and ceria NPs to mice and study the effects on the heart by recording the electrocardiogram of the mice. Reserve of Refractoriness, RoR, will be calculated by using the QT and RR intervals obtained from the collected ECG signals. This will be followed by studying the regulation of bio- and immono-chemical markers in the mice and also studying the uptake of carbon nanotubes by organs (lungs and liver) using confocal Raman and electron microscopy.

I.3 Reserve of Refractoriness

Recent experimental studies demonstrated that just a moderate pulmonary exposure to carbon nanotubes may trigger oxidative vascular damage which, in turn, may significantly accelerate the formation of atherosclerosis and atherosclerotic plaques[13]. However, it was also reported that acute exposure to ceria nanoparticles via inhalation may lead to cytotoxicity through oxidative stress response and ultimately lead to chronic inflammatory response with overloaded alveolar macrophages and neutrophils [14]. Although these findings conclusively demonstrated the importance of biochemical and immunological markers for identifying nanoparticle-induced oxidative stress and vascular damage, the association of such exposure with noninvasive electrophysiological factors is not understood. Even if monitoring of the cardiovascular system using electrophysiological measurements is one of the most robust biomedical tools, it is currently not adapted for applications in the environmental studies. The development of the non-invasive electrographic predictors of toxic effects on the human cardiovascular system is of a critical importance for public health and, indeed, warrants aggressive exploratory research. Moreover, various studies have reported that both carbon nanotubes and ceria nanoparticles have demonstrated both pro- and anti-oxidative stress responses. This makes CNTs and ceria nanoparticles ideal candidates to study nanoparticle-related cardiotoxicity. The objective of the work is to study the effect of CNTs and ceria NPs on cardiac response, monitored non-invasively, in mice subjected to exposure via intra-tracheal instillation.

CHAPTER II

LITERATURE REVIEW

II.1 Dependence of Toxicity on EN Characteristics

To understand EN toxicity, thorough characterization of properties and any change/variation in the properties that can lead to toxicity is important. From knowledge of toxicological properties of EN, it is understood that the most important parameter determining the adverse effects of ENs are dose, dimension and durability. But, recent studies show that there is a different correlation between properties of EN and their toxicological profiles leading to uncertainties in the dependence of toxicity in properties of EN such as particle size distribution, shape, size, agglomeration, chemical composition, purity, solubility, surface properties, physical properties (like density, crystallinity etc), bulk powder properties and last but not the least concentration dependent toxicity. The effects of these properties on toxicity are discussed later in this chapter. Some of the properties mentioned above are discussed in the following sections. In addition, the cellular assays that are used in the following sections are also discussed later.

II.1.1 Chemical composition dependent toxicity

Chemical composition is defined as the arrangement, type and ratio of atoms in molecules. The toxicity of nanomaterials is very much dependent on the chemical composition and different chemical composition exhibit different levels of toxicity. This is mainly attributed to the different ways of cellular interaction with different composition

of nanoparticles. The difference in atomic and molecular arrangement leads to different levels of cytotoxicity. A comparison study done by Zhang et. al. showed that graphene and single-walled CNTs (SWCNT) showed that they exhibit different levels of cytotoxicity on PC12 cells[15]. They performed LDH release assays which indicate that the cytotoxicity was higher in case of PC12 cells exposed to SWCNTs than that of cells exposed to graphene. Even though, both graphene and SWCNTs are mainly composed of carbon, the difference in atomic arrangement is attributed to different toxicities.

II.1.2 Size-dependent toxicity

In the past few decades, toxicological studies have demonstrated that smaller particles (<100 nm) have potential to be more toxic compared to larger counterparts. *In vitro* and *in vivo* studies conducted by exposing to EN have shown that smaller particles have greater toxicological effects. This is mainly attributed to the surface area which is higher in case of smaller sized particles. A recent study on size-dependent toxicity comparison of 20 nm and 100 nm silica nanoparticles on cutaneous tissue concluded that the cytotoxicity of 20 nm silica nanoparticles was higher than that of 100 nm nanoparticles[16]. This is highly attributed to the larger surface area offered by the 20 nm nanoparticle than that of the 100 nm nanoparticle. A recent work by Kim et al showed that silica NPs showed a size toxicity in A549 and HepG2 epithelial cells and also 3t3 fibroblasts[17] when they used monodispersed spherical silica NPs with diameters of 20-200 nm.

II.1.3 Surface area dependent toxicity

Smaller nanoparticles have a higher surface area and particle number per unit mass when compared to their larger counterparts. When particles of the same mass, chemical composition and crystalline nature are compared, toxicity was found to be greater for nanoparticles than their larger counterparts. This led to the understanding that the adverse effects imparted may be dependent on the surface area of the EN leading to change in the regulations based on dose and exposure limits. Larger surface area of EN leads to increased reactivity and in turn leading to increased adverse effects. The higher surface area of nanoparticles leads to a dose dependent increase in production of reactive oxygen species. Rabolli et al showed that toxicity of amorphous silica NPs showed that toxicity increases with increasing surface area when macrophage and fibroblasts were exposed to NPs with surface areas of 41, 283, 294, 300, 314, 331 m^2/g [18]. However, they also report that NP aggregation does not have implications on toxicity as much as surface area.

II.1.4 Concentration/dose dependent toxicity

Concentration can be described as the abundance of a constituent per total volume of the mixture. Concentration of EN is one of the reasons of agglomeration of particles. Even though, it depends on the solvent or the medium, it can be concluded that higher concentration of EN would promote agglomeration. Most aggregates formed as a result are observed to be larger than 100 nm, a size that seems to be the threshold for EN to exhibit adverse effects. Kim et al showed that monodisperse spherical silica NPs with diameters of 20-200 nm showed a dose dependent adverse effects when they were exposed to epithelial cells (A549 and HepG2 cells) and also 3t3 fibroblasts[17, 19]. They report that the

silica NPs show a dose dependent toxicity response when they exposed the cells to concentrations of 10, 50 ,100, 200 and 500 ug/mL over exposure periods of 24 and 72 hours.

II.1.5 Particle chemistry or crystallinity dependent toxicity

Particle chemistry is also an important factor to consider in understanding the toxicity of EN. Depending on the chemistries, EN can show different cellular uptake, sub-cellular localization and ability to produce reactive oxygen species. Nanoparticles can change crystal structure after interaction with water or liquids. For example, it is reported that zinc sulphide (ZnS) nanoparticles rearrange their crystal structure in the presence of water and become more ordered, closer to the structure of a bulk piece of solid ZnS[20]. Nanoparticles often exhibit unexpected crystal structures due to surface effects. This will contribute to different types of interactions with cells leading to various levels of toxicity depending on the arrangement of molecules.

II.1.6 Aspect ratio dependent toxicity

It was observed that particles with higher aspect ratio exhibit higher toxicity when compared to the particles of the same kind with lower aspect ratio. For example, single walled carbon nanotubes with higher aspect ratio were observed to create more pulmonary toxicity when compared to similar doses of spherical amorphous carbon or silica particles[21].

II.1.7 Surface functionalization dependent toxicity

Particle surface morphology could play an important role in toxicity of EN as it comes in contact with the cells and other biological material. Quantum dots of CdSe can

be rendered nontoxic when coated with functional groups[19]. Along with controlling toxicity, surface functionalization also changes various properties of EN like solubility, which can be used to a greater advantage.

Depending on composition, EN released into the environment can be a source of contamination. Surface chemistry is governed by the functionality and hence solubility, charge and adsorption/desorption characteristics should be taken into account as this changes the way EN interacts with biomolecules. The reactivity of the EN surface controls the potential to generate reactive oxygen species and in turn it's damaging potential. Size and size distribution is another important criterion as it influences the particle settling velocity, thus affecting mobility, potential transport, and bioavailability in the environment. The potential to transport across membranes and cause damage to cell organelles is also determined by EN size. A crystalline structure has more reactive sites as compared to amorphous materials hence having more toxicity, so morphology is another important aspect. Concentration and purity are other factors that affect toxicity. With various properties and their dependence, understanding toxicity is a challenge.

II.1.8 Dependence of toxicity on cell type

Along with the properties of the EN, the type of cell that the EN interacts with will also determine the toxicity. Even though, one cell type can exhibit toxicity to EN, it is not necessary another cell type should exhibit the same toxicity profile when exposed to the same EN. A recent work by Kim et al showed that monodisperse NPs of silica showed different trends in toxicity in three different cell lines i.e., A549 and HepG2 epithelial cells and also 3t3 fibroblasts when they used monodispersed spherical silica NPs with diameters

of 20-200 nm[17]. They report that HepG2 cells showed more toxicity with increasing concentration of silica NPs.

II.2 Concerns Related to Nanoparticle Exposure to Biological Systems

Nanoparticle usage in the CMP slurry composition is one of the thousand applications where nanoparticles are used and continue to have potential applications in the future. Looking at other side of the coin, potential concerns arise regarding environmental and health impacts of nanomaterial usage that follow nanomaterial applications. Reasons for increased usage of nanoparticles, their novel characteristics and exceptional behavior, can be a matter of concern as to how these novel characteristics change the material way of interactions with environment and biotic-abiotic system. Nanomaterials can enter the environment through effluent, spillage, consumer products and disposal, leading to their closer and larger interaction with environment and biotic system. Post exposure, nanoparticles may gain access to the biotic systems via lungs, dermal, wound tissues, intestinal tract either intentionally or unintentionally, posing serious health problems[22, 23]. Organisms can tolerate intake of nanoparticles to an extent; however, persistent or high concentration can damage the system and cause toxic effects. Intake of the nanoparticles might mean free mobility in the body fluids, owing to their small size and can be readily transported to different tissue and cellular systems[24]. Thus, nanoparticles not only cause adverse effects to the site of entry but also have potential translocate in the body, disseminate into secondary organs, enter cell membrane, lodge in mitochondria and trigger adverse effects[25]. According to EC-workshop in 2004 by Professor Jos Put at DSM Research, nanoparticles that can become airborne to form aerosol are perceived to be the

most dangerous type of nanoparticles, which are related to the enormously high surface to mass ratio. With the large surface area of 75-140 m^2, lungs can be the primary entry portal for inhaled particles[22]. It has shown by various studies, post inhalation and IV exposure that, nanoparticles exhibited prominent distribution in liver, urinary bladder and kidney in mice[26]. Number of other studies also show that nanoparticles have potential to translocate to various tissues like liver[27], kidney [28] and even brain [29].

II.3 *In-vitro* Models for Toxicity Analysis

Traditional toxicological approach to chemical testing involves animal testing as the means of hazard assessment, this strategy is costly and labor intensive. Though it is impossible to perform risk assessment without the *in vivo* analysis, it is becoming clear that animal testing cannot become the base model and test method for thousands of new chemicals and nanomaterials, where the toxicity and interactions vary with the properties of these materials[30]. In accordance to the National research council of US academy of Sciences (NAS), toxicological testing in the 21st century should undergo paradigm shift from a predominant observational science performed in whole animals to a target specific and predictive *in vitro* science utilizing mechanisms of injury and toxicological pathways to guide the judicious use of *in vivo* studies[30, 31]. Various cell lines have been used for the nano-bio interactions and toxicity analysis of the nanomaterials. As *in vitro* systems have an advantage of tissue specific analysis, the in vitro cell cultures can be chosen based on the exposure type, the cells likely to be exposed by a specific type of exposure and cell functions involved. For example, Human peripheral Blood lymphocytes used for the analysis of cellular binding/uptake of the surface-modified silica nanoparticles[32], murine

fibroblasts[33], recommended for cytotoxicity evaluation of compounds intended to be used in biomaterials, immortalized murine hippocampal cell line (HT22) for the neuroprotective effects of ceria nanoparticles, secondary target organs like kidney cells[34] and nerve cells[35]. As discussed, the lung is one of the key targets for the possible toxic effects of nanoparticles as a result of environmental, occupational or medicinal exposure[14, 36-38]. Various *in vitro* cell models like human alveolar epithelial cells (A549), human bronchial epithelial cells (Beas-2B) lung sub-mucosal cells (Calu-3) cells and alveolar macrophages[22] are used to understand the inhalation exposure of nanoparticles. Analysis of the uptake of nanoparticles using A549 cells would help understand the effect of inhalation exposure of nanoparticles and their diffusion capacity into lungs and their possibility to translocate to secondary organs[39].

II.4 Toxic Effects of Selected Metal Oxide Nanoparticles

II.4.1 Toxicity of silica nanoparticles

It is well established that crystalline silica causes adverse effects, whereas amorphous silica is considered safe by US Federal Drug Administration and hence used as a filter aid in food products, diagnostic devices and as negative control for toxicity analysis[33, 40]. Other applications include metal casting, refractory products and therapeutic drug delivery system[25, 41]. Recent *in vivo* and *in vitro* studies have shown that silica nanoparticles can have adverse effects. Intravenous administration of silica nanoparticles lead to the nanoparticle accumulation in liver and spleen, intranasal instillation caused inflammatory response[37, 42]. *In vitro* study where various sizes of silica nanoparticles (10, 150, and 500 nm) were exposed to the lung sub-mucosal cells, reported the exposure of 10

nm SiO_2 nanoparticle to Calu-3 cells resulted in increased cytotoxicity and cell death in a time- and concentration-dependent manner, with a lethal concentration of 9.7 μg/ml after 24 hours. Increase in MDA showed significant correlation to cell viability decrease at 18 hour. The 150 nm and 500 nm silica nanoparticles showed no significant toxic effects on Calu-3 cells. The 10nm SiO_2 nanoparticle caused toxicity associated with inflammation, release of ROS leading to apoptosis of cells[38]. Similar results were reported by Passagne et al., where 20 nm silica nanoparticles posed notable cytotoxic effects whereas 100 nm ones appear less toxic[43]. The IC 50 values for the two cell types used was different, IC 50 for the LLC-PK_1 was 66 ug/ml after 24 hour exposure, whereas for HK-2 IC 50 was 110.5 ug/ml, showing that the LLC-PK_1 cells are more susceptible to the cytotoxic effects of nano-silica and hence this shows that same particles interact distinctly with different cellular system. Both the studies concluded that smaller sized silica nanoparticles caused higher toxicity compared to particles larger than 100 nm. Further size dependent cytotoxicity of silica nanoparticles was reported by a study where mono-dispersed silica nanoparticles were exposed to human endothelial cells, showed that smaller sized silica nanoparticles caused cytotoxic cell damage and decreased cell survival of EAHY926 cells, analyzed by MTT and LDH assays. Silica nanoparticles of sizes 14 nm, 15 and 16 nm showed higher LC 50 values (33 to 47 $\mu g/cm^2$) compared to larger nanoparticles of 104 nm and 335 nm (1095 and 1087 $\mu g/cm^2$) by MTT assay[44]. Contrary to these results, Lin W et al., reported that there was no significant difference between cytotoxicity of two silica nanoparticles (15 nm and 46 nm), whereas both the particles were more cytotoxic compared to crystalline silica (used as positive control)[39]. There was dose-dependent

toxicity observed, accompanied by ROS production and decreased glutathione levels, which showed that silica nanoparticles cause toxic effects via induction of oxidative stress to A549 cells. No size dependence may be due to the aggregation of silica nanoparticles in the cell culture media, shown by hydrodynamic sizes of 590 nm and 617 nm for 15 nm and 46 nm respectively, by DLS measurement[39].

Nanoparticle size is important in determining the interactions and adverse of nanoparticles on cells and further aggregation state of nanoparticles is another important factor, which can change the properties of nanoparticles like size and surface and therefore change the cellular interaction of nanoparticles. The impact of aggregation on toxicity was analyzed by Rabolli et al., where toxicity of stable mono-disperse and aggregated silica nanoparticles was compared by exposing them to macrophage and fibroblast cells. It was found by WST1 assay, that the ED_{50} (6-9 μg/ml and 15-22 μg/ml, in macrophage and fibroblast cells, respectively) were not affected by the agglomeration and it was shown that the surface area but not the agglomerated state of nanoparticles determine the toxic effect of silica nanoparticles[18].

Toxicity analysis of amorphous silica is more variable due the diversity of possible structures compared to the crystalline silica[45]. As the surface chemistry, size and shape are important considerations for nanoparticle toxicity, there is need to characterize nanoparticles in detail considering the systemic variations of these particles due to the synthesis process. Studies concentrating on the silica nanoparticles based on the synthesis process are not studied in detail. Recent studies have shown that the physiochemical differences in fumed silica and colloidal silica are clearly manifested in the different

patterns of inflammation, toxicity and hemolysis[45]. Nanoparticle interaction is also dependent on the method of preparation of nanoparticles. Silica nanoparticles (SiNPs) can be distinguished as different forms based on method of synthesis including fumed silica, which are produced as dry aggregates under high-temperature flame[46], and precipitated, colloidal, or mesoporous silica, which are made via molecular condensation of silanol groups in aqueous solution or under hydrothermal conditions[26]. It has very low density and higher surface area and works a great thickener or reinforcing filler. Fumed silica has very low density and higher surface area and works a great thickener or reinforcing filler, which is more likely to become airborne poses a higher risk for environmental exposure, studies are deemed necessary to establish the toxicity potential of the fumed silica nanoparticles. The literature reviewed so far was concentrated on the colloidal silica nanoparticles, studies concerning with toxicity analysis based on the method of preparation are scarce. In the toxicity analysis conducted on human bronchial epithelial cells (Beas-2B), it was found that 1mg/l of fumed silica (7 nm) decreased the cell viability to 83.9% after 24 hour exposure compared to control cells. Whereas the porous silica of same concentration caused decreased cell viability (79.9%), showing that the porous silica particles might have greater toxicity compared to fumed silica particles. This was confirmed by further analysis on ERK and nuclear NRf-2 and the numbers of cells with DNA contents in subG1 phase. The similar fumed silica particles (7 nm) were used for this study to compare the CMP fumed silica nanoparticles. The results from the cell viability will be discussed further.

Studies to understand the aggregation of nanoparticles and their effect on biological system was analyzed with fumed silica nanoparticles as well[45]. Fumed silica nanoparticles

of 7-14 nm were used to evaluate the effect of aggregation on cytotoxicity of A549 cells using conventional cytotoxicity assays and metabolomics. The dispersion state of the nanoparticles was analyzed using DLS and TEM. The nanoparticles were well dispersed in the cell culture media at 25-100 ug/ml, however they sediment rapidly in concentration dependent manner. The nanoparticles caused a dose-dependent increase of ROS and cell membrane damage to in A549 cells at 4 hour and cell viability was lost after 48 hour exposure. The fumed silica nanoparticles used share a similar primary sizes, but they exhibited distinct time- and concentration- dependent dispersion patterns. The dose-effect patterns were not the same for different exposure times and the relation fitted better with polynomial regression compared to linear regression. The study demonstrated that fumed SiNPs caused both acute (due to the direct nanoparticle interaction with the cell) and delayed toxicity due to the nanoparticle aggregates leading to oxidative stress, damage to cell membrane and mitochondrial dysfunction. This suggests that not only the particle size but also, the properties of nanoparticles in the dispersed media and interaction of the nanoparticles with the cell culture media (protein corona formation) determines the toxicity of nanoparticles to the cell culture system.

Size, surface area and aggregation state of nanoparticles are the properties that need to be studied for better understanding the interaction of nanoparticles with cellular system. In a recent study conducted by Lankoff et al., the uptake of aminopropyl/vinyl- modified silica nanoparticles by lymphocytes was more efficient than that of vinyl-modified and unmodified silica nanoparticles[32]. The hydrodynamic size of the aminopropyl/vinyl-modified silica nanoparticles (176.7±5.1 nm) was less compared to the other two types of

silica nanoparticles, vinyl-modified and unmodified silica nanoparticles (235.4 ± 4.9 nm and 266.3 ± 7.2 nm respectively), showing the uptake is higher for the smaller sized nanoparticles. This may suggest that the nanoparticles modified with aminopropyl/vinyl were dispersed better leading to lower dynamic sizes compared to the others. Thus, surface charge and surface properties of nanoparticles play important role in determining the interaction and fate of nanoparticle with cellular systems.

II.4.2 Toxicity of ceria nanoparticles

As a lanthanide element oxide and strong properties like high thermodynamic affinity to oxygen and sulfur, ceria nanoparticles are one of the important nanomaterials, finding applications in a wide variety of areas for catalysis, solar cells, fuel cells, phosphor/luminescence, abrasives for chemical mechanical planarization (CMP), gas sensors, oxygen pumps and many more. W. Lin et al evaluated the cytotoxic effects of 20-nm ceria nanoparticles on exposure to A549 cells[47]. Cell viability was analyzed using sulforhodomine B method, after exposure to 3.5, 10.5 and 23.3 ug/ml of ceria nanoparticles as a function of dose and exposure time. Oxidative stress indicators like ROS production, glutathione, malondialdehyde, α-tocopherol, lactate dehydrogenase were analyzed. Cell viability decreased as a function of ceria nanoparticles concentration and exposure time. After 72 hours of exposure, cell viability decreased to 88.0 %, 67.7% and 53.9% for the cell cultures exposed to 3.5, 10.5 and 23.3 ug/ml of ceria nanoparticles respectively. The extent to cell membrane breakage of A549 cells was revealed by LDH levels in cell medium which increased to 14.5%, 32.1% and 70.5% respectively. The oxidative stress analysis showed that DCF fluorescence intensity increased by 70%. 139% and 181%

compared to control cells, after exposure to 3.5, 10.5 and 23.3 ug/ml ceria nanoparticles for 72 hours. The ROS production compared to the control cells showed a dose-dependent response. Mittal et al., study aimed at understanding the molecular mechanism underlying the cytotoxicity of ceria nanoparticles on A549 cells, where the internalization of the ceria nanoparticles was analyzed by the flow cytometry analysis[36]. The flow cytometry analysis showed there was dose and time dependent increase in the SSC intensity, which correlates to the increased granularity of the cells as a marker for the nanoparticle uptake by the cells. The ceria particles were internalized and caused cell death and morphological changes. The cell death increased to 9.62%, 11.69%, 15.34% and 18.98% after 48 hours of exposure to 10, 25, 50 and 100 ug/ml of ceria nanoparticles, analyzed by the propidium iodide uptake method. The oxidative stress analysis showed that, the ROS production increased in the cells in dose dependent and time dependent manner. DCF fluorescence intensity increased by 240%, 266% and 288% after 6 hours exposure to 25, 50 and 100 ug/ml, respectively as compared to the control cells. This was accompanied by the constant decrease in the antioxidant, GSH levels. The cell death was found to be apoptic shown by loss in mitochondrial membrane potential and increase in annexin-V positive cells and confirmed by immunoblot analysis. It was concluded by the study that ROS mediated DNA damage and cell cycle arrest play a major role in ceria nanoparticles induced apoptotic cell death in A549 cells[36].

II.4.3 Toxicity of alumina nanoparticles

Nanoscale alumina can be beneficial in the orthopedic implants. It is believed that the use of nanometric aluminum oxide could solve the current problems associated with

implantation by enhancing osseo-integration and preventing graft rejection. Nanometric alumina could be also used for magnetodynamic therapy. Aluminum oxide nanoparticles are produced by thermal decomposition of a precursor obtained in the reaction of an aluminium organic compound and aluminium alcoholate with oxygen and water vapor from the air. As alumina nanoparticles have potential applications as the biomedical materials, study was conducted to assess the adverse effects of nanoscale Al_2O_3 on murine fibroblasts (L929), recommended for cytotoxicity evaluation of compounds tended to be used in biomedical materials and normal human skin fibroblasts (j BJ). The alumina nanoparticles showed decrease in cell viability to less than 10% compared to the control cells. From the EZU4 test, at the concentration as high as 400 ug of Al_2O_3/ml the average cell viability after incubation with Al nanoparticles was 96.51% for human fibroblasts, and 91.53% for murine fibroblasts. It was shown that Al_2O_3 nanoparticles did not induce apoptosis of cells, although they can penetrate into cells, which was seen microscopically and also confirmed by ICP-OES [48]. Another study conducted for the comparison of the cytotoxic and genototoxic effects of titanium oxide and aluminum oxide nanoparticles in Chinese hamster ovary (CHO-K1) cells, showed that the cell viability decreased after 24 hour exposure to nanoparticles used in this study and in a dose dependent manner with changes in lysosomal and mitochondrial dehydrogenase activity[49]. The cell viability decreased to 40% when exposed to 100 ug/ml of TiO_2 nanoparticles, whereas the cell viability was even lower for the cells exposed to Al nanoparticles for same concentration, as shown by neutral red (NR) uptake analysis. Results from MTT assays showed that the cell viability was decreased significantly when exposed to both nanoparticles for

concentration values equal to or higher than 5 ug/ml. Genotoxic effects analyzed by MN frequencies significantly increased when the cells were exposed to 0.5 and 1ug/mL TiO_2 and 0.5–10 ug/mL Al_2O_3[49].

II.5 Cellular Uptake of Nanoparticles

It is already established that nanoparticles cause adverse effects when they interact with the cellular system. They may interfere with the complex machinery by disturbing the cellular components, thus for a better understanding of the effects of the nanoparticles on the cellular system, their intra-cellular localization is important to be analyzed. However the possibilities to monitor the cellular location of nanoparticles are scarce and major toxicological concern is the possible uptake of nanoparticles via different pathways like endocytosis, phagocytosis etc. The possible uptake mechanism can provide insights on the localization and the type or extent of cellular damage to cells, organs or organisms. One of the strongest techniques used for the particle uptake and localization with the cells is fluorescent labeling of particles to determine their intracellular localization. Silica nanoparticles fluorescently lagged (70 nm, 200 and 500 nm) were used for the uptake and IC localization in HeLa cells using confocal laser scanning fluorescence microscopy, from which it was demonstrated that the silica nanoparticles were not distributed throughout the cell, but they were primarily found inside vesicular compartments. There was localization of all sizes of nanoparticles in endosomes, but the lysosomes incorporation was preferentially by 70 nm nanoparticles[50]. Another study using fumed silica nanoparticles of three sizes 7nm, 20nm and 50 nm, tagged with fluorescein isothiocyanate (FITC) were used for understanding the cellular uptake and cytotoxicity. Fluorescence microscopy and

flow cytometry showed the presence of FITC-nanoparticles in cytoplasm and nucleus in HepG2 cells[51]. Another powerful method for the uptake analysis of the nanoparticles is the electron microscopic techniques, transmission electron microscopy and scanning electron microscopy. In a study conducted by Lesniak et al., A549 cells were exposed to 50 nm silica nanoparticles in serum- free and serum containing media, fixed and ultrathin sections of 80 nm were obtained using a diamond knife using ultramicrotome. These sections of A549 cells were observed under TEM for the localization and uptake of nanoparticles in the cell organelles, which showed that the cells exposed to silica nanoparticles in the serum-free media lead to the accumulation of nanoparticles[52]. Transmission electron microscopy was used for the cellular uptake of Al2O3 and TiO2, magnetite particles showed the incorporation in cytoplasm-based vesicles via endocytosis in A549 cells and no evidence of nanoparticles in the nucleus[53, 54]. Electron microscopy has very good resolution but involves time consuming sample preparation and sectioning and further limited by the number of sections and number of images to be examined. Fluorescent techniques are quicker but require labeling the nanoparticles prior to their exposure with cells, which is essentially chemically modifying the molecules with a fluorescent molecule, which may change the physicochemical properties of the nanoparticles on a whole. This means that the entire cell can be analyzed for the nanoparticle localization at once, for faster and non-invasive methods. Raman microscopy is one non-invasive, label-free, alternative technique capable of measuring the distribution of nanoparticles, provided the nanoparticles and nanostructures show Raman active vibration modes. The vibrational spectra can be decomposed to analyze the cellular location and distribution in various regions of the cell.

Study conducted by Lopis L et al, analyzed the cellular distribution of ceria, CNT and alumina nanoparticles[53].

II.6 Oxidative Stress as a Mechanism of NP Toxicity

Under normal coupling conditions, ROS are generated at low levels during mitochondrial electron transport of aerobic respiration or by oxidoreductase enzymes and metal catalyzed oxidation during cellular metabolism, which play vital roles in cell signaling including apoptosis, gene expression and activation of cell signaling cascades and maintenance of homeostasis. Detoxification mechanisms like antioxidant defenses and enzymes like Glutathione (GSH), vitamin C, α- tocopherol and ascorbic acid, which may be overwhelmed at higher ROS production levels due to oxidative stress from external or internal imbalances. Hence, oxidative stress is defined as the disturbance in the prooxidant-antioxidant balance that is (the balance between oxidative pressure and antioxidant activities) in favor of the prooxidant, leading to potential damage[55]. ROS production and oxidative stress is the best-developed paradigm for the toxicity of inhaled ultrafine particles[7]. Though there is admittedly difference between the ultrafine particles and the engineered nanoparticles, it is worth noting that nanomaterials involve ROS production and the induction of oxidative from the toxicity studies conducted. Nanoparticles can generate ROS through the interaction of the surface area or cellular system and are hypothesized as key player's nanoparticles mechanism of toxicity[1, 2, 56]. Thus, oxidative stress via ROS production is one of the major and primary paradigm for the nanoparticle toxicity, where the nanoparticles can mediate DNA damage, lipid peroxidation and mediate cytotoxic pathways like apoptosis and inflammation. There can be varied mechanisms of

the ROS production in cells, via nanoparticle interaction with the cellular components or via phagocytosis-related formation of ROS (Figure 2.1)[57]. For example, uptake of the nanoparticles via phagocytosis can lead an activation of membrane-bound NADPH oxidase, which catalyzes oxygen to superoxide leading to toxicity. Small particles with large surface area have shown to cause injurious effects by the production of ROS and oxidative stress[2, 58]. Nanoparticle injury can also proceed by non-oxidant paradigms like binding of protein corona causing fibrillation and toxic ion release. The ROS generation and oxidative stress reported by the toxicological studies on silica, ceria and alumina nanoparticles are reported in the respective sections above. As shown in Figure 2.2, ROS mediation is one of the intermediate steps involved in the regulation of various biomarkers within a cell.

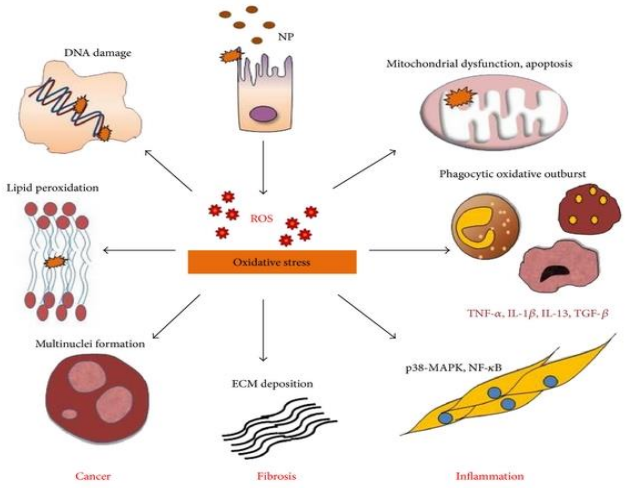

Figure 2.1. Nanoparticle Toxicity Mediated by Induction of Oxidative Stress[59]

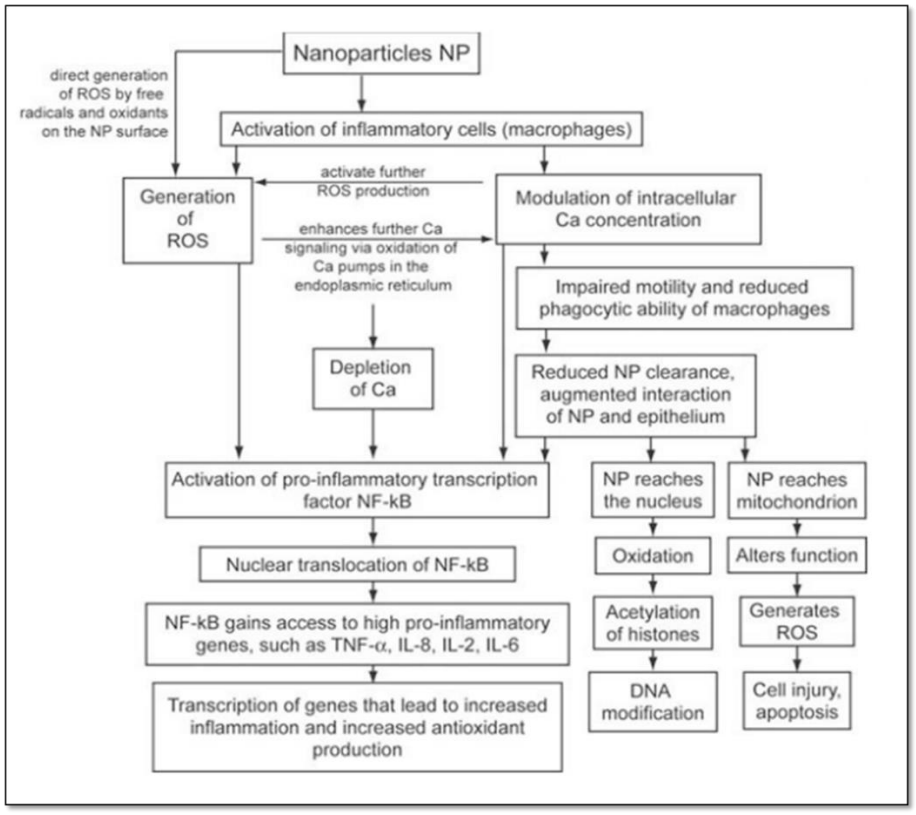

Figure 2.2. Various Possible Events by which Nanoparticles Exert Toxic Effects at Cellular Level

CHAPTER III

CHARACTERIZATION AND PRELIMINARY TOXICITY ANALYSIS

III.1 CMP Slurry Nanoparticle Characterization

III.1.1 Characterization of nanoparticle size and morphology using transmission electron microscopy

Transmission electron microscopy was used for analyzing the particle size, shape and dispersion state of colloidal silica, fumed silica, ceria and alumina slurry nanoparticles which are presented in Figure 3.1. The colloidal silica slurry nanoparticles were spherical, fumed silica particle have a characteristic interlocked chain structure (characteristic due to the method of preparation), ceria slurry contained particles with variety of shapes, larger particles exhibited cuboidal structure and also slight crystalline character, represented by the electron beam diffraction forming a shadow around these bigger particles (this is mostly a characteristic of crystalline particles). Alumina slurry contained nanoparticles with irregular shape making difficult to distinguish the primary particle size. The primary particle sizes and the statistical evaluation of the size distribution were performed by Image J and Origin software (Table 2). The colloidal slurry nanoparticles were found to be 32 ± 10.23 nm, fumed silica slurry nanoparticles were found 84 ± 40.5 nm, ceria slurry nanoparticles of 42 ± 20.24 nm and alumina slurry nanoparticles of 54.3 ± 48.46 nm, showing a wide size distribution. Though the particle size analysis from TEM and Image J

does not exactly correlate with the information provided from Cabot, the average particle diameters were found to be at the lower end of the sizes provided (refer to Table 1). Further TEM characterization also showed that the slurry nanoparticles are highly dispersed.

Table 3.1. Average Diameters and Zeta Potential of Slurry Nanoparticles in Water

Sample	Concentration (mg/ml)	Z-average diameter	Zeta potential
		Water	Water
Colloidal Silica Slurry NS-0813-1	0.0203	52.53 nm	-22.8
	0.203	48.54 nm	-24.3
	2.03	46.21 nm	-28.4
Fumed Silica Slurry NS-0813-2	0.0334	161.7 nm	-45
	0.334	159.3 nm	-46
	3.34	157.9 nm	-53.9
Ceria Slurry NS-0813-3	0.0052	154.4 nm	-0.0813
	0.052	143 nm	0.l45
	0.52	141.2 nm	49.2
Alumina Slurry NS-0813-4	0.0201	119.5 nm	45.2
	0.201	119.4 nm	59
	2.01	115.5 nm	58.3

III.1.2 Analysis of particle size distribution using dynamic light scattering

Nanoparticles were further characterized using DLS for size and stability in deionized water (Table 1). The DLS measurements delivered similar values as reported by Cabot, demonstrating that the particles are stable in the aqueous solutions. Further the particle size distribution was evaluated at different concentrations, which will be later used for the cell based analysis. The measured PSD and zeta potential showed that the slurry particles are highly dispersed and stable even at high concentrations.

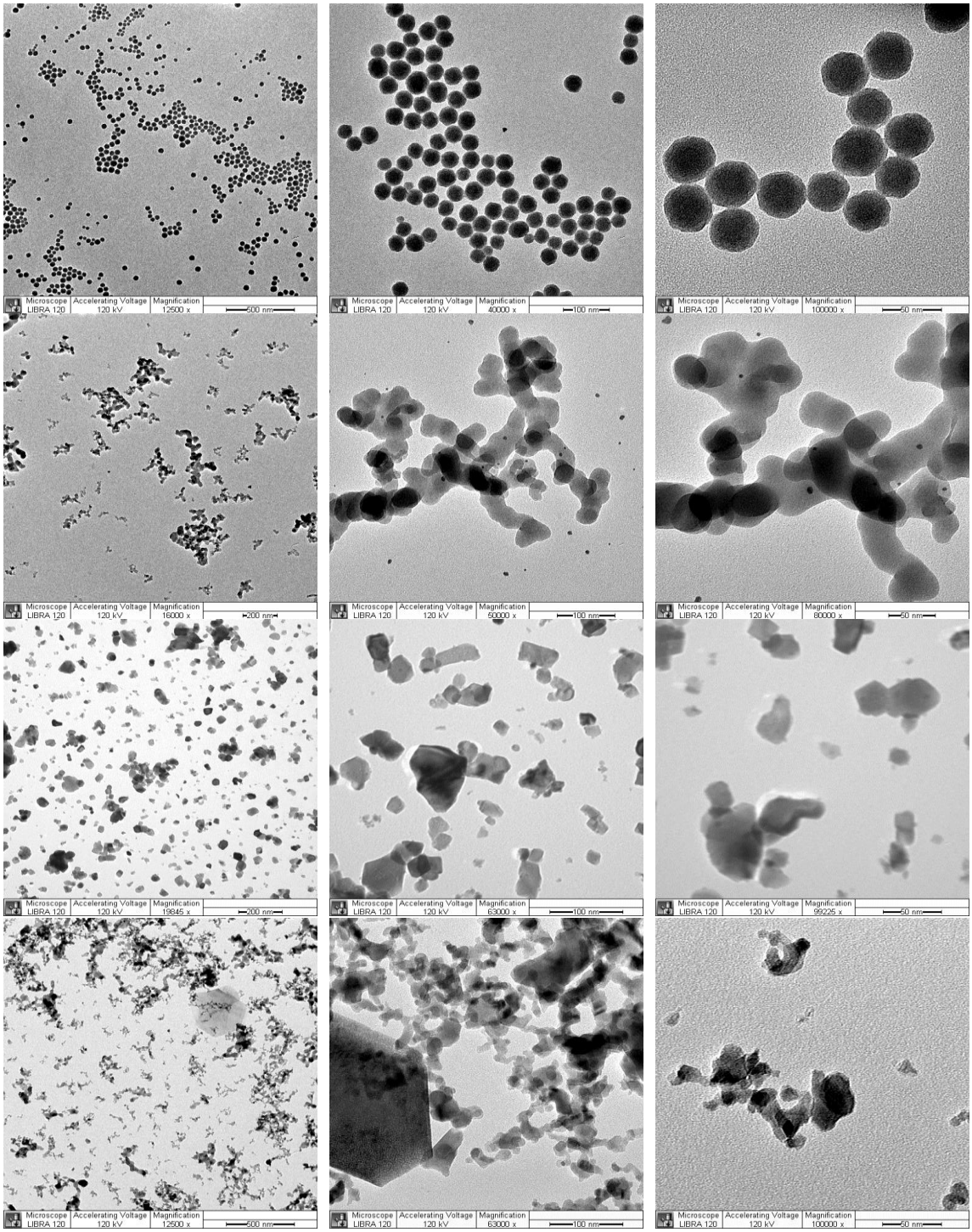

Figure 3.1. TEM images of Slurry Nanoparticles; Row 1- Colloidal Silica, Row 2- Fumed Silica; Row 3-Ceria; Row 4-Alumina

The silica particles, both colloidal and fumed silica showed higher negative zeta values, showing the negatively charged high dispersed particles. Ceria and alumina slurry particles recorded high positive zeta potentials, again showing that the particle is highly stable, but positively charged. The zeta potential values were shown to be slightly lower at the lower concentrations for ceria and alumina nanoparticles in the aqueous medium.

III.1.3 Scanning electron microscopy and energy-dispersion spectroscopy

The energy dispersion spectra of the slurry particles confirmed the presence of silica, ceria and alumina in the samples (Figure 3.2). The scanning electron microscopy images of the slurry nanoparticles are displayed as insets in figure 3.2.

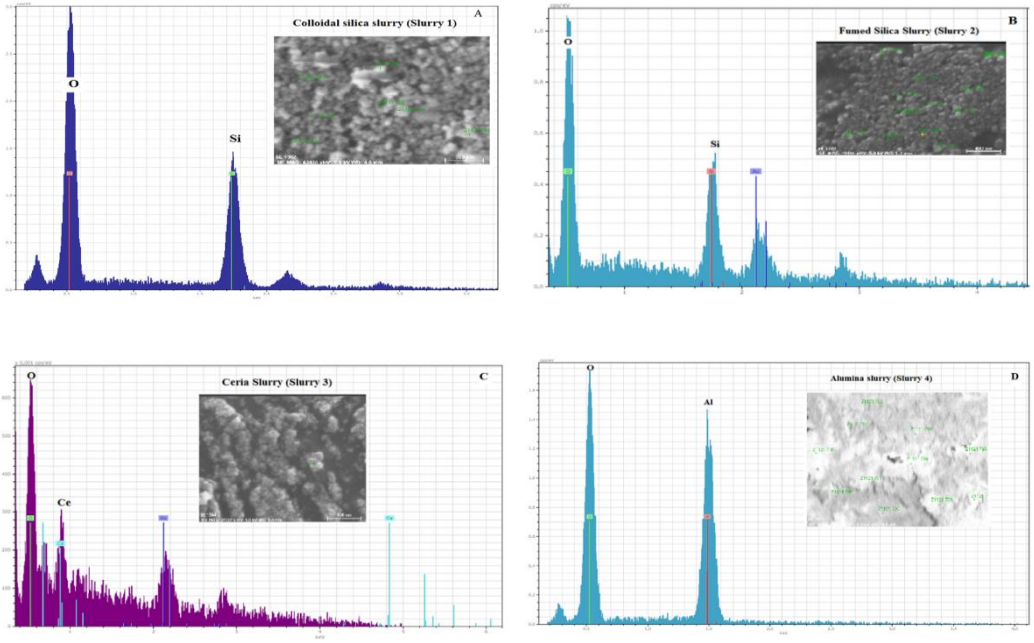

Figure 3.2. Energy Dispersion Spectra of a) Colloidal Silica, b) Fumed Silica, c) Ceria and d) Alumina Slurry Nanoparticles

III.1.4 Inductively coupled plasma-optical emission spectroscopy

ICP-OES data showed that the slurry samples, slurry 1, 2, 3 and 4 contained silica, ceria and alumina particles respectively (Figure 3.3). The percentage of silica, ceria and alumina content in the slurries was analyzed using ICP-OES and the results agree with the information provided from by Cabot/SRC (refer to table 1). As recorded, the fumed silica slurry had the highest percentage of solids (5%) and the ceria had the least percentage of solids (1%).

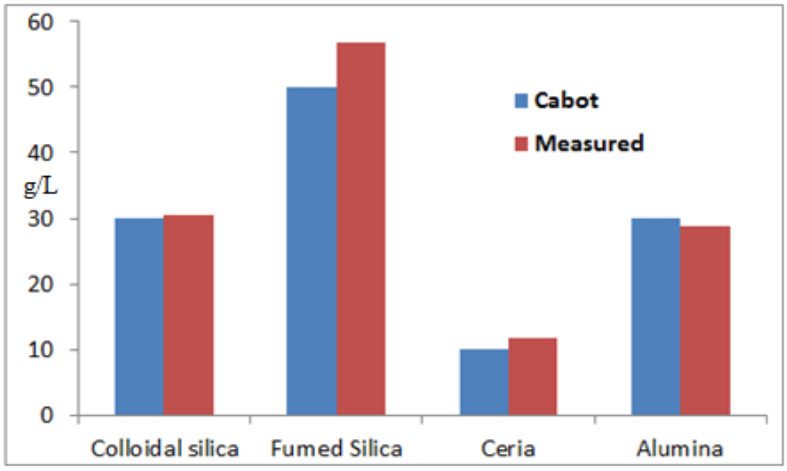

Figure 3.3. ICP-OES Data of Slurry Nanoparticles

III.1.5 X-ray diffraction spectroscopy

XRD is known for understanding the crystalline character of materials. It can also give information on the amorphous nature of the samples by broad peaks of x-ray diffraction. Comparison of the slurry samples with the corresponding undispersed particles showed that the slurry samples contained silica, ceria and alumina particles (Figure 3.4).

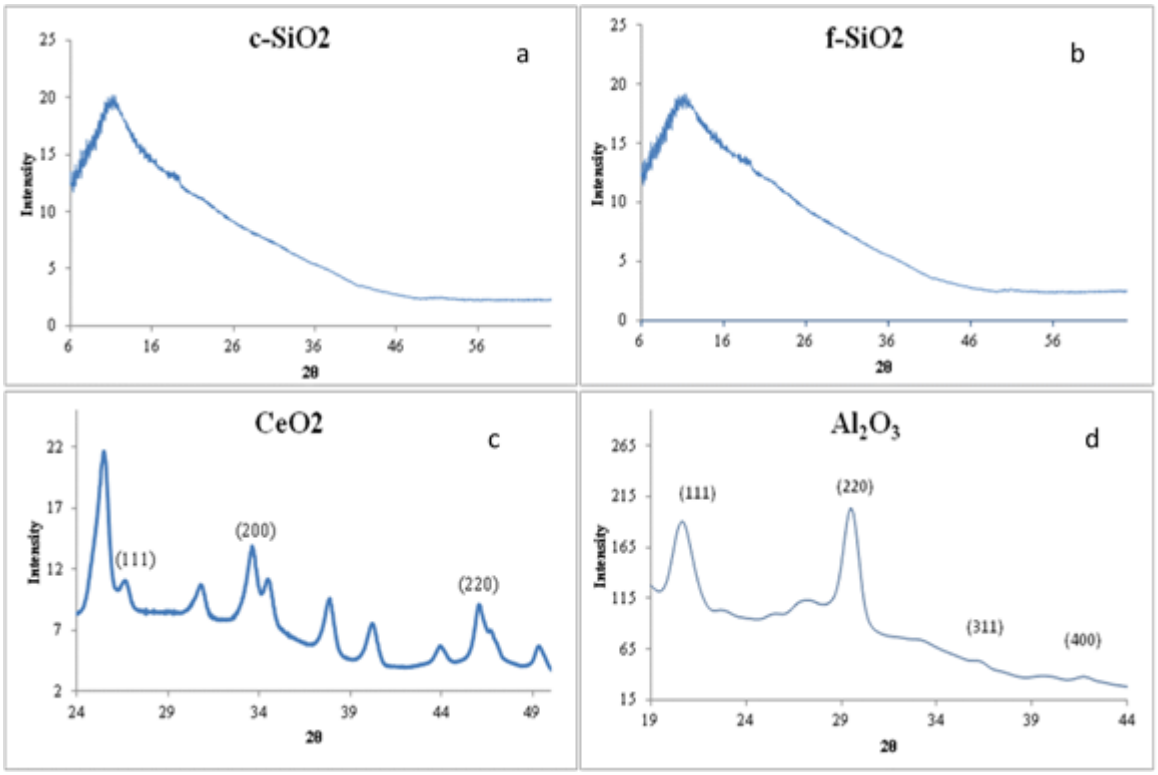

Figure 3.4. XRD of Silica (a and b), Ceria (c) and Alumina (d) NPs in Slurry

The colloidal silica slurry (slurry 1) sample correlates with the pristine/undispersed silica samples and exhibit amorphous nature (shown by broad peaks). The x-ray diffraction data of the ceria slurry (slurry 3) sample showed that it contains ceria by comparing with the diffraction pattern of pristine/undispersed ceria, though there are slight differences in the intensity and peaks for few crystallographic planes. The XRD data showed slight crystalline character of the ceria slurry nanoparticles, which was also observed from transmission electron microscopy which may be due to the short range order of the ceria powder or small percentage of crystalline particles present in the sample. The slurry 4 contains alumina shown by the comparison of alumina slurry (slurry 4) and

pristine/undispersed alumina diffraction patterns. The different peaks of x-ray diffraction are also used to differentiate type of alumina particles.

III.2 A549 Cell Culturing and Maintenance

Adherent Human lung epithelial cells (A549 cells) were used for this study. Cells were grown in F12-K media supplemented with 10% FBS and 1% antibiotic solution. A549 cells are adherent and confluent cells can be analyzed under light microscope as simple indication by percentage area of cell culture flask covered by monolayer of cells. Easy indication of the cell death or abnormal growth can be the morphology analysis and detachment of cells from the flask surface.

Complete cell culture media with 10% serum was used for cell viability, membrane integrity and cellular uptake analysis, whereas serum-free media and 1% serum supplemented media was investigated for ROS production analysis. Cell growth in the serum free media was different, as they did not spread on the flask surface and the number was low as compared to the cells grown in complete cell culture media. Though cells grown in media supplemented with 1% serum were shown to have less cell density compared to the cells grown in complete cells culture media, the morphology was comparatively similar (Figure 3.5). Hence, complete cell culture media was used for cell viability, membrane integrity and uptake analysis. Cell culture media supplemented with 1% FBS was used for the intracellular ROS production.

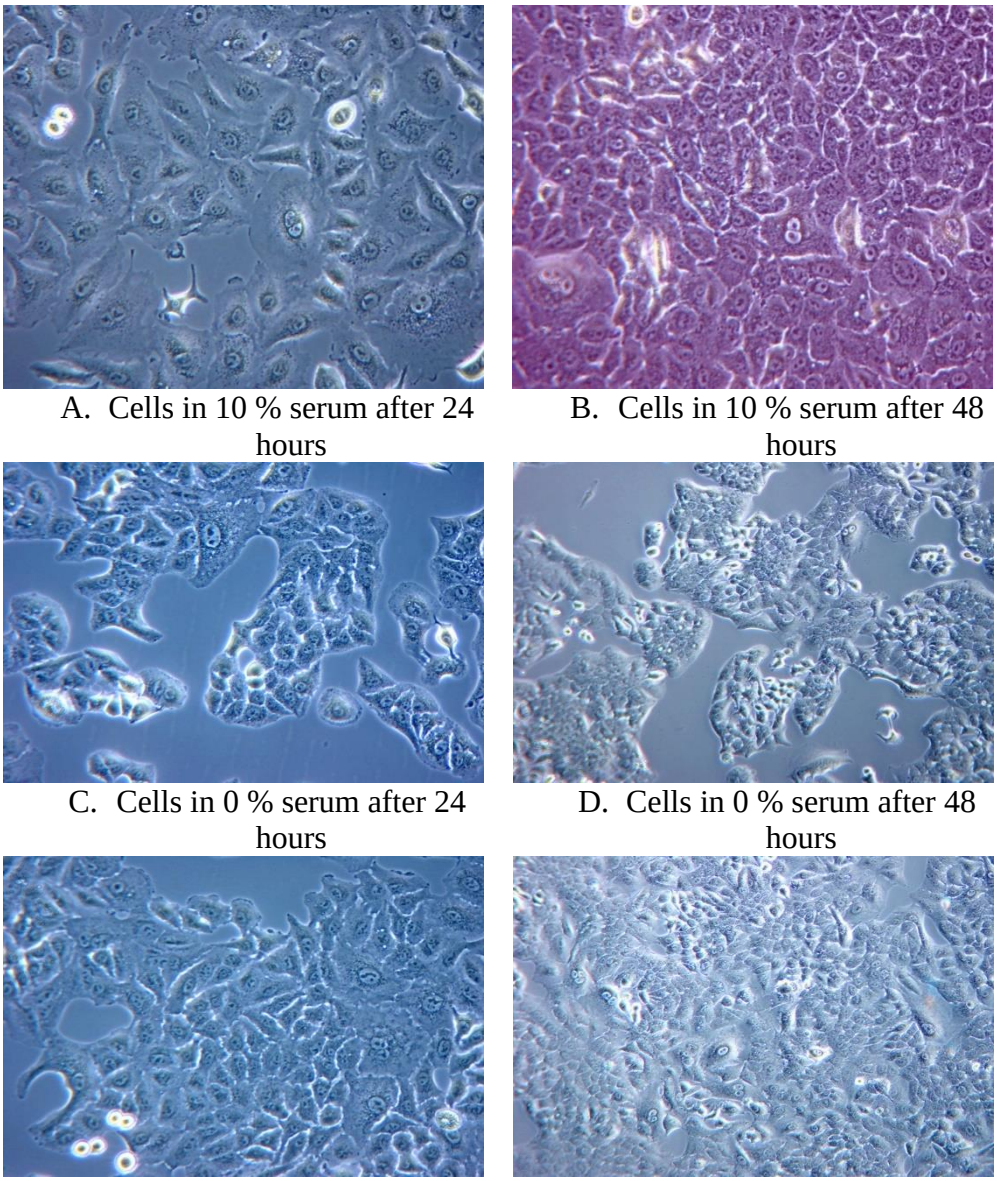

A. Cells in 10 % serum after 24 hours

B. Cells in 10 % serum after 48 hours

C. Cells in 0 % serum after 24 hours

D. Cells in 0 % serum after 48 hours

E. Cells in 1 % serum after 24 hours

F. Cells in 1% serum after 48 hours

Figure 3.5. Cell Morphology at Different Serum Concentrations (A to F) of Cell Culture Media

III.3 Cell Based Assays

III.3.1 Nanoparticle dispersions for cell based assays

The slurry concentrations of 2.03, 3.34, 0.52 and 2.01 mg/ml for colloidal silica slurry, fumed silica slurry, ceria slurry and alumina slurry, respectively, were used as highest concentration of each of the slurries. As the slurries were colloidal dispersions, the concentrations were prepared by simply volume dispersions in the media. The concentrations provided were used as the highest concentrations and further two magnitudes of dilutions (medium and low concentration) were prepared from the concentrated slurries using cell culture media (1 ul and 0.1 µl in 1 ml). Similar concentrations were used for the corresponding undispersed particles which were weighed and suspended in the cell culture media; 2.03 mg/ml for colloidal silica, 3.34 mg/ml for fumed silica, 0.52 mg/ml for ceria and 2.01 mg/ml for alumina nanoparticles and microparticles. The concentrations followed for the cell viability and membrane integrity studies and pH recorded for different concentrations of all four slurries used are tabulated (Table 3). The pH of the slurries was observed to be close to the pH of the cell culture media, irrespective of the original acidic/basic pH of the slurries (refer to Table 1).

III.3.2 Cell morphology analysis

As an early indication of the nanoparticle induced stress, changes in cellular morphology were analyzed. The cells were exposed to low and high concentration of the slurry nanoparticles for 24 hours and observed under light microscope for morphological changes. Colloidal silica nanoparticles at lower concentration did not affect the cell density and the morphology of the cells (Figure 3.6B), but at higher concentration, the cell density

decreased greatly accompanied by cells membrane shrinkage and lose of normal cell shape compared to the control (Figure 3.6C). Fumed silica slurry nanoparticles at higher concentration had adverse effect on the cell density (also seen by cell viability analysis) and the cells completely lose their normal shape, exhibit round shape and membrane shrinkage which are clearly seen in the microscopy images (Figure 3.7B and 3.7C).

Table 3.2. Nanoparticle Concentrations used for Cell Based Assays

Slurry sample		**Concentration (mg/ml)**	**Volume of slurry sample (µl)**	**pH**
Colloidal silica slurry (Slurry 1)	High (S1 H)	2.03	10	7.55
	Medium (S1 M)	0.203	1	7.74
	Low (S1 L)	0.0203	0.1	7.78
Fumed silica slurry (Slurry 2)	High (S2 H)	3.34	10	8.2
	Medium (S2 M)	0.334	1	7.83
	Low (S2 L)	0.0334	0.1	7.76
Ceria slurry (Slurry 3)	High (S3 H)	0.52	10	7.7
	Medium (S3 M)	0.052	1	7.74
	Low (S3 L)	0.0052	0.1	7.73
Alumina slurry (Slurry 4)	High (S4 H)	2.01	10	7.72
	Medium (S4 M)	0.201	1	7.81
	Low (S4 L)	0.0201	0.1	7.85

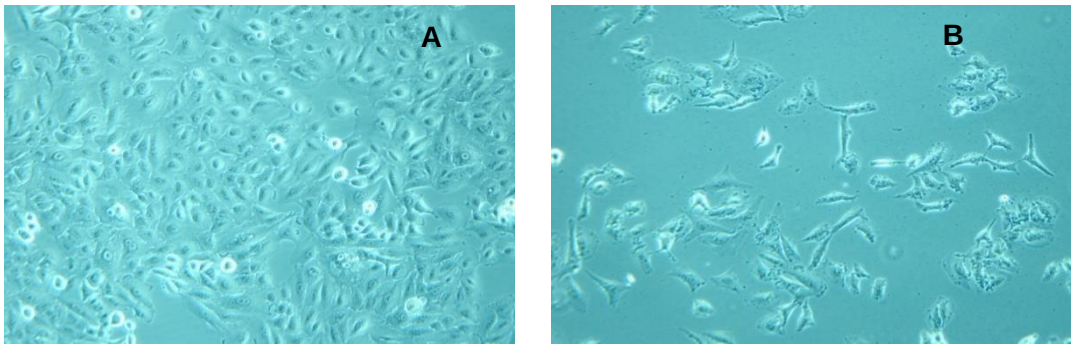

Figure 3.6. Cell Morphology Analysis after Exposure to Colloidal Silica Slurry Nanoparticles; A) Control Cells and B) Cells Exposed to High Concentraiton

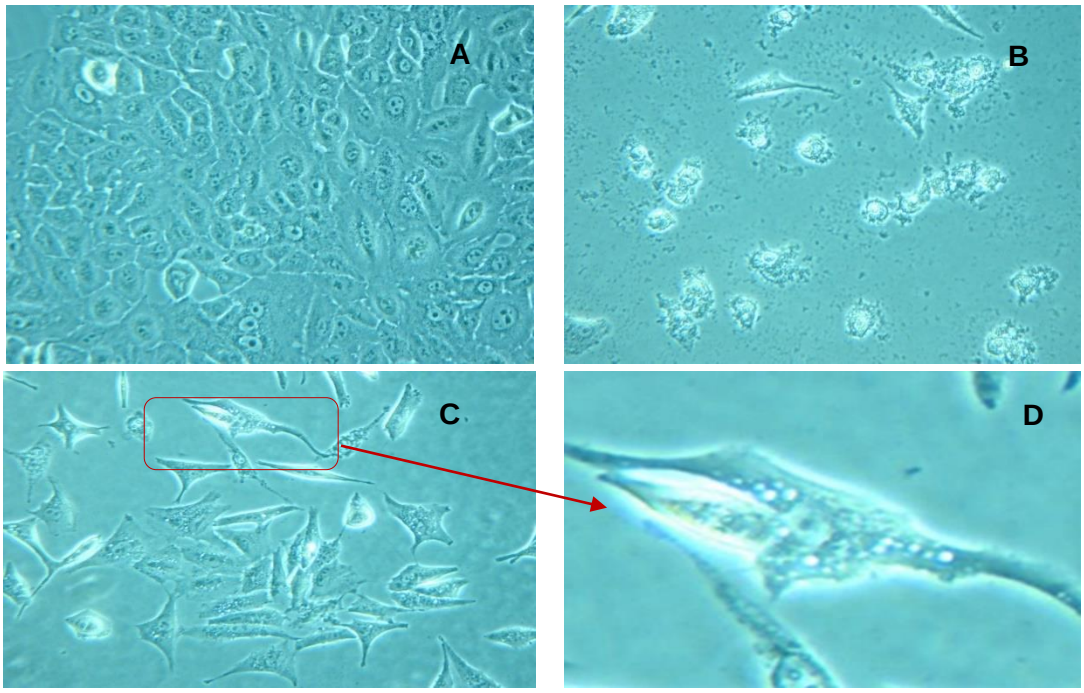

Figure 3.7. Cell Morphology Analysis after Exposure to Fumed Silica Slurry Nanoparticles; A) Control Cells, B) and C) Cells Exposed to High Concentration, and D) Enlarged Cell Showing Formation of Vesicles

III.3.3 Cell viability and membrane integrity analysis

A549 cells (from same passage number and same flask) were exposed to different concentrations of slurry nanoparticles for 48 hours and cell viability was analyzed using MTT reduction (Figure 3.8A) and membrane integrity was analyzed using LDH assay (Figure 3.8B). The cell viability decreased to 93 %, 86% and 19% compared to control in cells exposed to low, medium and high concentrations of colloidal silica slurry nanoparticles respectively (Figure 3.8A). The viability decreased to 84%, 78% and 10.4% compared to control, when exposed to low, medium and high concentrations of fumed silica slurry nanoparticles respectively. Cell viability of A549 cells did not decrease significantly compared to the control when exposed to ceria slurry nanoparticles (not less than 95%) and alumina slurry nanoparticles (not less than 85%).

From the membrane integrity analysis it was shown that fumed silica slurry nanoparticles caused higher membrane damage compared to colloidal silica slurry Nanoparticles, which is in agreement with the cell viability data. The extracellular LDH concentration was evaluated to be 14.4%, 121% and 240% compared to control for cells exposed to low, medium and high concentrations of colloidal silica slurry Nanoparticles respectively. The extracellular LDH was found to be 113%, 170% and 245% compared to control, when exposed to low, medium and high concentrations of fumed silica slurry nanoparticles respectively. Cells exposed to ceria nanoparticles and alumina nanoparticles did not cause significant cellular membrane damage compared to control cells (Figure 3.8B). Cell viability data agrees with the membrane damage analysis, therefore cell

viability was used for further analysis for effect of exposure time and concentration of nanoparticles on cells.

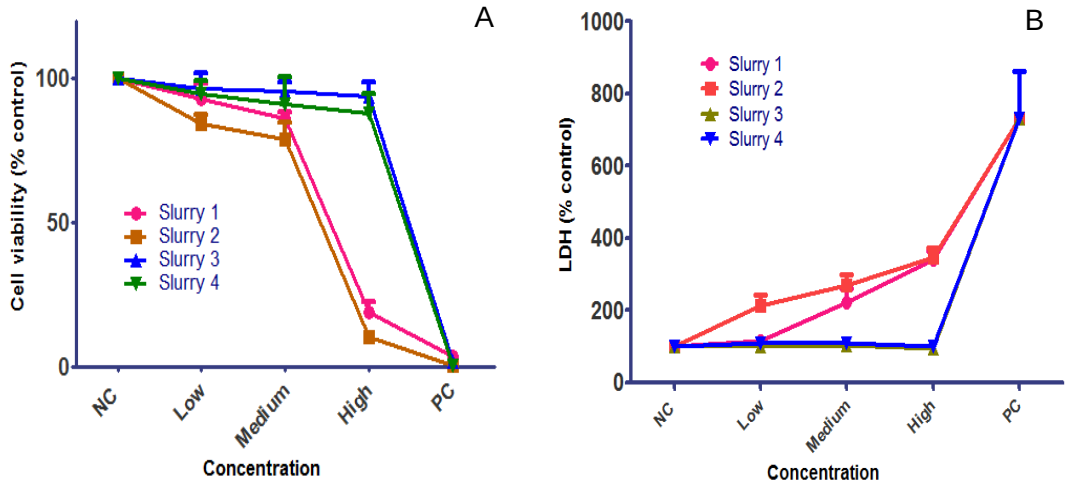

Figure 3.8. Cell Viability and Membrane Integrity Analysis after Exposure to Slurry Nanoparticles

(A: Cell viability and B: membrane integrity of cells exposed to low, medium and high concentrations of the four slurry nanoparticles. Slurry 1- colloidal silica slurry nanoparticles, Slurry 2- fumed silica slurry nanoparticles, Slurry 3- ceria slurry nanoparticles and Slurry 4- alumina slurry nanoparticles.)

III.3.4 Cell viability and membrane integrity analysis of slurry supernatants

The slurry compositions as discussed earlier are a mixture of abrasive nanoparticles with other chemicals to stabilize them and ease the material removal during polishing of wafers. To investigate the effect of these chemicals on cellular toxicity, the slurries were centrifuged at 200,000 rpm to remove the nanoparticles and the supernatants were used to evaluate the effect on cells (Figure 3.9). The two groups, MTT and LDH, are separated by

50 y data points for clarity. The was no significant decrease in the cell viability and/or increase in the LDH release due to membrane damage compared to control after exposure to all the slurry supernatants, showing that the cell viability decrease presented in the previous section was from nanoparticles and the chemicals in the slurry did not affect the cellular function.

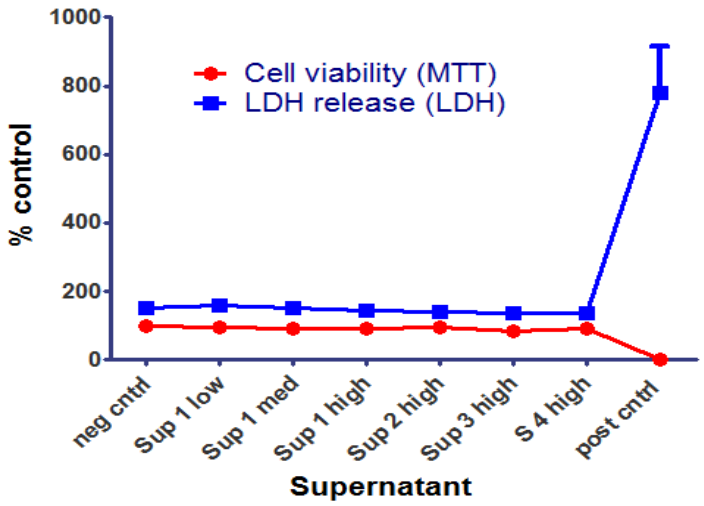

Figure 3.9. Cell Viability and Membrane Integrity Analysis after Exposure to Supernatants

III.3.5 Oxidative stress analysis

III.3.5.1 Analysis of intracellular ROS production. Intracellular reactive oxygen species (ROS) production was used as a marker for the oxidative stress analysis in cells exposed to nanoparticles and microparticles. ROS production in the cells was evaluated by DCF-fluorescence, which after exposure to undispersed particles at different concentration did not show significant increase in the ROS production, whereas there was significantly lower fluorescence detected from the cells exposed to colloidal silica and fumed silica

slurry nanoparticles (Figure 3.10). There was no significant increase in the DCF fluorescence when cell were exposed to the alumina nanoparticles (not greater than 13%, compared to the control cells. As the cell viability decreased to 86%, 80% and by 19.7 % for 24 hour exposure for colloidal silica and 83, 83.7 and 11.43 for 24 hour exposure to fumed silica slurry nanoparticles, the decrease in fluorescence could be due to the low cell number and leakage of DCF dye from the cell membrane, as indicated by the cell membrane integrity analysis. Hence normalization of the DCF- fluorescence data was required for total number of cells.

*III.3.5.2 Analysis of ROS production after normalization to cell number***.** Procedure 2 described in the materials and methods section was used for the ROS production analysis and fluorescence is represented as relative fluorescence unit (normalized to 10,000 cells). The results showed that the DCF-fluorescence normalized to 10,000 cells, increased with the increasing concentration with respect to the control cells (Figure 3.11). Intracellular ROS production increased to 152%, 143.7 % and 182.3 % after 24 hours and 137 %, 142 % and 194% after 48 hours for the cells exposed to low and medium concentration of the colloidal silica slurry nanoparticles compared to control cells. ROS production increased to 118%, 125.7% and 190% after 24 hours and 155.8 %, 134.8 % and 189.5 % after 48 hour exposure to low, medium and high concentration of fumed silica slurry Nanoparticles. There was dose dependent increase in ROS production compared, but there was no significant difference between the 24 hour exposed group and 48 hour exposed group.

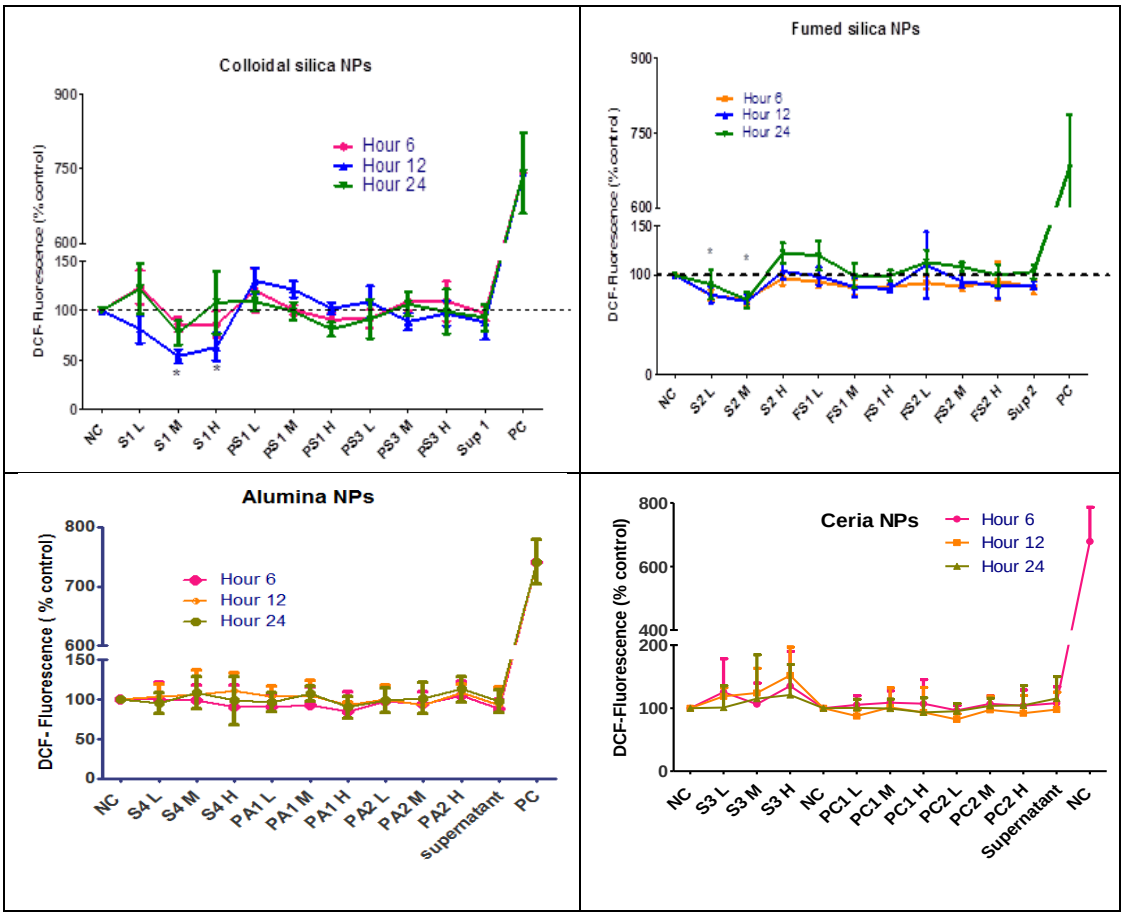

Figure 3.10. DCF- Fluorescence after Exposure to Slurry Nanoparticles and Undispersed NPs and MPs

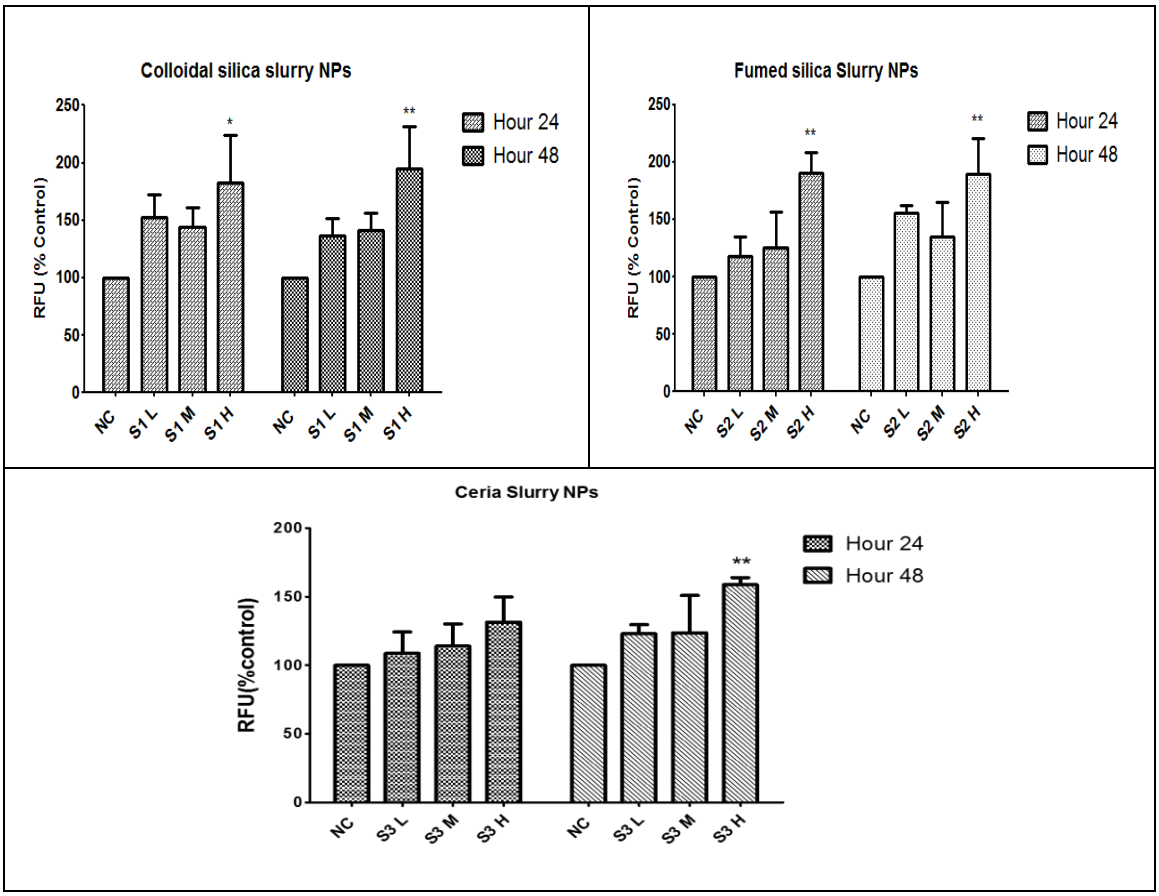

Figure 3.11. ROS Production in Cells on Exposure to Slurry Nanoparticles

III.3.6 In vitro Cellular Uptake of EN

Cellular uptake was studied using ICP-OES, confocal Raman and ECIS measurements. These techniques were selected to study the uptake without further any surface modification. Moreover ECIS, unlike most end-point techniques, is an established technique for real time and longitudinal measurements. The highest concentrations (from table 2) and exposure time of 48 hours were chosen to study the uptake of the NP slurries – colloidal silica (2.03 mg/mL), fumed silica (3.34 mg/mL), ceria 3 (0.52 mg/mL) and alumina slurry (2.01 mg/mL). In case of ICP-OES and confocal Raman studies, the cells

were washed 10 times with PBS to eliminate NPs that are adhered on the cell membrane. For ICP-OES and Raman measurements, slurries dispersed in media were used for comparison. Figure 3.12A shows the ICP-OES measurements after digesting slurry exposed cells, using standard protocols. It can be observed that there is significant cellular uptake of NPs for all the slurries.

Even though there is clear evidence of uptake of all the slurries from ICP-OES data, we could only confirm ceria NP uptake in confocal Raman measurements. Figure 3.12B shows Confocal Raman spectra for only cells, dried ceria slurry, ceria NPs and cells after exposure to ceria slurry for 48 hours. Ceria has a Raman peak around 450 cm^{-1} Raman shift. It can be observed from the Raman spectra that there is sharp peak indicating clear evidence of ceria NPs in the cells. It can be concluded from the spectra that the intensity of the peak goes down which could be due to the concentration of ceria NPs internalized in the cells. Also, there was a slight shift in the peak if we compare ceria NPs to dried ceria slurry and to ceria slurry exposed to cells. This could be because of the presence of other constituents in case of the dried slurry and due to the cellular components in case of NPs in cells.

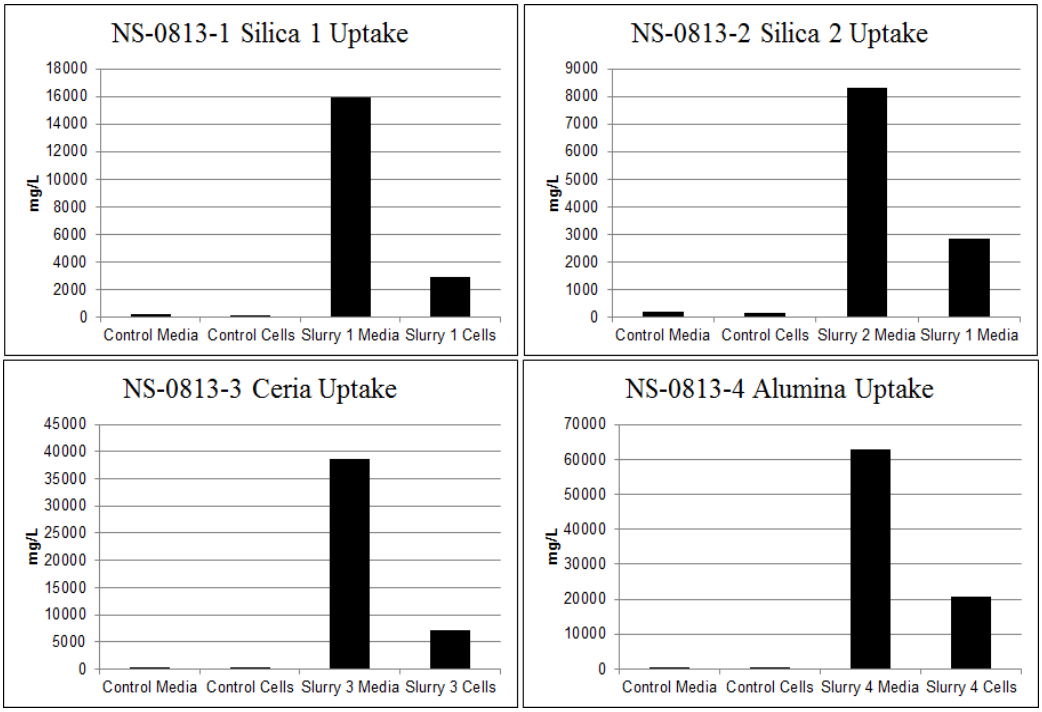

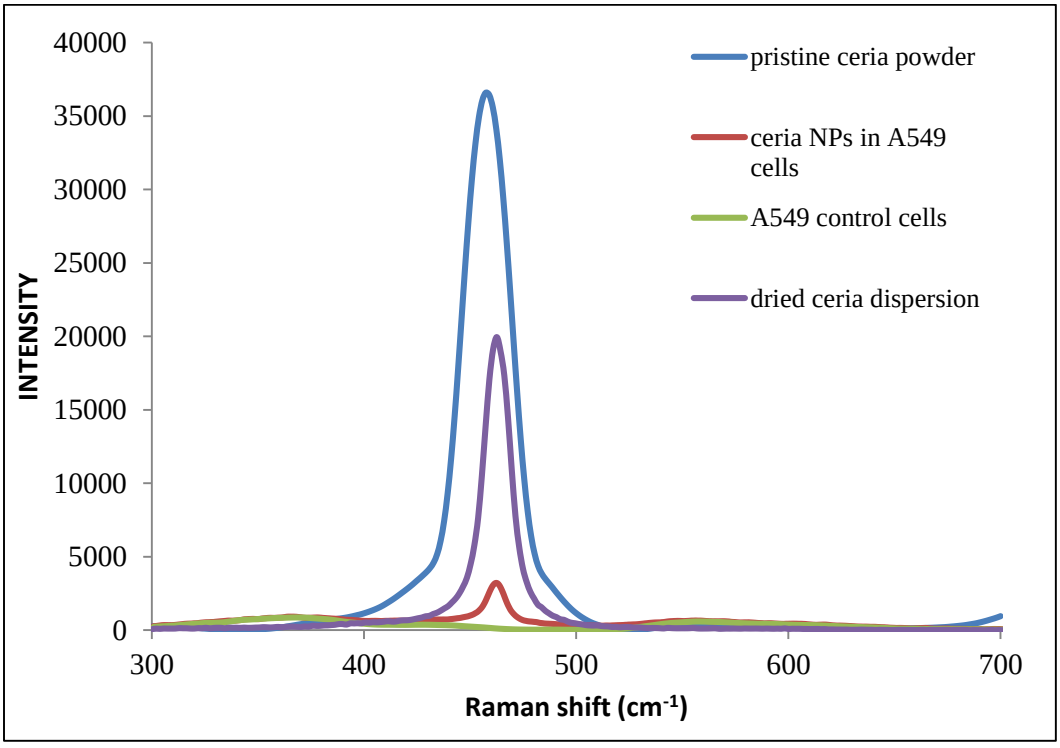

Figure 3.12. a) ICP-OES Data of Cells Exposed to Slurries and b) Confocal Raman Spectral Comparison Indicating Cellular Uptake of Ceria NPs from Ceria Slurry

CHAPTER IV

TIME AND DOSE-DEPENDENT CELLULAR TOXICITY OF SILICA NANOPARTICLE BASED SLURRIES USED IN CHEMICAL MECHANICAL PLANARIZATION PROCESS: EFFECT OF NANOPARTICLE CHARACTERISTICS

IV.1 Introduction

Monitoring exposure and understanding the Environmental, Health and Safety (EHS) of engineered nanomaterials (ENs) is of enormous importance to the semiconductor industry. According to the 2013 International Technology Roadmap for Semiconductors (ITRS), a number of ENs in the form of inorganic nanoparticles (NPs) such as amorphous silica, ceria and alumina, nanotubes (multi-walled and single-walled carbon nanotubes), nanowires (gallium-arsenide nanowires), and thin sheets (graphene) are slated for introduction in semiconductor front-end manufacturing, interconnect, lithography, assembly and packaging from now through 2028. However, at present, the only known use of ENs in high volume semiconductor manufacturing is the nanoscale abrasives made of either amorphous silica, ceria or alumina nanoparticles (NPs) of sizes between 20 and 200 nm for a widely used semiconductor manufacturing process called Chemical Mechanical Planarization (CMP)[11]. According to BCC research, nearly 60% of the total $1.7 billion worldwide market for NPs in 2012 was used for CMP processes[60]. The CMP process is used to achieve local and global planarity on a variety of materials including dielectrics, semiconductors, metals, polymers, and composites. Achieving near-perfect planarity is

critical in the manufacturing of integrated circuits and many other semiconductor processes including optical lithography, multi-level metallization and damascene technology and for many other semiconductor processes including optical lithography, multi-level metallization and damascene technology. Planarization is achieved by a combination of chemical reactions and mechanical polishing using slurries made up of unbound nanoscale abrasives of either silica, ceria or alumina NPs, oxidizing chemicals and other additives. Of the various abrasive NPs used in the CMP processes, amorphous silica NPs hold the largest share with an estimated 2.4 million metric tons used in 2014[61]. However, little is known on possible cellular interactions and cytotoxic potential of silica NP slurries to manufacturing personnel and impact in waste streams, which are potential gateways for release of used NPs to the environment. Much of the work on amorphous silica NP toxic effects have focused on pristine NPs with or without surface modification[17]. However, it is well-known that NP toxicity depends not only on its physical and chemical properties and on how those properties influence cells or tissues but also on their dispersion conditions[62]. Subtle differences in NP size, shape, composition, type, aggregation, surface reactivity and dispersion media conditions can affect their interactions and toxicity[17, 18, 44]. It is therefore essential to investigate and understand the effect of "true" NP slurries or formulations (NPs well-dispersed in a slurry matrix), as used in a manufacturing setting, on cytotoxicity and cellular interactions rather than pristine NPs[63]. In addition, it is also important to carefully characterize the physical and chemical properties of a NP at various stages throughout its lifecycle. The overarching objective of the EHS community including the semiconductor industry, as noted in a recent article is to develop predictive capability for assessment of

human and environmental toxicity, along with correlating toxicity with physiochemical properties.

The silica nanoparticles that have been chosen for this study have already been used in real applications in semiconductor fabrication for chemical mechanical planarization (CMP) of wafers. However, the fact that the threshold levels of toxicity of these nanoparticles have not been reported yet makes it really important to study the toxicity of these nanomaterials since the waste from the CMP process is directed into water streams. It was reported by a study conducted at a semiconductor process development and fabrication facility reported that alumina and silica particles were identified in the work space[64]. Another study investigating the filters of the conventional waste water treatment (WWT) system reported that nanoparticles may be captured incidentally by the existing system without size-selectivity for nanoparticles[64, 65]. This provides evidence for the possibility of airborne NPs being exposed to the personnel, especially by inhalation, working with the CMP tool, filtration and waste water treatment systems.

To use ENs with high efficiency for various applications, it is necessary for the NPs (NPs) to exist in a highly dispersed state in order to have high surface area, which is one of the major advantages nanomaterials offer when compared to their larger counterparts. However, due to surface charge and functionalization of NPs, they form aggregates changing the size, due to which linear trends in concentration/dose dependent reactivity are not observed. The objective of this study is to investigate the effects of EN attributes such as size, surface area, surface charge and aggregation on their toxic potential. The NPs in CMP slurries are highly dispersed with high dispersion stability in order to facilitate

uniform polishing of wafer surfaces. Hence, these NPs become excellent candidates to study the effect of aggregation.

It is well established that crystalline silica causes adverse effects, whereas amorphous silica is considered safe by US federal Drug administration and hence used as a filter aid in food products, diagnostic devices, therapeutic drug delivery system and negative control for toxicity analysis[66]. Amorphous silica NPs can be distinguished as different forms based on method of synthesis including fumed silica, which are produced as dry aggregates under high-temperature flame, and precipitated, colloidal, or mesoporous silica, which are prepared via molecular condensation of silanol groups in aqueous solution or under hydrothermal conditions.

In this study, we have evaluated the toxic potential along with lethal doses of toxicity of colloidal and fumed silica NPs on A549 cells. Also, this paper will provide understanding on the influence of size and aggregation of colloidal and fumed silica NPs on their toxicity. For this purpose, highly dispersed and undispersed NPs of similar size and microsize particles were included in the study. The physicochemical properties of the ENs were characterized using dynamic light scattering (DLS), zeta potential, transmission electron microscopy (TEM), inductively coupled plasma optical emission spectrometry (ICP-OES), fourier transform infrared (FT-IR) spectroscopy and BET surface area analysis. In order to relate this study to inhalational exposure we have chosen adenocarcinomic basal alveolar lung epithelial cells (A549 cells), which form the lining of the respiratory tract, as the *in vitro* model to study the toxicity of the NPs. From the results, it was observed that both highly dispersed colloidal and fumed silica NPs showed dose

dependent toxicity, where high toxicity was observed for the highest dose, over exposure periods of 6, 12, 24, 48 and 72 hours whereas the undispersed NPs exhibit a reverse trend. From comparison of these results with characterization of the NPs, it can be concluded that aggregation of silica NPs is responsible for the observed trends of toxicity.

IV.2 Materials and Methods

IV.2.1 Nanoparticles

CMP slurries composed of colloidal silica and fumed silica was supplied by Cabot Microelectronics through SRC (Semiconductor Research Corporation). Undispersed colloidal silica NPs of 80 nm (silica nanospheres) were purchased from NanoComposix (CA, USA) and fumed silica NPs of 7 nm and 200 nm were purchased from Sigma-Aldrich (MO, USA). The composition and size of the dispersed NPs and sizes of the undispersed particles as reported by the company (Table 4.1a and 4.1b).

Table 4.1. Size and Composition of the Dispersed Samples and Sizes of Undispersed Particles

Sample	Composition	pH	Size(nm)
Colloidal Silica (NS-0813-01)	3% precipitated Silica, adjusted with acetic acid	2.5-4.5	50-60
Fumed silica (NS-0813-02)	5% silica, adjusted with KOH	10	120-140

Undispersed Particles	Size
Colloidal Silica (PS1)	80 nm
Colloidal Silica (PS3)	1-3 um
Fumed Silica (FS1)	7 nm
Fumed Silica (FS2)	200-300 nm

IV.2.2 Materials

Trypan blue, fetal bovine serum (GE Health care), F12K media -and DPBS (Corning cellgro, VA), penicillin-streptomycin-glutamine (Hyclone gibco, life technologies, NY) trypsin, MTT cell proliferation Assay kit (Vybrant, Molecular probes, Oregon) and LDH cell integrity assay kit (Pierce, Thermo Scientific, IL).

IV.2.3 Dynamic light scattering and zeta potential

Particle size distribution (PSD) and zeta potential were measured using a Malvern Instruments ZEN3600 Zetasizer Nano-ZX which emloys a HeNe laser (633 nm) and scattering angel of 175°. The silica NP dispersions were dispersed in water and cell culture media for measurements and the measurements were conducted by using a refractive index of 1.54. Approximately 1 ml of the samples were loaded in the zeta cells and placed in the cell holder for measurements. Three measurements of ten runs each were conducted for each sample and the average of the three measured values were reported.

IV.2.4 Transmission electron microscopy

A Carl Zeiss Libra 120 Plus TEM Microscope was used to acquire electron micrographs of the NPs to characterize the samples for size and morphology. NPs were dispersed in DI water at very low concentrations and sonicated for 10 minutes. The copper grids were glow discharged to make them hydrophilic and a drop of the sample was put on the copper grid and allowed to air dry and used for analysis at 120 kV and an emission current of 3-6 μA. The images were further processed by Image J software for the particle size analysis.

IV.2.5 X-ray diffraction (XRD) analysis

XRD patterns were obtained using Agilent Technologies Oxford Gemini X-Ray Diffractometer to understand the crystallinity of the NPs. For this purpose the NP dispersions were dried to a constant mass at 125 ^{0}C. The samples were irradiated by a molybdenum source at a voltage of 50 mV and a current of 30 mA.

IV.2.6 Inductively coupled plasma-optical emission spectroscopy (ICP-OES)

Silica dispersion were diluted (varying amounts) and digested overnight in 1% HF (3-4ml total vol). Digested samples were vortexed heavily before analysis. The samples were analyzed in a Varian 710 Axial ICP ES using "OneNeb" low flow nebulizer with double pass cyclonic spray chamber (borosilicate glass) and axial quartz torch for high dissolved solids. A manual calibration was performed for .1, .5, 1, 5 ppm standards and the concentrations of silica were determined by data interpolation in the calibration curve.

IV.2.7 Attenuated total reflectance fourier-transform infrared (ATR-FTIR) spectroscopy

Infrared spectra were obtained using a Varian 670 FTIR Spectrometer using an ATR accessory equipped with a diamond crystal. The spectra were obtained with 1.5 sensitivity and 120 scans per sample.

IV.2.8 A549 cell culture and maintenance

A549 cells was purchased from (ATCC), cells were maintained in F12 K media supplemented with 10% FBS and 1% pencillin and grown at 37°C in a 5% CO2 humidified environment. Cell cultures with 95% or higher viability were used for the experiments. Cell count and cell viability was analyzed using trypan blue dye exclusion test and a haemocytometer. NP and MP dispersions for cell based experiments were prepared by

dispersing the particles into complete cell culture media and sonicated prior to exposure to cells. All the cell based experiments were carried out in complete cell culture media supplemented with 10% serum.

IV.2.9 NP concentrations

The concentrations of three orders of magnitude (high, medium and low) with the highest concentration being 2.03 and 3.34 mg/ml for colloidal silica and fumed silica NP dispersions, respectively, were chosen. The concentrations were prepared from the stock using cell culture media (1 ul and 0.1 µl in 1 ml). Similar concentrations were used for the corresponding undispersed particles (both nano- and micro-particles) which were weighed and suspended in the cell culture media. Figure shows MTT cell viabilities of A549 cells. The toxicity analysis was performed by exposing the chosen concentrations of NPs to A549 cells.

IV.2.10 Cell viability analysis

Cell viability was measured using the 3-(4, 5-dimethylthiazol-2-yl)-2, 5-diphenyltetrazolium bromide (MTT) reduction assay. The MTT assay uses mitochondrial activity as a measure of cell viability. The cells were seeded in 96 well (3200 cells per well) plates at a density of 10,000 cells per cm^2 area for 24 hours. After the cells adhere, media was replaced with fresh media along with triplicates of different concentrations of the slurries and corresponding NPs and incubated for different time points (6, 12, 24, 48 and 72 hours). After incubation, the cell viability assay was performed using the MTT cell viability kit. The media was replaced with 100 ul of fresh media (phenol-red free media was used for MTT analysis, as recommended by the kit manufacturers). Immediately after

this the absorbance was measured at 570 nm for the background subtracttion to account for the interference due to media components and NPs remaining attached to the cells and surface. MTT assay was performed by loading 10 µl of the reagent A (MTT tetrazole) and incubated for 4 hours for the insoluble purple formazan crystal formation. 100 µl of reagent B (SDS, solubilizing agent) was added to the wells and incubated further overnight and the absorbance was measured at 570 nm. The results were analyzed using Graphpad (Prism) and cell viability was represented as the percentage of negative control and one way Analysis of variance (tukey test) was used to evaluate the statistical significance with 95% confidence. Two way ANOVA with Bonferroni post-test was used for comparing time points and groups.

IV.2.11 Membrane integrity analysis

Lactate dehydrogenase (LDH) is a cytosolic enzyme present in cells which is released into the cell media when the cell membrane is damaged. Membrane integrity can be analyzed by LDH concentrations in the cell media. LDH analysis was performed by using Thermo scientific pierce LDH cytotoxicity assay kit. A549 cells were seeded in a 96 well plate with a density of 10,000 cells per cm^2 area of the plate (3200 cells per well). After cell adherence, the cell media was replaced with fresh media and the cells were exposed to triplicates of different concentrations of the dispersed and undispersed particles. After 48 hours for exposure, 50 µl of the supernatant was transferred to another 96 well plate and 50 µl of the reaction mixture was added to each well. 15 ml of the reaction mixture was prepared by mixing 0.6 ml of assay buffer to 11.4 ml of substrate mix (lysophilizate). The plate was incubated for 30 minutes at room temperature and then 50 ul of the stop

solution was added to stop the reaction and absorbance was measured at 490 and 680 nm for LDH analysis using a spectrophotometer. The results were analyzed using statistical software Prism and LDH concentration in the cell media was represented as the percentage negative control and one-way ANOVA was used to evaluate the statistical significance with 95% confidence.

IV.3 Results

IV.3.1 Characterization

Prior to studying toxicity, the NPs were thoroughly characterized in order to better understand the physicochemical properties of the ENPs and then for shape, composition, particle size distribution, and dispersion stability. Figure 4.1 shows the TEM images of dispersed colloidal and fumed silica NPs. The colloidal silica NPs were spherical and fumed silica NPs have an interlocked chain structure which could be due to the method of synthesis (fumed silica is produced as dry aggregates under high-temperature flame and colloidal silica is produced via molecular condensation of silanol groups in aqueous solution or under hydrothermal conditions).

NPs were further characterized for size and dispersion stability using DLS and zeta potential measurements. The DLS measurements showed PSD of 46±0.2 and 147.8±5.1 for colloidal silica and fumed silica NPs, respectively. The values were similar to those reported by Cabot (supplier of dispersed NPs), demonstrating that the particles are stable in aqueous solution. The zeta potential measurements indicated high negative values of -21 and -50 for colloidal and fumed silica NPs, respectively, demonstrating high dispersion

stability and negative surface charge of the NPs which in turn compliment the low standard deviations in the PSD measurements. The surface area of the highly dispersed NPs, measured using a BET surface area analyzer, was found out to be 99.509 m^2/g for colloidal silica and 50.997 m^2/g for fumed silica. The composition of the dispersed NPs was analyzed using ICP-OES, XRD, FT-IR and Raman spectroscopies. The ICP-OES analysis validated that the concentrations of the NPs were 30.45 g/L for colloidal silica and 56.94 g/L for fumed silica compared were in agreement with 30 g/L and 50g/L, respectively, reported by Cabot (Figure 4.2).

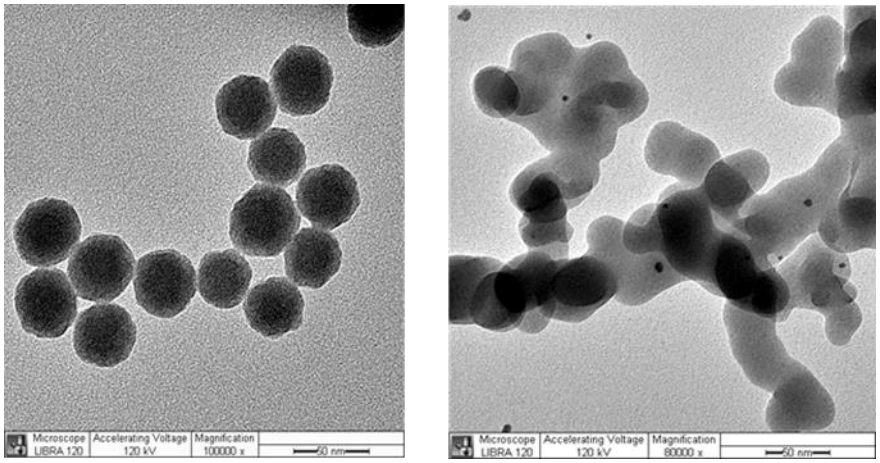

Figure 4.1. TEM Images of Dispersed A) Colloidal and B) Fumed Silica NPs

IV.3.2 Cellular toxicity analysis

Concentrations for cellular analysis were chosen by considering the process of CMP where the slurries are diluted by water before being washed off from the CMP tool and directed to the waste water systems. The concentrations of three orders of magnitude (high, medium and low) were chosen with the highest concentration being 2.03 and 3.34

mg/ml for colloidal silica and fumed silica NP dispersions, respectively. The concentrations were prepared from the stock using cell culture media (1 ul and 0.1 µl in 1 ml). Similar concentrations were used for the corresponding undispersed particles (both nano- and micro-particles) which were weighed and suspended in the cell culture media. Figure shows MTT cell viabilities of A549 cells. The toxicity analysis was performed by exposing the chosen concentrations of NPs to A549 cells. The concentrations used for the cell viability and membrane integrity studies and pH recorded for different concentrations of all four slurries used are tabulated (Table 4.2).

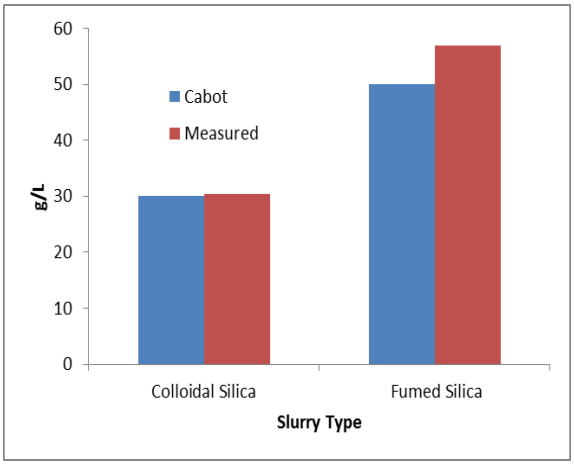

Figure 4.2. ICP-OES Quantification of Colloidal and Fumed Silica Dispersions in Comparison to the Values Reported by Cabot Microelectronics

The pH of the slurries was observed to be close to the pH of the cell culture media, irrespective of the original acidic/basic pH of the slurries (refer to Table 3.2). The comparison of TEM images dispersed and undispersed colloidal silica NPs is represented in Figure 4.3A and 4.3B .The undispersed particles tend to agglomerate even after

sonication and the interface boundaries are evident from the TEM images. This was further confirmed from the DLS-particle size distribution measurements which showed high dispersion stability for dispersed NPs compared to the undispersed particles used for the study (Figure 4.3C and 4.3D). The dispersed NPs did not show significant change in the size even at higher concentrations, whereas the undispersed NPs purchased commercially showed significantly higher particle sizes reaching to micrometer range at higher concentrations.

Table 4.2. NP Concentrations used for Cell Based Assays and the Recorded pH for each Concentration

Sample		Concentration (mg/ml)	Volume of sample (µl)	pH
Dispersed colloidal silica NPs	High (S1 H)	2.03	10	7.55
	Medium (S1 M)	0.203	1	7.74
	Low (S1 L)	0.0203	0.1	7.78
Dispersed fumed silica NPs	High (S2 H)	3.34	10	8.2
	Medium (S2 M)	0.334	1	7.83
	Low (S2 L)	0.0334	0.1	7.76

IV.3.3 Cell viability and membrane integrity analysis

Figure 4.4 shows the compilation of results from cell viability and membrane integrity analysis of A549 cells exposed to dispersed colloidal and fumed silica NPs for 48 hours. The cell viability decreased to 93 %, 86% and 19% compared to control, when exposed to low, medium and high concentrations of colloidal silica NPs, respectively (Figure 4.4A). The viability decreased to 84%, 78% and 10.4% compared to control, when

exposed to low, medium and high concentrations of fumed silica dispersed NPs, respectively.

From the membrane integrity analysis it was shown that fumed silica NPs caused higher membrane damage compared to colloidal silica NPs, which is in agreement with the cell viability data. The extracellular LDH concentrations (Figure 4.4B) was found to be 14.4%, 121% and 240% compared to control for cells exposed to low, medium and high concentrations of colloidal silica NPs, respectively, and 113%, 170% and 245% compared to control, when exposed to low, medium and high concentrations of fumed silica NPs, respectively. The cell viability data compliments the membrane integrity analysis, and so cell viability was used for further analysis for effect of exposure time and concentration of NPs on cells.

To investigate if the effects observed were due to the NPs or other constituents in the dispersions, both the dispersions were centrifuged at 200,000x to remove the NPs and the supernatants were used to evaluate the effect on cells. It was observed that there was no significant decrease in the cell viability and/or increase in the LDH release due to membrane damage compared to control cells after exposure to the supernatants, indicating that the effects observed were from NP interaction with the cells and that the other components of the dispersions did not exhibit any effect on cellular function.

IV.3.4 Exposure time and concentration dependence on cell viability of A549 cells exposed to colloidal Silica NPs and MPs

Cell viability of A549 cells after exposure to different concentrations of dispersed and undispersed colloidal silica MPs and NPs (undispersed colloidal silica NPs sizes - 80 nm and 1-3 microns) was evaluated. These results showed that cell viability decreased to 99%, 91 % and 32 %, compared to control cells after 6 hour exposure (Figure 4.5A). The viability further decreased to 86 %, 83% and 21 % after 12 hour exposure (Figure 4.5B), 86%, 80% and 19.7 % for 24 hour exposure (Figure 4.5C), 92%, 85 % and 18% for 48 hour exposure (Figure 4.5D) to medium and high concentration of dispersed colloidal silica NPs, respectively. The cell viability was found to be higher in case of A549 cells exposed to NPs for 72 hours (Figure 4.5E) compared to the 48 hour exposure group shown by 100%, 95% and 34% compared to control cells exposed to low, medium and high concentrations respectively. Even though the viability did not decrease significantly, the trends showed that the cell viability was lower in case of cells exposed to lower concentrations of the undispersed NPs. The cell viability improved as the concentration of the NPs increased and the cells were no longer affected by the undispersed particles at higher concentrations as compared to the lower concentrations. A reverse trend was observed for the dispersed NPs- as the concentration increased the cell viability decreased greatly compared to the control, proving the dose dependency of cellular toxicity due to dispersed colloidal silica NPs.

From the two way analysis of variance, the different exposure times and concentrations of the dispersed NPs were tested for statistical significance. The results showed that the exposure time had significant effect on the cell viability with a p value of

0.0009, showing that greater exposure times would cause decreased cell viability and toxicity to cells, except for the group exposed to 72 hours. The viability improved and observed to be similar with the group of 6 hour exposure. The concentration of dispersed NPs was always the dependent factor with a p value of less than 0.0001. It was further analyzed that concentration does not have same effect on all the exposure time points and the interaction was not significant (p value = 0.333).

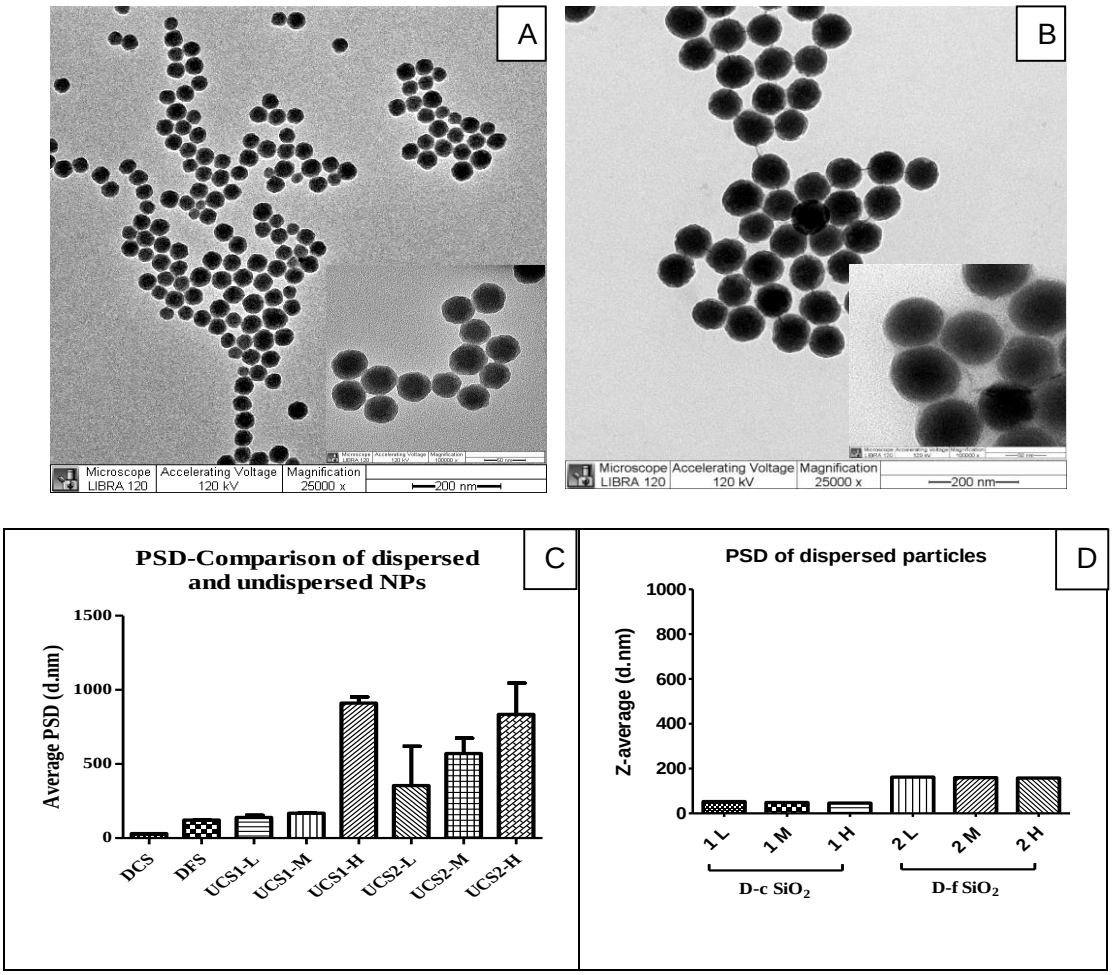

Figure 4.3. TEM Images of A) Dispersed and B) Undispersed Colloidal Silica NPs. PSD of CMP C) Dispersed and D) Undispersed NPs at Different Concentrations used in Cellular Analysis

IV.3.5 Exposure time and concentration dependence on cell viability of A549 cells exposed to fumed silica NPs and MPs

Cell viability of A549 cells after exposure to different concentrations of dispersed and undispersed (7 nm and 200 nm) fumed silica MPs and NPs was analyzed. It was observed that dispersed NPs were found to be toxic shown by decrease in cell viability (Figure 4.6). The cell viability decreased to 83%, 78% and 12.5 % after 6 hour exposure to low, medium and high concentration respectively (Figure 4.6A). The viability was found to be 81.6% , 77.4% and 8% after 12 hour exposure (Figure 4.6B), 83%, 83.7% and 11.43% for 24 hour exposure (Figure 4.6C), 84%, 78% and 10% after 48 hour exposure (Figure 4.6D)and 95%, 73% and 12.5 % after 72 hour exposure (Figure 4.6E) to low, medium and high concentration respectively. The undispersed fumed silica NPs of 7 nm diameter showed toxicity at lower concentrations with cell viability decreasing to 80%, 72.5%, 64%, 73% and 77 % after 6, 12, 24, 48 and 72 hours of exposure, respectively. The decrease in cell viability was not higher than that caused by dispersed NPs. The medium and higher concentrations of 7 nm particles did not significantly decrease the cell viability (not less than 88%). The fumed silica NPs of 200-300 nm showed slight cell viability decrease to 72% and 77.7 % at lower concentrations after 12 and 24 hour exposure, respectively. From cell viability analysis of both the undispersed particles it can be stated that the change is size does not show toxic effects at the higher concentrations. It was observed that with increasing concentrations the viability improved in case of undispersed fumed silica NPs whereas a reverse trend was observed for their dispersed counterparts. Three concentrations of both dispersed (S1) and undispersed colloidal silica NPs 2.303 mg/ml as high concentration,

0.2303 mg/ml as medium concentration and 0.02303 mg/ml as low concentration. PS 1 refers to 80 nm undispersed silica and PS 3 refers to 1-3 microns undispersed silica. From the two way analysis of variance using bonferroni post-tests to compare the replicates, it was observed that the dispersed fumed silica NPs did not show significant change on cell viability (p value of 0.93) where the time accounted for 0.1% of the total variance. There was no significant difference between the groups treated for different time points, showing the NPs has almost same effect independent of the exposure time. The concentration has a bigger effect than time with a p value of <0.0001.

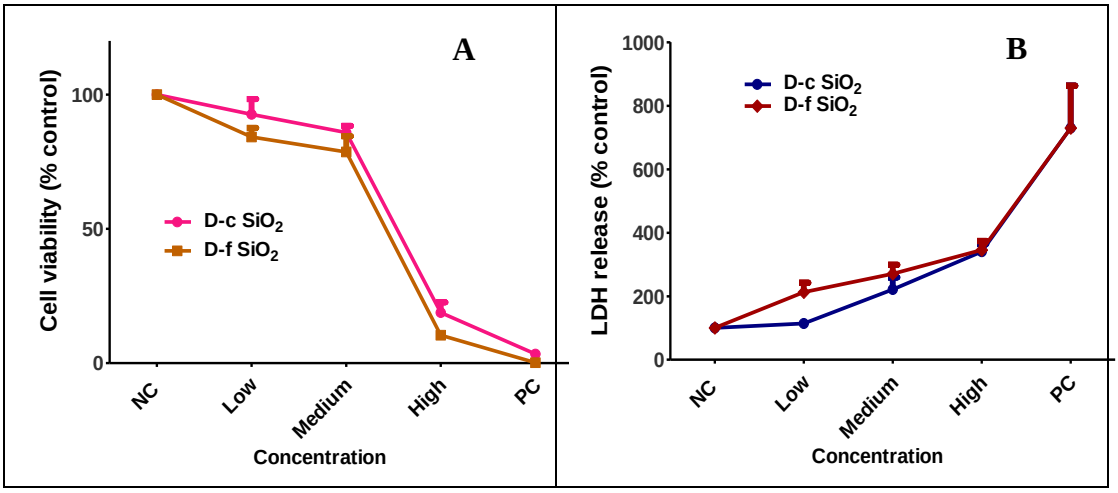

Figure 4.4. A) Cell Viability and B) Membrane Integrity of Cells Exposed to Low, Medium and High Concentrations of Dispersed Colloidal and Fumed Silica NPs

Figure 4.7 shows trends in cell viability with changing size, surface area, PSD and surface charge of colloidal and fumed silica NPs. It was observed that cell viability decreased with increasing surface area indicating that toxicity of colloidal and fumed silica NPs increases with increasing surface area. Further, it can also be inferred from the size

and PSD date, with increasing size and PSD cell viability increased, i.e. toxicity decreased with increasing size and PSD of colloidal and fumed silica NPs. In case of surface charge, there was no proper trend for colloidal silica but, cell viability increased with increasing surface charge. The results from surface area, size and PSD are in good agreement with those findings in literature. With increasing surface area, the reactivity of material increase and so does toxicity. However, with increasing size and PSD, the uptake of NPs by the cells will be limited and thus less toxicity.

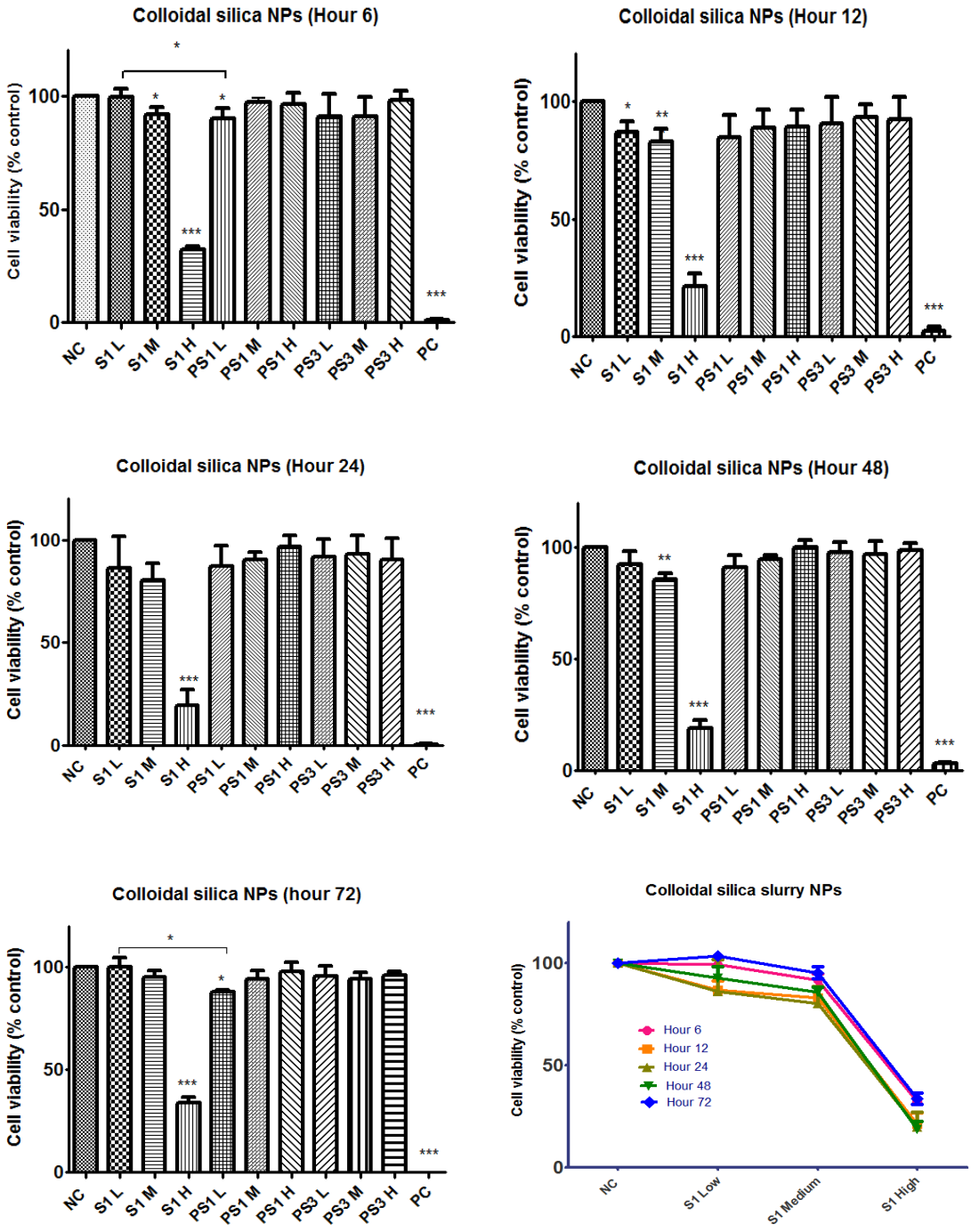

Figure 4.5. Cell Viability of A549 Cells after Exposure to Colloidal Silica NPs and MPs for 6 hours, 12 hours, 24 hours, 48 hours, 72 hours, and Trends of Concentration and Time Dependence on Cell Viability

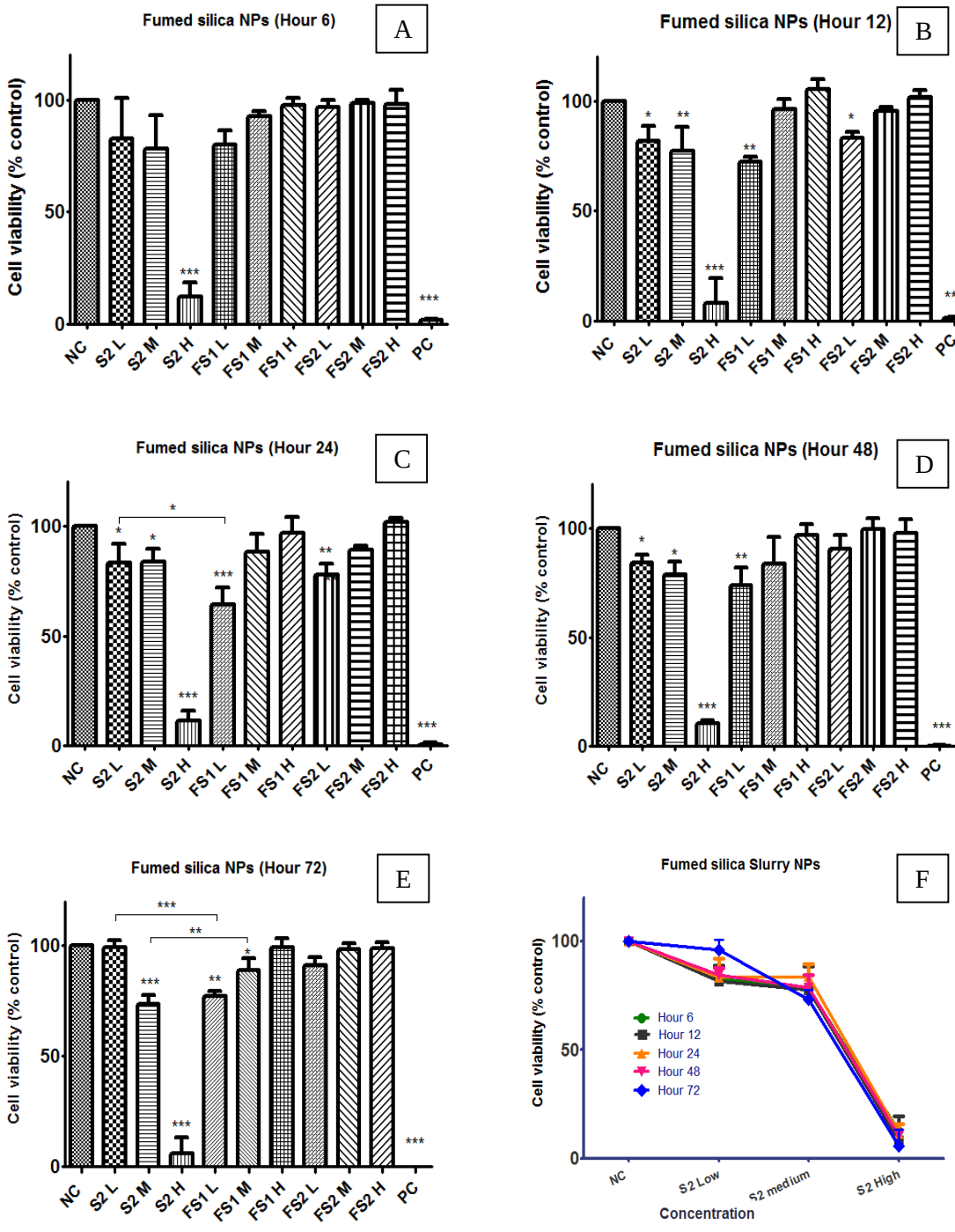

Figure 4.6. Cell Viability of A549 Cells after Exposure to Fumed Silica NPs and MPs for A) 6 hours, B) 12 hours, C) 24 hours, D) 48 hours, E) 72 hours, and F) Trends of Concentration and Time Dependence on Cell Viability

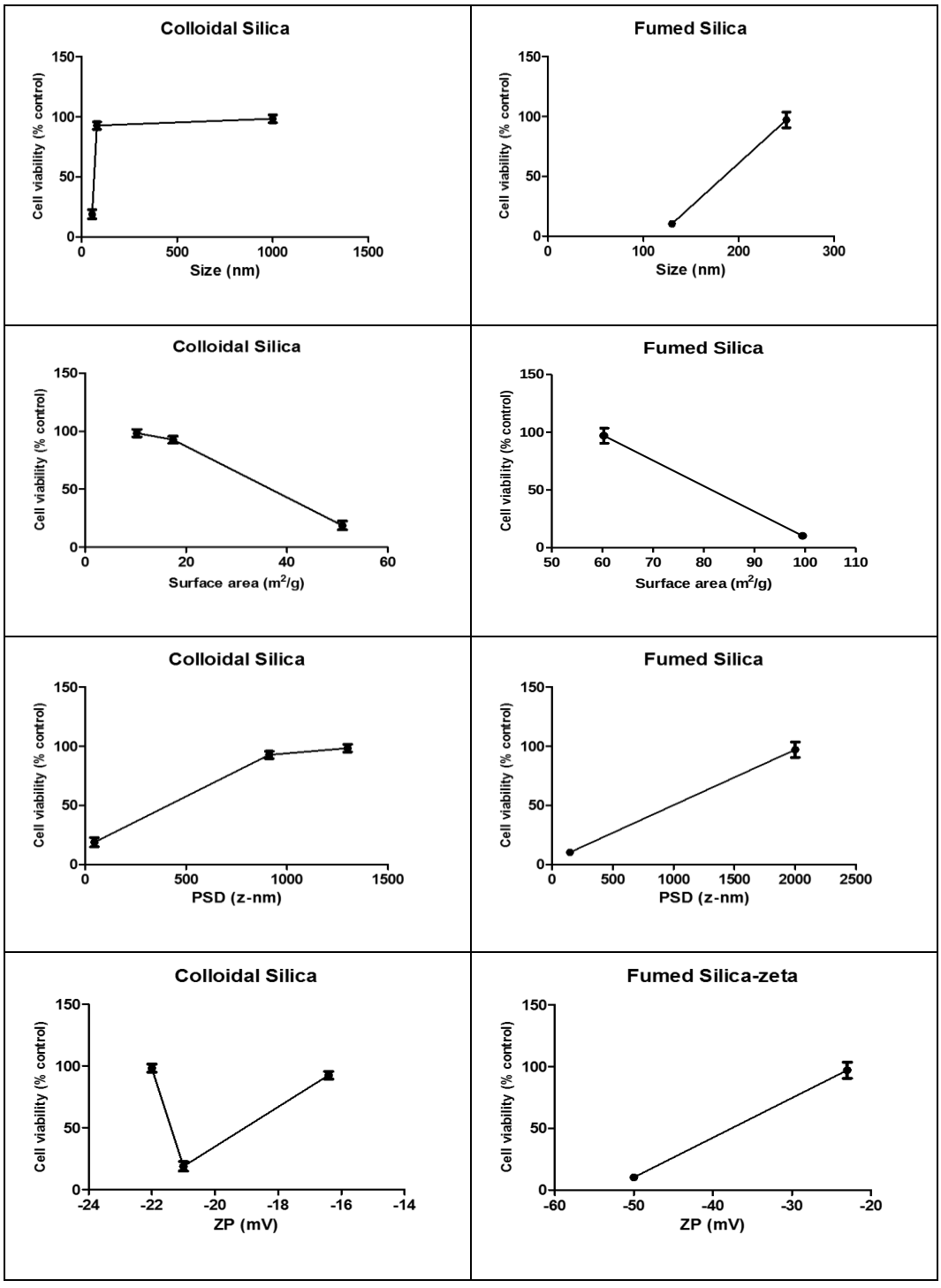

Figure 4.7. Trends of Cell Viability with Changing Physicochemical Properties (Size-column 1, Surface Area- column 2, PSD-column 3 and Surface Charge-column 4) of Colloidal (left column) and Fumed (right column) Silica NPs

IV.4 Discussion

Aggregation of NPs, which is mainly attributed to surface charge on NPs, is one of the major factors that is accounted for the observed differences in the properties and performance of NPs. ENs are often stabilized with charges on their surface via electrostatic repulsion to prevent aggregation to increase the surface area and therefore show highest possible activity. The negatively or positively charged NP surfaces make them highly reactive and receptive to cell surfaces due to their interaction with cations and anions as a part of cell cycle and functionality.. It was found that both positively and negatively charged NPs are responsible for mitochondrial membrane potential disruption suggesting that both charged ligands conjugated on NPs can lead to disorder in cell growth and functionality. Therefore, the NP surface properties needs to be examined with care to ascertain cellular activities.

The CMP NPs used in this study are stabilized by mechanical dispersion methods to form highly uniform dispersion and prevent agglomeration to attain uniform planarity and high MRR. The pH of the NP dispersion of colloidal silica and fumed silica used in this study are acidic and basic, respectively. The selected pH helps in maintaining a surface charge on the NPs and improve the stability by avoiding agglomeration by electrostatic repulsion and also to provide charge the surface for NPs and wafer surface interactions. Thus NPs in the dispersions may either be positively charged or negatively charged in solution, when they are exposed to cell cultures. The high dispersion and charged surfaces of disperseed NPs would have facilitated high reactivity of NPs with the cell surface and

increased interaction with the cell system facilitating their uptake causing adverse effects. The high dispersion of the NPs also ensures the small particle size by preventing agglomeration, showing that smaller the size of particles, higher toxicity and/or uptake by the cellular system, which was confirmed by TEM images and PSD measurements.

In our study, the undispersed particles showed a reverse trend from that observed with dispersed NPs, lower concentration showed slight toxicity to cells whereas at higher concentration, the cell viability was not affected, showing that the particles agglomerated which decreased the reactivity with cellular system, seen from DLS data. When the 48 hour exposure group was used to compare the effects of dispersed and undispersed particles, there was significant difference between the groups. Importantly, effects of undispersed NPs and MPs were similar, indicating that these particles behaved like MPs at higher concentration, which was shown by the DLS data. Another interesting trend observed from cell viability after exposure to fumed silica particles was the size dependent toxicity, where the 7 nm undispersed fumed silica NPs showed higher toxicity at lower concentration, when compared to the dispersed particles and 200 nm particles. But again at higher concentration, the undispersed particles did not show any effect on the cell viability and only the dispersed particles showed decreased cell viability. The differences observed in the cell viability of dispersed and undispersed NPs show that the agglomeration state is an important physicochemical property of the NPs for their toxicity assessment.

It was observed that dispersed fumed silica NPs were slightly toxic compared to dispersed colloidal silica NP, though the fumed silica particles are of larger size. This

suggests that the fumed silica can have high toxicity potential which is in agreement with other studies reported earlier. This also highlights the importance of difference in surface chemistry, reactivity, and/or NP morphology. Further fumed silica NPs were >100 nm, particles in the range of 100-500 nm can still behave as NPs exhibiting unique properties, suggesting the fact that there is no exact range for the nanoscale[67]. Another explanation to this could be the breakdown of the NP agglomerates, as the fumed silica NPs are synthesized from small primary sizes and the agglomerated chainlike structure is due to the flame synthesis method. It could be possible that these agglomerates are breaking down to smaller sized particles after exposure to cells, as reported in the case of colloidal silica agglomerates[68]. The cell membrane damage shown from the extracellular LDH release, is a feature of necrotic cell death, showing that increased concentration of colloidal and fumed silica causes increased number of cells to die of necrosis. These results are consistent with previously reported potential of membrane damage by amorphous silica NPs[69]. Further there was slight differences observed from the sequence of cell viability and membrane damage could result from the relative apoptotic and necrotic cell death[70].

With good agreement with the literature, the toxicity of both colloidal and fumed silica NPs increase with increasing surface area[18]. It was observed that colloidal NPs (both dispersed and undispered) did not show similar toxicity profiles. This could be attributed to aggregation in undispersed colloidal silica NPs which lead to a very small decrease in cell viability. As discussed in the above sections, similar trends were found with changing PSD of colloidal silica NPs. From this we can conclude that toxicity of colloidal and fumed

silica NPs not only depends on traditional variables such as time and dosage of exposure, but also on physicochemical characteristics of NPs such as size, surface area, PSD and surface charge.

CHAPTER V

UPTAKE AND TOXICITY OF CERIA NANOPARTICLES

V.1 Introduction

Ensuring the safety of Engineered Nanomaterials (ENs) is of enormous importance especially due to their unique physicochemical properties and applications. This is especially true in the case of dispersed ENs, which contains nanosized (< 100 nm) particles. At this time, there are no US regulations in place for specific ENs or products that contain ENs, with a few exceptions. While it is likely that most ENs will be safe, the uncertainty about their novel physiochemical properties and how they may relate and interact with environmental and biological systems has generated considerable concern[71]. In this study, we will try to address some of the concerns particularly in regards to cellular uptake and toxicity of ENs. For the purpose of this study, we have chosen well dispersed ceria NPs. The objective of this work is to (a) comprehensively characterize physicochemical properties of EN of ceria using established analytical and metrology techniques and (b) understand their behavior particularly, cellular uptake and toxic potential in relevant media and biological systems. The goals of this study are to understand the toxicity of ENs using biochemical and analytical/spectroscopic techniques.

Ceria NPs are used for CMP in semiconductor fabrication to achieve uniform planarity on wafer surfaces[12]. Along with usage in CMP, Ceria NPs have been found to be useful in

catalysts, solid oxide fuel cells, and as photolytic and thermolytic water splitting agent[72]. Ceria NPs have been found to be both reactive oxygen species (ROS) generating and inhibiting. This makes ceria NPs a suitable candidate as a therapeutic agent, if tailored with precise control. Even though ceria is considered a potential candidate for various application, bio implications of ceria are not completely understood. There are a few studies in the recent past showing discrepancies in the behavior of ceria which portray ceria as both toxicity inducing and inhibiting. Most of the studies report that regulation of ROS is the major mechanism by which ceria imparts either a positive or a negative effect in biological environment[73]. With the contradicting reports about bio-interactions, uptake and internalization of ceria NPs becomes important to understand. Most of the studies reported up to date on uptake and internalization of ceria NPs have been performed on functionalized ceria NPs, especially using fluorescent molecules[74]. It is believed that modifying the surface of a NP will alter its behavior, in this context its bio interactions. In this study, we will try to address some of these concerns related to bio interactions of ceria NPs considering an inhalational model (A549 cells) without surface modification.

V.2 Materials and Methods

V.2.1 Ceria NPs

The electrostatically stabilized, highly dispersed ceria NPs used in this study were obtained from Cabot Microelectronics. The dispersion is composed 1% ceria NPs with a particle size of 60-100 nm and the dispersion had an overall pH of 3-4. For the sake of comparison in the cell viability and membrane integrity studies, another set of undispersed ceria NPs in the nanometer and micrometer range with the dimensions of 50-105 nm and

1-2 μm, respectively, were used. These undispersed ceria NPs were purchased from Nanoamor, Houston, TX.

V.2.2 Characterization

The ceria NPs were comprehensively characterized using various microscopic and analytical techniques including TEM (Carl Zeiss Libra 120 Plus TEM Microscope), ICP-OES, Confocal Raman (Horiba Xplora Confocal Raman Microscope System), FT-IR (Varian 670 FTIR Spectrometer equipped with an ATR accessory), XRD (Agilent Technologies Oxford Gemini X-Ray Diffractometer using a Molybdenum source at a voltage of 50 mV and current of 30 mA), BET-surface area analysis (Nova Quantachrome 2200e BET surface area analyzer), DLS and Zeta potential measurements (Malvern Instruments ZEN3600 Zetasizer Nano-ZX). The slurries were dried to perform BET, XRD, and TEM. The ceria NP dispersion was dried as described in the previous section for XRD, BET and Confocal Raman.

V.2.3 Cell viability assay

A549 cells (adenocarcinomic human alveolar basal epithelial cells, ATCC® CCL-185™) were obtained from the American Type Culture Collection (Manassas, VA) and were cultured in F-12K media supplemented with 10% (v/v) FBS in a 37 °C incubator with 95% air and 5% CO2. The dye 3-(4,5-dimethylthiazol-2-yl)-2,5-diphenyltetrazolium bromide (MTT) was used to quantitatively evaluate the cell viability of A549 cells after exposure to the slurries. MTT is converted to purple formazan crystals by mitochondrial reductase enzymes that are present in viable cells. The amount of formazan produced is proportional to the number of cells and can be measured using a spectrophotometer. The

MTT assay kit was purchased from Sigma Aldrich. A549 cells were seeded in 96 well plates at a density 10,000 cells/cm^2. After seeding, the cells were incubated for 24 hours to allow time for attachment. The media was changed after 24 hours of incubation and the NP at concentrations of 0.52, 0.052 and 0.052 mg/mL were added. After 48 hours of incubation, the media was changed and then the cells were incubated for an additional 24 hours after which the cells were treated with MTT reagent and incubated for four hours. After four hours, purple formazan crystals were formed. The crystals were dissolved using the MTT solvent and the absorbance was measured at 570 nm. The absorbance was compared to the controls (positive-lysis buffer and negative-untreated cells) and one-way Anova test was performed to analyze the significance of the results with a confidence interval of 95%.

V.2.4 Membrane integrity assay

Cell culture conditions were as in the previous section. Lactate dehydrogenase (LDH) was used to evaluate the membrane integrity of A549 cells exposed ceria NPs. Lactate Dehydrogenase (LDH) is a stable cytoplasmic enzyme present in most cell types and leaks out of cells into the media if there is damage to the plasma membrane. LDH catalyses the oxidation of lactate to pyruvate through the reduction of nicotinamide adenine dinucleotide (NAD) to NADH. The activity of LDH is determined by measuring the absorbance at 490 nm to analyze the amount of LDH present in the cell culture media. The LDH assay kit was purchased from Sigma Aldrich. A549 cells were seeded in 96 well plates at a density 10,000 cells/cm^2. After seeding, the cells were incubated for 24 hours to allow time for attachment. The media was changed after 24 hours of incubation followed

by the addition of the NPs at concentrations mentioned in the previous section. After 48 hours of incubation, the assay was performed and the absorbance was collected at a wavelength of 490 nm. The absorbance was compared to the controls (positive-lysis buffer and negative-untreated cells) and one-way Anova test was performed to analyze the significance of the results with a confidence interval of 95%.

V.3 Results and Discussions

V.3.1 Characterization

Nitrogen adsorption-desorption isotherms were collected for the dried ceria NPs and surface area was calculated based on extension of Langmuir Theory. The surface area was calculated to be 16.979 m^2/g. Figure 5.1 shows TEM image of dried ceria NPs which indicate that the particle size of the NPs was in the range of 60-100 nm which is consistent with the size obtained from the manufacturer. The NPs in slurry form, as obtained by the manufacturer, were characterized by DLS, which indicated PSD of 145.3±2.6 d. nm when diluted 100x in water and 187.3±3.2 when diluted 100x in F12-K media, and zeta potential measurements, which indicated the charge to be 42.7±1.4. The XRD, Raman and ICP-OES analysis indicated the presence of the ceria NPs and DLS and TEM characterization confirmed the size of the NPs. Even though DLS measurements indicated bigger sized NPs, this could be due to dilution of NPs in media and water. In addition, ICP-OES data validated that the concentrations of the NPs were same as that provided by the manufacturer. The XRD data (Figure 5.2) of dried ceria NPs showed important peaks that are consistent with most ceria NPs which is consistent with literature and the FT-IR spectra (Figure 5.3) also confirmed the presence of ceria NPs by the peaks present between

550 and 700 cm^{-1} which are from the Ce-O bonds. The FT-IR spectra was obtained from the ceria NP dispersion and it indicated the presence of other functional groups like hydroxyl, huge peak at 3306 cm^{-1} and carbon double bond at 1648 cm^{-1}.

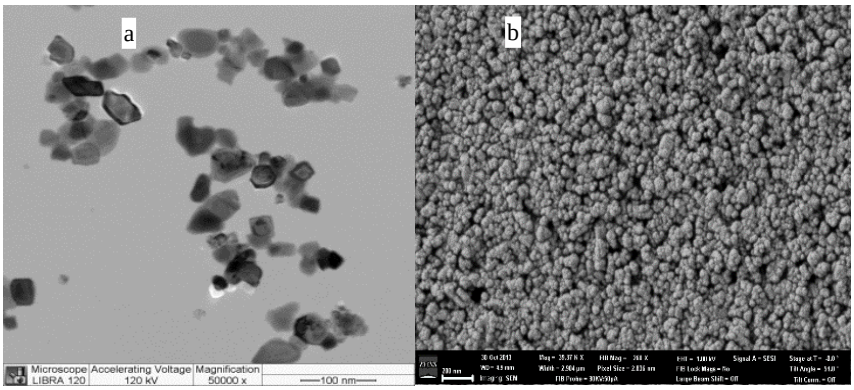

Figure 5.1. a) TEM and b) SEM Image of Ceria NPs

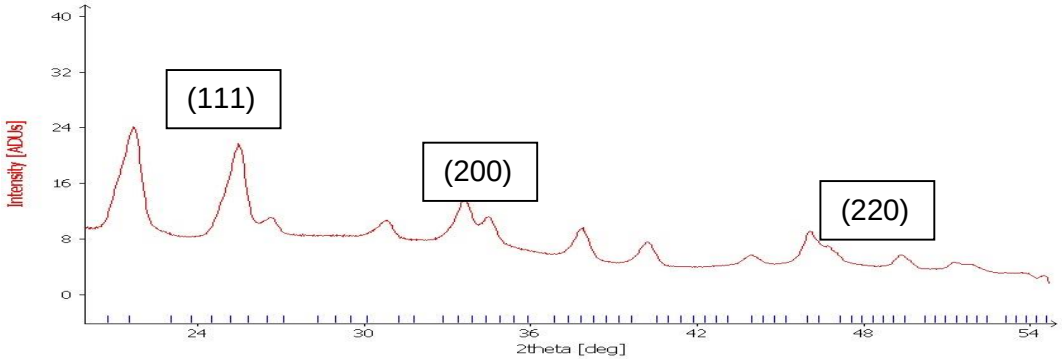

Figure 5.2. XRD Spectrum of Dried Ceria NPs

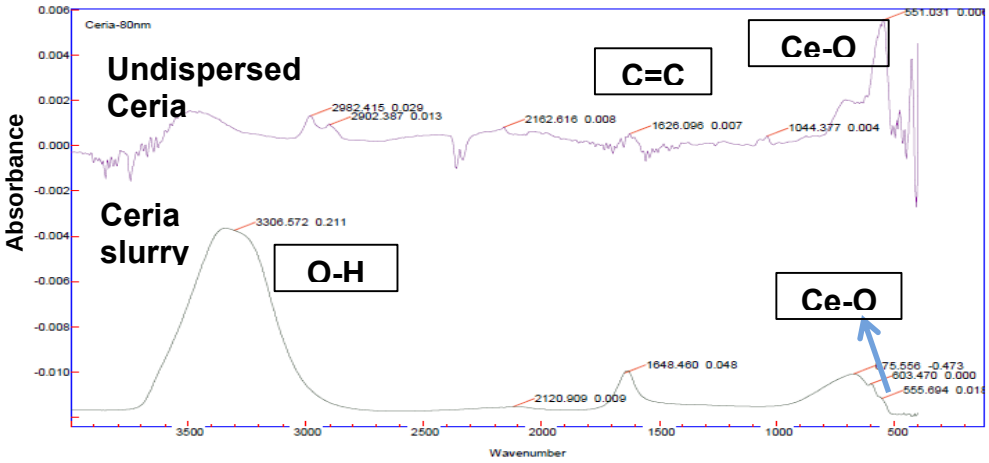

Figure 5.3. ATR FT-IR Spectral Comparison of Ceria NPs

V.3.2 Cellular toxicity

MTT (cell viability) and LDH (membrane integrity) assays were performed on A549 cells after exposing the cells to the ceria NPs for 48 hours. The assays were conducted in a 96 well plates and lysis buffer was used as the positive control. The MTT and LDH assays indicated that ceria NPs showed no toxic effects. The same experiments were carried out on undispersed ceria NPs (same properties as dispersed ceria used throughout the study) to study any differences in toxicity due to aggregation and significance of stable dispersion in the results collected. In figure 5.4 three concentrations of ceria Slurry NPs (S3) and pristine ceria Nanoparticles and microparticles with 0.52 mg/ml as high concentration, 0.052 mg/ml as medium concentration and 0.0052 mg/ml as low concentration. PC1 refers the pristine ceria (50-105 nm) and PC2 refers to pristine ceria (1-2 microns). For these experiments, the undispersed ceria NPs were dispersed in the culture media (F12k media) by sonication for 30 minutes to make the same concentration as the dispersed NPs. But,

they showed aggregation unlike the dispersed NPs which got dispersed uniformly even after diluting in media. Figure 5.5 shows the MTT and LDH results.

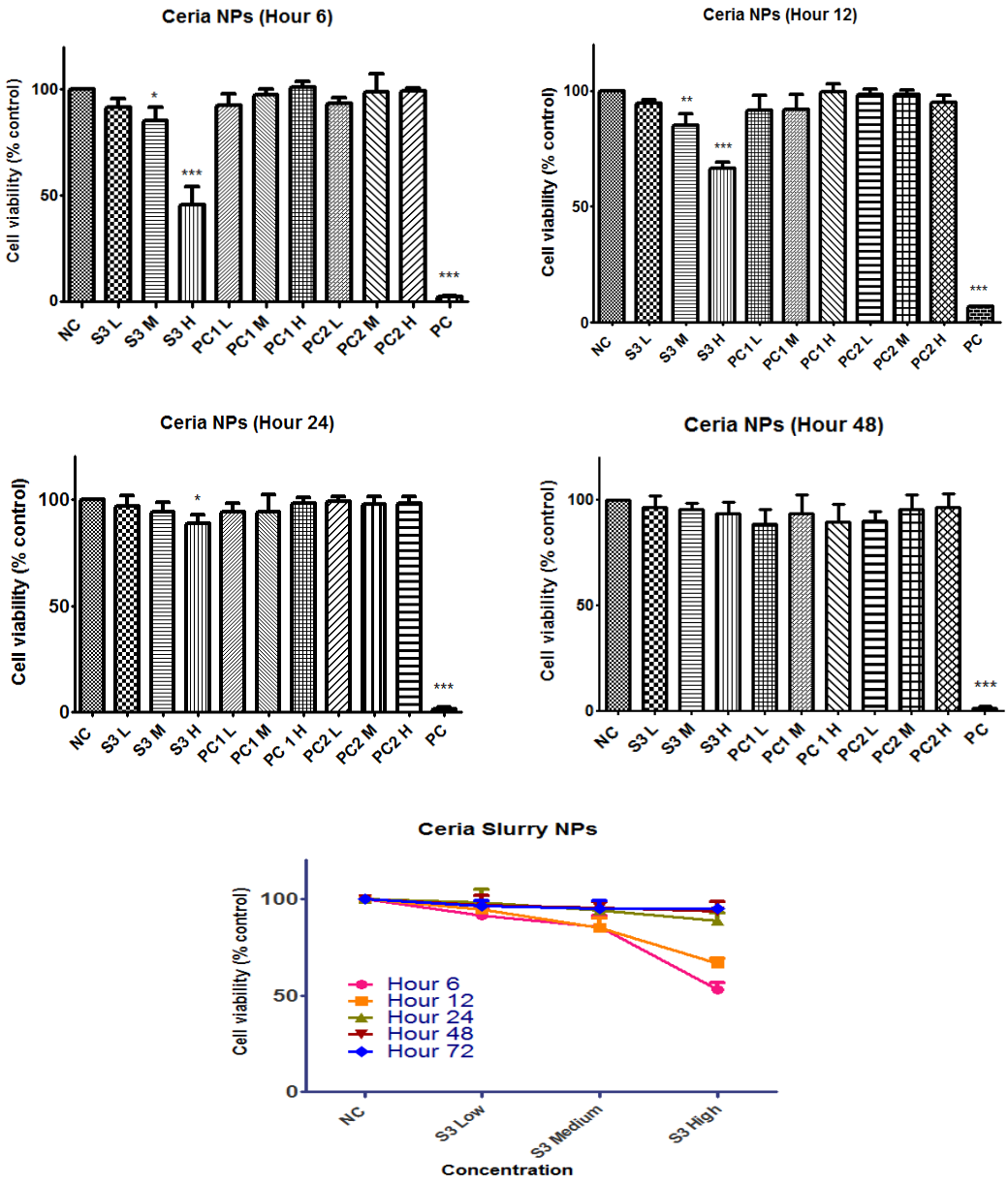

Figure 5.4. Cell Viability of A549 Cells Exposed to Ceria NPs and MPs for a) 6 hours, b) 12 hours, c) 24 hours and d) 48 hours

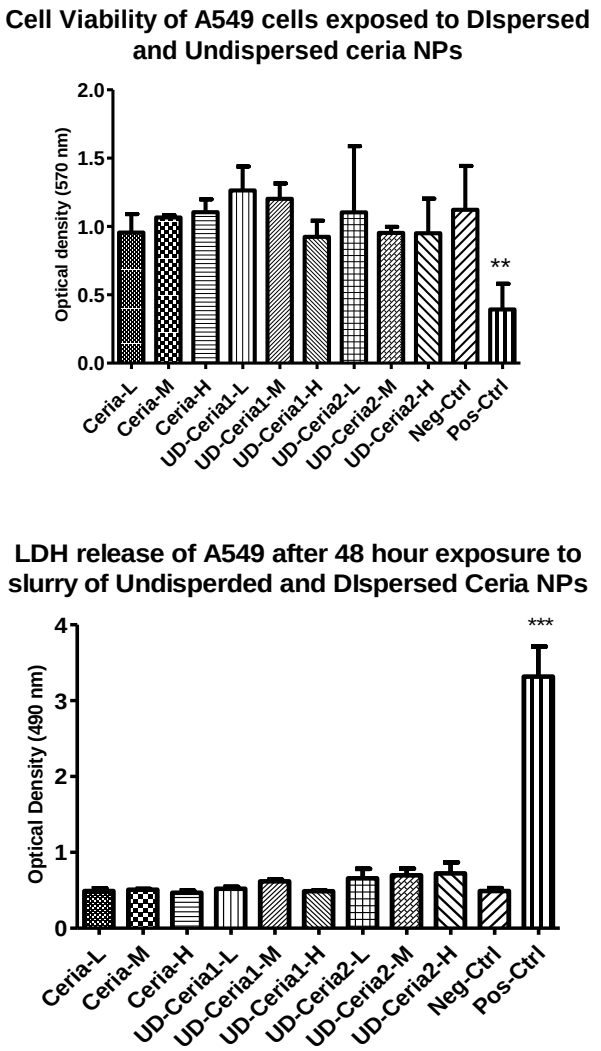

Figure 5.5. a) MTT and b) LDH Assays Performed on A549 Cells Exposed to Ceria NPs

(The optical density is a direct measure of cell viability. One-way ANOVA was performed on the data using a significance level of 0.05 (95% confidence intervals); *** - 99.9% confidence interval; ** - 99% confidence and * - 95% confidence interval.)

V.3.3 Cellular uptake and internalization

Cellular uptake and internalization were measured using ICP-OES and confocal Raman techniques. These techniques were selected to study the uptake without further surface modification. The highest concentration of 0.52 mg/mL was chosen to conduct all the uptake experiments with exposure time of 48 hours. In case of ICP-OES and confocal Raman studies, the cells were washed 10 times with PBS to eliminate NPs that are adhered on the cell membrane. For ICP-OES and Raman measurements, slurries dispersed in media were used for comparison. Figure 5.6 shows Confocal Raman spectral comparison of control cells, dried ceria NPs, undispersed ceria NPs and cells after exposure to ceria NPs for 48 hours. Ceria has a Raman peaks between 450 and 465 cm^{-1} Raman shift. It can be observed from the Raman spectra (Figure 5.6) that there is significant peak indicating clear evidence of ceria NPs uptake into the cells. It can be concluded from the spectra that the intensity of the peak goes down which could be due to the concentration of ceria NPs internalized in the cells. Also, there was a slight shift in the peak if we compare ceria NPs to dried slurry and to ceria NPs exposed to cells. This could be because of the presence of other constituents in case of the dried slurry and due to the cellular components in case of NPs in cells. Figure 5.7 shows the ICP-OES measurements after digesting slurry exposed cells, using standard protocols. It can be observed that there is significant cellular uptake of ceria NPs. As expected, there are no levels of ceria in control media and control cells and ceria dispersed in media at a concentration of 0.52 mg/mL showed highest concetration of ceria. This provides additional evidence to the Confocal Raman studies indicating clearly that ceria NPs were localized with in the cells.

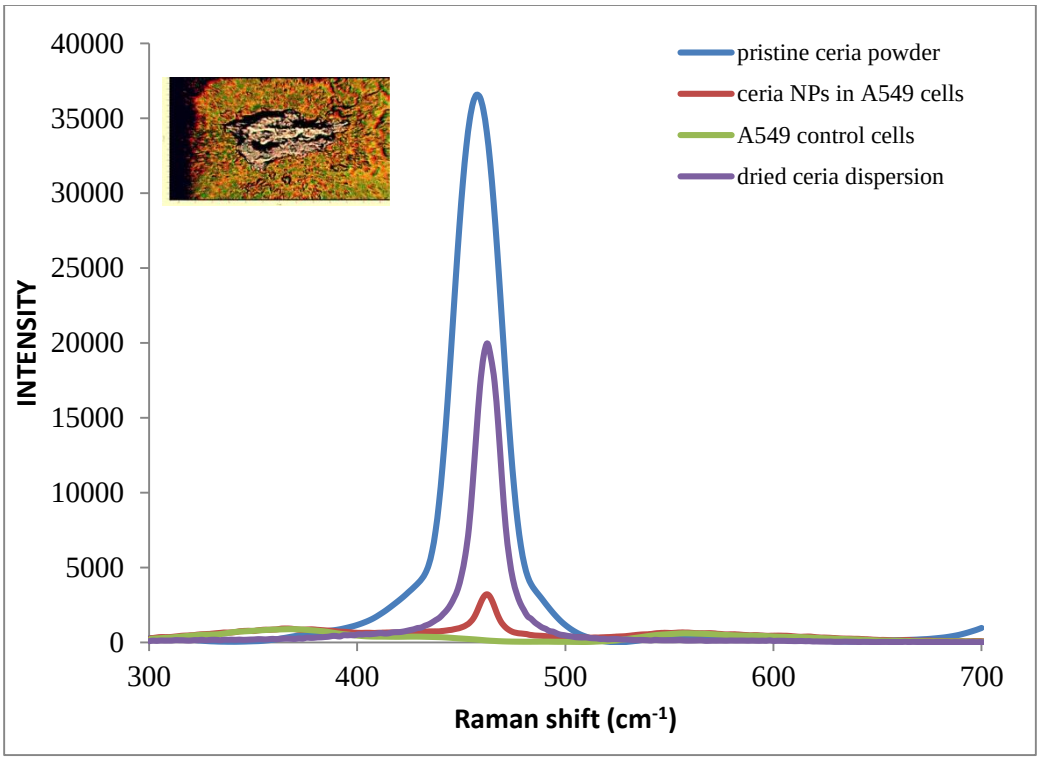

Figure 5.6. Confocal Raman Spectra Demonstrating the Uptake of Ceria NPs by A549 Cells

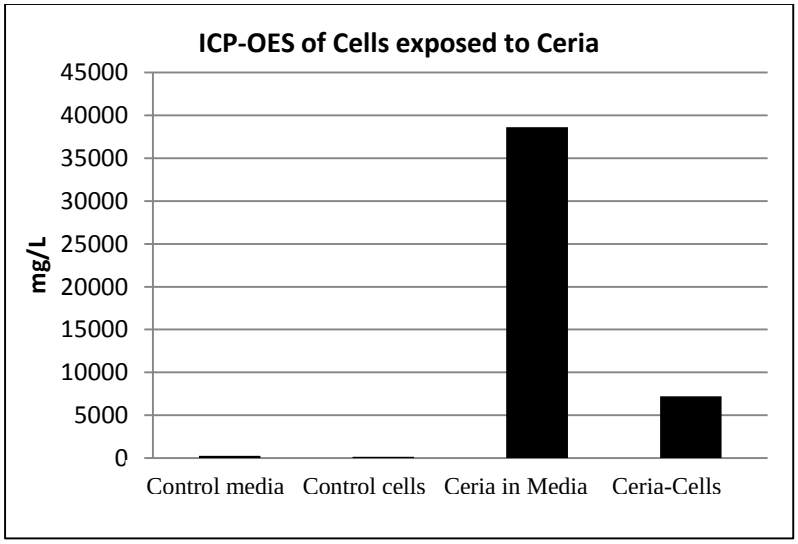

Figure 5.7. ICP-OES Data Demonstrating the Uptake of Ceria NPs by A549 Cells Performed after a Two Day Exposure Period

The hypothesis about cell death contradicts the toxicity data (MTT and LDH assays) which showed no toxic effects on the cells. Even though there is promising evidence, the mechanism by which the NPs exert an effect has to be further investigated along with the mechanism by which the NPs get internalized into the cells.

V.3.3.1 Nanoparticle internalization and distribution. Raman spectra of the ceria slurry nanoparticles and cells after exposure to ceria slurry nanoparticles is displayed in Figure 5.8, along with the control cells (not exposed to the nanoparticles) and Raman spectra of just the ceria slurry nanoparticles. The Raman spectra from the ceria slurry nanoparticles showed a single band around 455 cm^{-1}. The spectra observed in the cells also showed a single band at around 453 cm^{-1}. Confocal microscopy allows for the recording of Raman spectra in all three dimensions with an accuracy limited by the resolution of the device. The special mapping was performed in z-direction and XY planes, by assuming Z-plane to be close to the equatorial plane of the cell with an increment of 2.5 μm from -30 to 30 μm. The maximum intensity was observed at z = -2.5 and -5 μm. From the z scans, there is clear evidence of the nanoparticle internalization into the cells; further inhomogeneous distribution can be confirmed by the phonon band intensities (Figure 5.8). The red and light blue in Figure 5.8 represent the highest and lowest intensity respectively. Similar analysis was performed keeping the z plane constant and in different x and y spots on the cell as spot 0 chosen close to the nucleus of the cell (Figures 5.9 and 5.10). The varied intensities at different spots confirm the inhomogeneous distribution of ceria Nanoparticles in the cell. The maximum intensity was observed at a spot x= -10 μm and y= 5 μm (Figure 5.10) . There was low but ceria band seen at around the spot chosen

(around nucleus), this do not necessarily mean the entry of ceria nanoparticles into the nucleus as the ceria particles beneath or just above the nucleus can contribute to the Raman spectra. Variations were observed in the position of the ceria peak from 443 to 447 cm^{-1}, which may be due to the surface modification in the different regions of the cell or may be due to the nanoparticle interactions resulting in the disorder of the oxygen lattice, as mentioned. Similar variations were also seen in the z-planes.

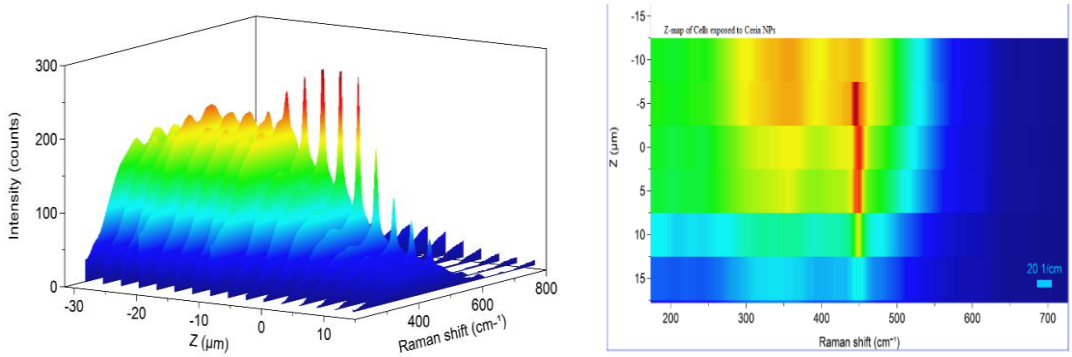

Figure 5.8. Raman Spectra of A549 Cells Exposed to Ceria NPs at Different Z-Planes

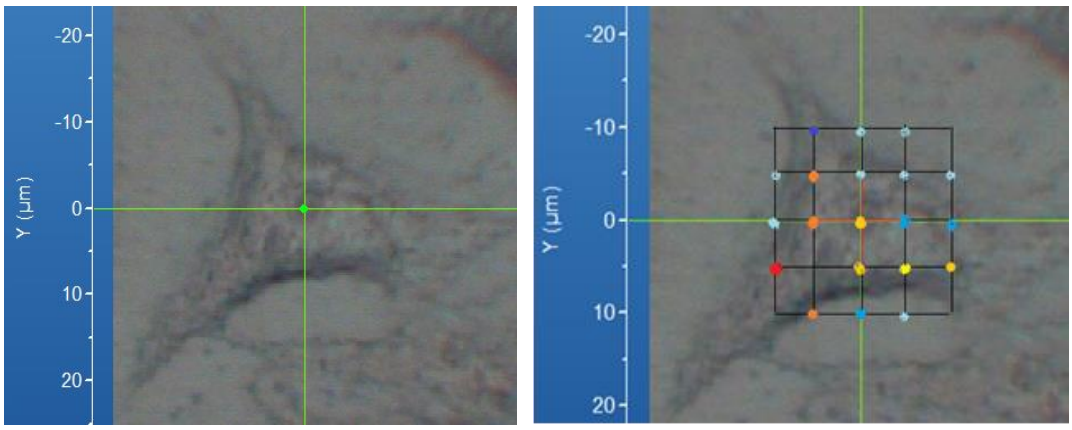

Figure 5.9. Cell Selected for the XY Map with Overlay of Intensities

Ceria nanoparticles showed decrease in cell viability for 6 and 12 hour exposure, but longer exposures did not affect the cell viability to a significant extent. Antioxidant/prooxidant property of ceria nanoparticles have been reported earlier. This may be due to the initial stress to the cells or the ceria nanoparticles can be dispersed for shorter times and then for longer times they settle down, which would have reduced the cellular interaction. It was observed from Raman analysis that after 24 hour of exposure the ceria particles were detected in cells, may be the initial cell loss is due to the period of uptake of nanoparticles. In agreement with Celardo et al, it has we observe that ceria nanoparticles exhibit antioxidant effect (cytoprotective response) to secondary oxidative stress stimulus, after cellular uptake[75]. The intrinsic mixed valence state of ceria (Ce^{3+} and Ce^{4+}) can also contribute to its antioxidant properties[75, 76]. Further shorter time periods and mechanism of uptake have to be investigated to understand the ceria nanoparticles. Ceria slurry nanoparticles showed increase in the DCF-fluorescence though ceria nanoparticles did not show toxicity at 24 hour and 48 hour exposure from both cell viability and membrane integrity analysis. Ceria nanoparticles have shown to produce spontaneous generation of ROS under abiotic conditions and also the intrinsic material property of ceria (Ce^{3+} and Ce^{4+}) could contribute to the oxidation of DCFH to DCF (fluorescence). Ceria nanoparticles shown internalization and inhomogeneous distribution in cells, observed from Raman spectra analysis.

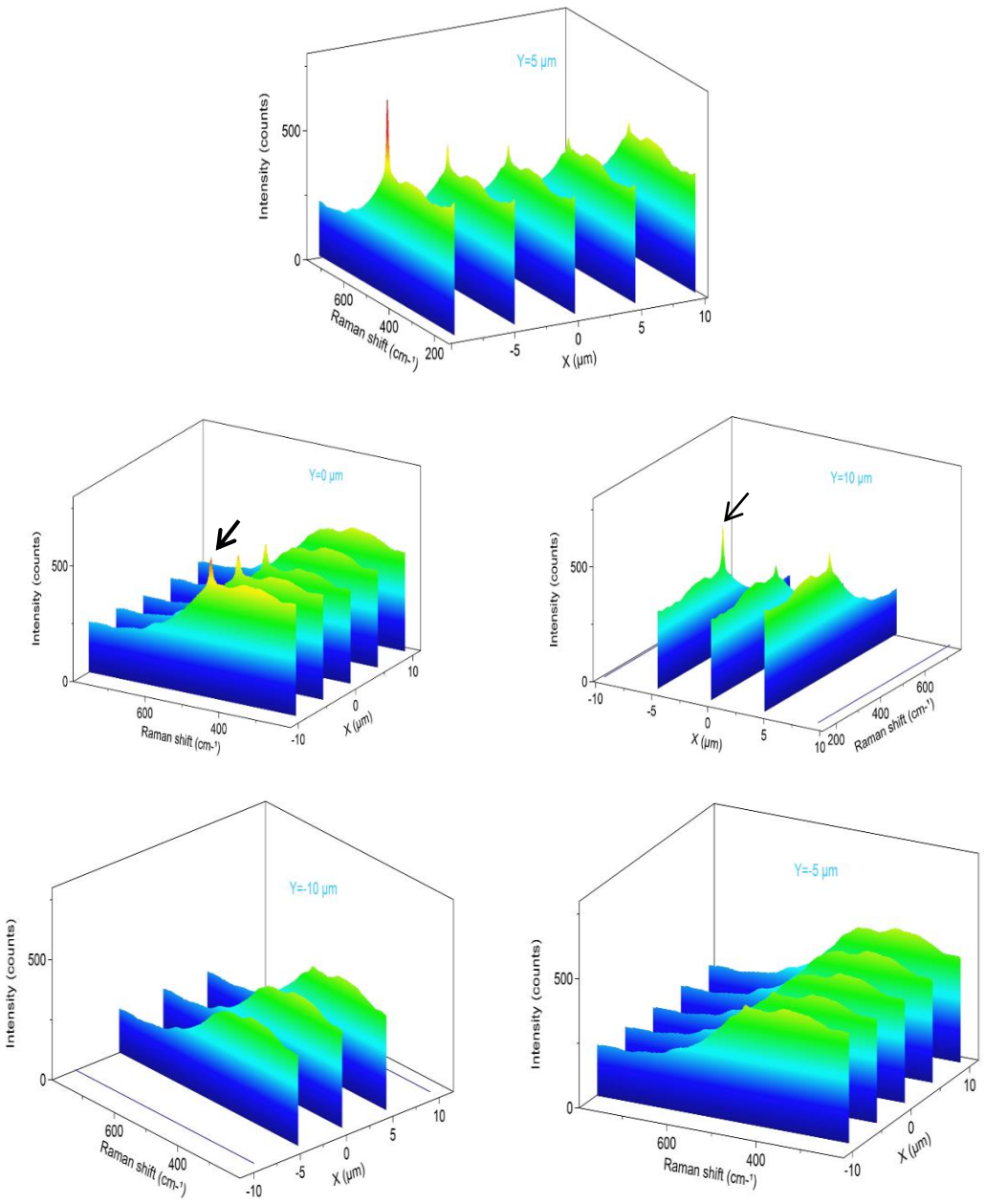

Figure 5.10. Raman Spectra of Cell Exposed to Ceria Slurry Nanoparticles taken at Different XY Spots

CHAPTER VI

ASSESSING THE CHANGES IN PHYSCICOCHEMICAL PROPERTIES AND CELLULAR TOXICITY OF PRE- AND POST-CMP SILICA SLURRY

VI.1 Introduction

Chemical Mechanical Planarization (CMP) is a key enabling technology for the semiconductor industry to achieve both local and global planarization on a variety of materials including dielectrics, semiconductors, metals, polymers, and composites[77]. One of the application of CMP is the elimination of topographic variations in order to achieve near-perfect layer planarity on many different length scales from nano- to meso- and micro-scales. Achieving near-perfect planarity is critical for semiconductor processes such as optical lithography, multi-level metallization and damascene technology[78]. CMP slurries typically consist of fine abrasives made of either alumina, ceria or silica nanoparticles (of sizes between 20-200 nm), along with oxidizing chemicals and various additives[12, 78]. In a typical CMP process, as the nanoparticle-based slurries are dispensed on a rotating wafer surface, a polishing pad is engaged in a polishing action to planarize the wafer surface. The interaction between the wafer surface, the pad, and the nanoparticles in the slurry provide mechanical removal, while the oxidizing chemistry facilitates the removal process. As stated earlier, the abrasive inorganic oxide nanoparticles are an important constituent for CMP process. These CMP nanoparticles constitute nearly 60% of the total $1 billion worldwide market for nanopowders in 2005[79]. In spite of such large-scale use of engineered

nanoparticles in the CMP process, little is known about the human workplace exposure on biological systems as well as on environmental fate, behavior and impact. In particular, colloidal silica nanoparticles (c-SNPs) formed by liquid phase by precipitating a Si precursor (e.g., Na2SiO3) is used widely in the CMP processes[80]. About 2.4 million metric tons of silica NPs was used in 2014 by the semiconductor industry[61]. Therefore, the goal of this study is to (a) characterize the physical and chemical properties of pristine CMP slurries (called henceforth as "pre-CMP slurries") made of colloidal silica nanoparticles (c-SNPs) and used CMP slurries/waste (called henceforth as "post-CMP slurries") and (b) investigate and compare *in vitro* cellular toxicology and uptake of pre-CMP and post-CMP slurries after exposure to human respiratory cell lines.

Although engineered nanoparticles are generally believed to be relatively innocuous, toxicity and cellular behavior assessments conducted thus far have varied widely depending on their physicochemical properties, dispersion state and assessment method. No comprehensive toxicity assessment have been reported thus far on the effect of nanoparticles in pristine and used CMP slurries on exposure to human lung cell lines. Studies conducted at semiconductor process development and fabrication facility have reported workplace residues of amorphous silica, ceria and alumina nanoparticles in the size range of 100-500 nm[64]. Furthermore, on-site wastewater treatment (WWT) systems are not designed to remove nanoparticles. Current literature indicate that SNPs, are typically not removed by conventional biological wastewater treatment processes. A recent study showed that because existing WWT systems have no size selectivity for nanoparticles, a high probability of these materials entered the municipal wastewater

streams[65]. In light of these significant unknowns in the use and fate of engineered nanoparticles, particularly for colloidal SNPs, we pursued a comprehensive study to assess the impact of CMP nanoparticles (both before and after CMP) on the respiratory biological system from inhalational exposure. This understanding of toxicity is critical in order to facilitate, in future design of environmentally benign nanoparticles. Furthermore, this study will also (a) correlate physiochemical properties to cellular toxicity and (b) identify the physicochemical factor responsible for adverse or benign effects of nanoparticles[10].

VI.2 Materials and Methods

VI.2.1 Silica slurry and characterization

The Klebosol 1501-50 colloidal silica slurry was purchased from Dow chemicals, MI. The concentration and size of NPs, and pH of the slurry are listed is Table 1. The slurries were characterized using a Carl Zeiss Auriga-BU FIB FESEM Microscope Scanning Electron Microscope for particle size, Carl Zeiss Libra 120 Plus Transmission Electron Microscope for morphology and size, Agilent Technologies Oxford Gemini X-Ray Diffractometer for crystallinity, Micromeritics ASAP 2020 surface area analyzer for surface area measurements, Malvern Instruments ZEN3600 Zetasizer Nano-ZX for particle size distribution and zeta potential, and Varian 670 Attenuated Total Reflectance Fourier Transform-Infrared Spectrophotometer for functional groups.

VI.2.2 Chemical mechanical planarization

CMP was performed on an IPEC Avanti 472 polisher. Silicon oxide (blanket) wafer was polished for 4 minutes using a Dow® IC1000™ perforated polishing pad with Carrier/platen speed of 60/30 rpm, down pressure of 2.0.psi, back pressure of 4.5 psi and

slurry rate of 200 ml/min with in-situ pad conditioning and continuous sweep. The slurries were collected at the pad for 0, 1, and 3 minute timepoints for post-CMP characterization and cytotoxicity analysis. A sample from the final pad rinse was also collected and analyzed. Collections were made by redirecting slurry excess from the edge of the pad using UHV aluminum foil into polypropylene centrifuge tubes.

VI.2.3 Cytotoxicity analysis and uptake

Both the pre- and post- CMP cellular studies were performed using 1, 100 and 10000 times dilution of slurry samples. This was done by taking into considering the fact that the CMP wastes are extensively diluted before being directed into waste water streams. All the cytotoxicity and cellular uptake experiments were conducted on A549 (adenocarcinomic human alveolar lung epithelial) cells at a seeding density of 10, 000 cells/cm^2. For cellular studies, MTT (3-(4, 5-dimethylthiazol-2-yl)-2, 5-diphenyltetrazolium bromide) reduction assay, a widely used method for assessing cell viability was used. For uptake studies, a quantitative spectroscopic method, Inductively Coupled Plasma-Optical Emission Spectroscopy was used. The slurries were dispersed in media before exposure to cells for both cytotoxicity and uptake studies by sonication for 30 mins. The highest concentrations were chosen for each NP for uptake studies.

VI.3 Results and Discussion

VI.3.1 Pre- and post-CMP slurry characterization

The slurries were comprehensively characterized using microscopic and analytical techniques to understand their physicochemical properties and to correlate these properties to the measured cytotoxicity and cellular uptake behavior. The pre- and post-CMP slurries

were dried before performing BET, XRD, SEM and TEM analysis. Figure 6.1A and 6.1B show the SEM, EDX and TEM images of pre-CMP colloidal silica NPs with particle size of around 50 nm. The inset in Figure 6.1A indicates the presence of silicon. The FT-IR spectra (Figure 6.1C) showed clear evidence for the presence of Si-O peak at ~1100 cm^{-1}, along with C=C and O-H stretching at ~1650 and ~3400 cm^{-1}, respectively. This may indicate the presence of possible organic molecules and aqueous and/or basic component such as hydroxide additives. The XRD spectrum (Figure 6.1D) indicated the amorphous structure of colloidal SNPs in the low-angle region. The post-CMP measurement of XRD, SEM and TEM did not show any significant change at the different CMP time-points.

The particle size distribution (PSD) and zeta potential of pre- and post-CMP slurries are listed in Table 6.1. It can be observed that the PSD did not change much before and after the CMP process. However, the zeta potential, which is an indication of NP stability in solution varied from -36.5 for pre-CMP slurry to -15.8 and 0.2 for 1 minute post-CMP and pad rinse (after 4 minutes) respectively. The high negative zeta potential indicates that colloidal silica NPs in the slurry are very well dispersed. However, this NP stability progressively decreases with the CMP process and with water dilution during CMP. The BET surface area calculated from Nitrogen adsorption-desorption isotherms obtained on dried SNPs in pre- and post-CMP slurries were measured to be 37.99 and 39.70 m^2/g for pre-CMP and post-CMP slurries (after 3 minutes) respectively. Figure 6.2 shows the FT-IR spectra of post-CMP slurry samples collected at 0, 1 and 3 minutes of polishing, and from pad rinse (after 4 minutes). These spectra were obtained from 1x dilution samples. It can be observed from the spectra that Si-O bond ~1100 cm^{-1} is significant at all time-points

of CMP, but not significant at pad rinse time-point. This could be due to minimal availability/concentration of silica NPs after pad rinsing with copious amount of water. In summary, the results obtained from pre- and post-CMP slurry characterization did not show any significant change in the physicochemical properties of SNPs used in the slurry, except an appreciable change in the zeta potential of post-CMP NP slurries.

Table 6.1. Particles Size Distribution (PSD) and Zeta Potential Measurements of Pre- and Post-CMP Slurries

Sample Name	***PSD (z-nm)***	***Zeta Potential (mV)***	***BET surface area (m^2/g)***
Pre CMP slurry	73.4±3.55	-36.75±0.5	37.99
Post CMP - 1 minute	74.11±2.4	-15.8±1.1	
Post CMP - 3 minute	71.89±0.7	-24.3±0.7	39.70
Post CMP – pad rinse	82.115±0.72	0.2±0.1	

VI.3.2 Cellular analysis of pre- and post-CMP slurries

MTT (cell viability) assay was performed after exposing A549 human lung epithelial cells to 1x, 100x and 10,000x dilution of pre- and post-CMP slurries for 48 hours. The studies were conducted in a 96-well plate format by adding 10 µL of the sample to a total volume of 150 µL in each well and lysis buffer was used as the positive control. Cell media was used as negative control in these experiments. It is important to note that cell viability and cellular toxicity are inversely related, a higher value of MTT means lower toxicity. The results of the MTT assay were plotted as percent negative control.

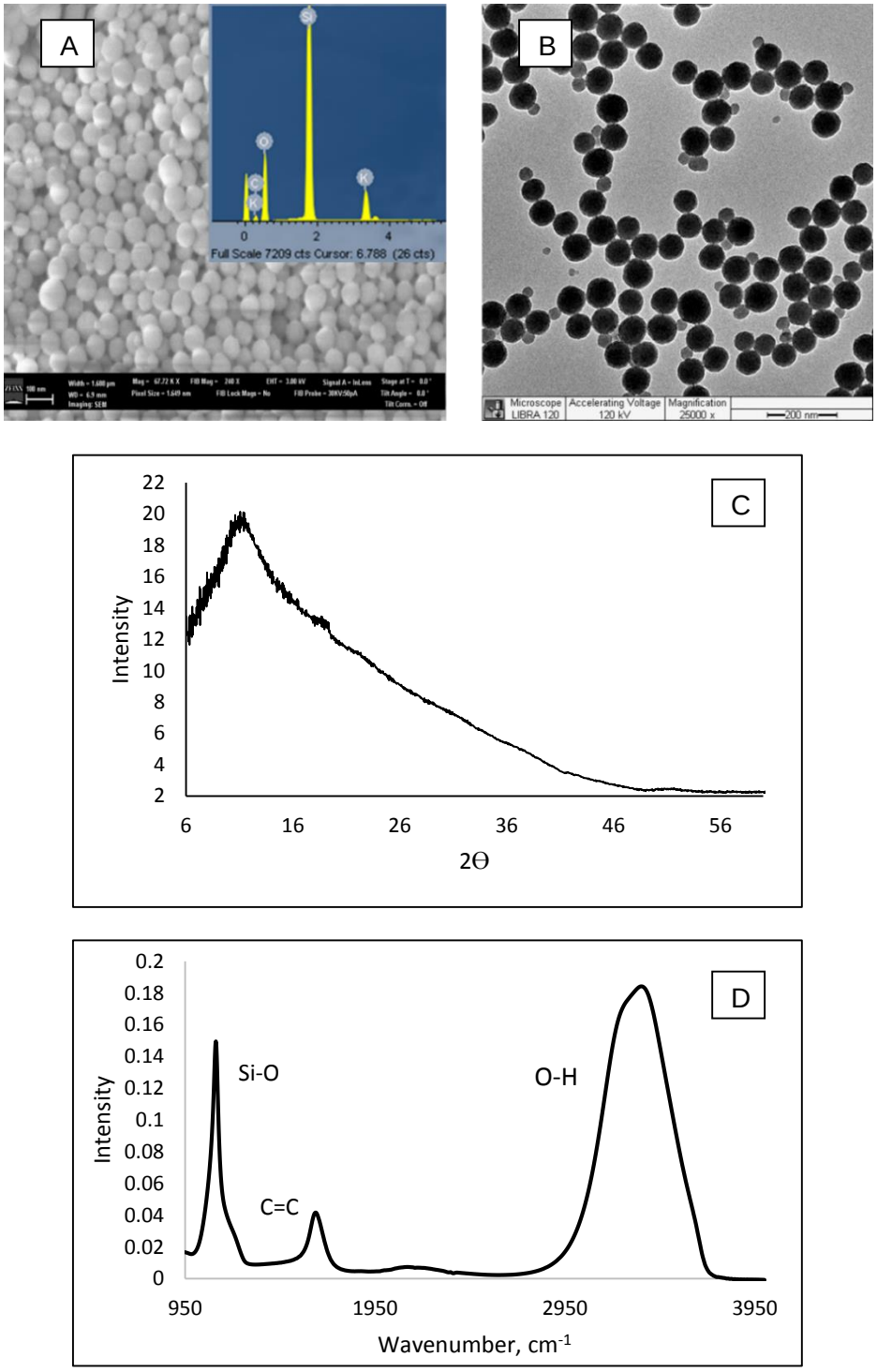

Figure 6.1. A) SEM Image (inset-EDX analysis), B) TEM image, C) FT-IR, and D) XRD Spectra of Colloidal Silica Slurry

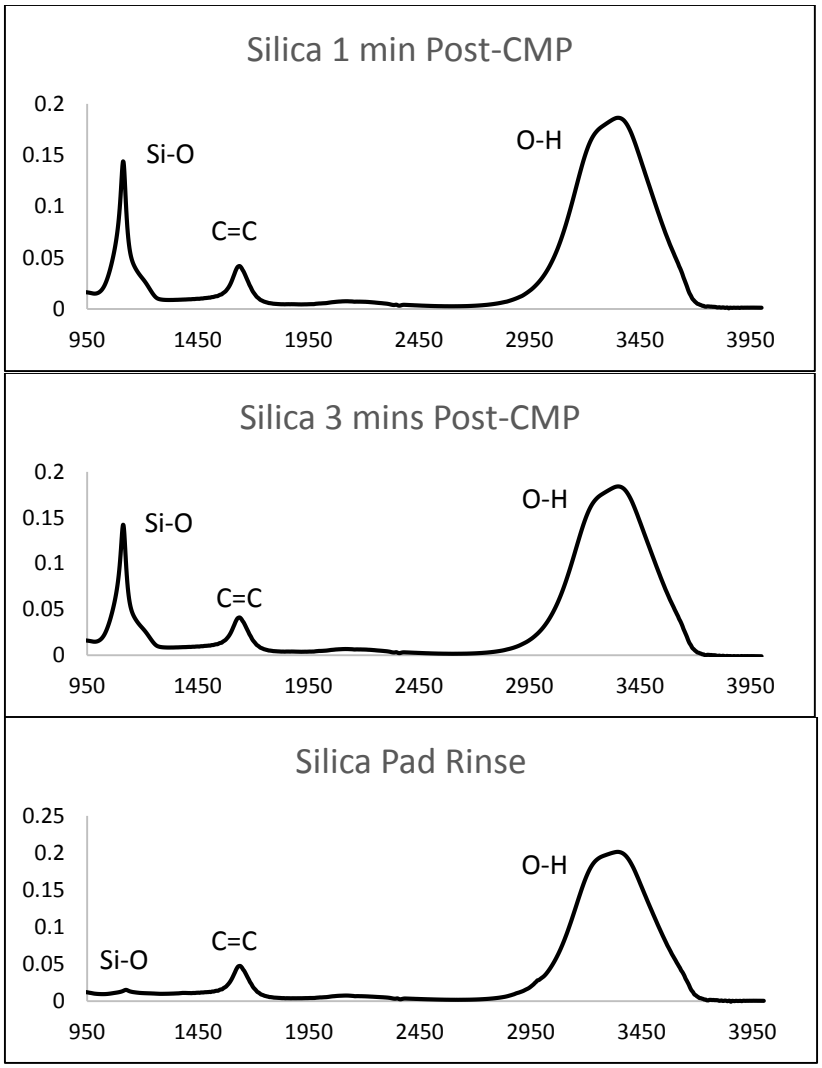

Figure 6.2. FT-IR Spectra of Post-CMP Wastes Collectrd after A) 0 mins, B) 1 min, C) 3-4 mins, and D) Pad Rinse after Polishing

Figure 6.3 shows the MTT assay which indicates that all the silica nanoparticle-based pre- and post-CMP slurries showed some toxicity at 1x dilution, however at 100x and 10,000x dilutions, both pre- and post-slurries showed minimal to no toxicity at all. Samples from pad rinse step (after 4 minutes of CMP) showed absolutely no toxicity for all the dilutions tested. This study further illustrates the importance of serial dilution and/or

waste treatment in minimizing or eliminating cellular toxicity. This is in agreement with our previous studies, where we showed that concentrated silica NPs and not the other components in the slurry are responsible for toxicity[81].

So, if the concentration of silica NPs in the slurries is reduced by serial dilution (at least by 100x), the effect of cellular toxicity can accordingly be minimized or eliminated. The high cellular toxicity observed at 1x dilution may be due to the high solid content in slurry or may be due to the highly basic nature (pH 10.8) of the slurry. However, with the serial dilution, the pH is close to the physiological pH (or cell media pH of 7.8). This effect is validated by the observance of minimal or low toxicity in case of A549 cells exposed to 100x and 10,000x dilutions of pre- and post-CMP slurries. In summary, from the cellular viability studies, it can concluded that no significant difference in cellular toxicity was observed on exposure to pre- and post-CMP slurries after serial dilution.

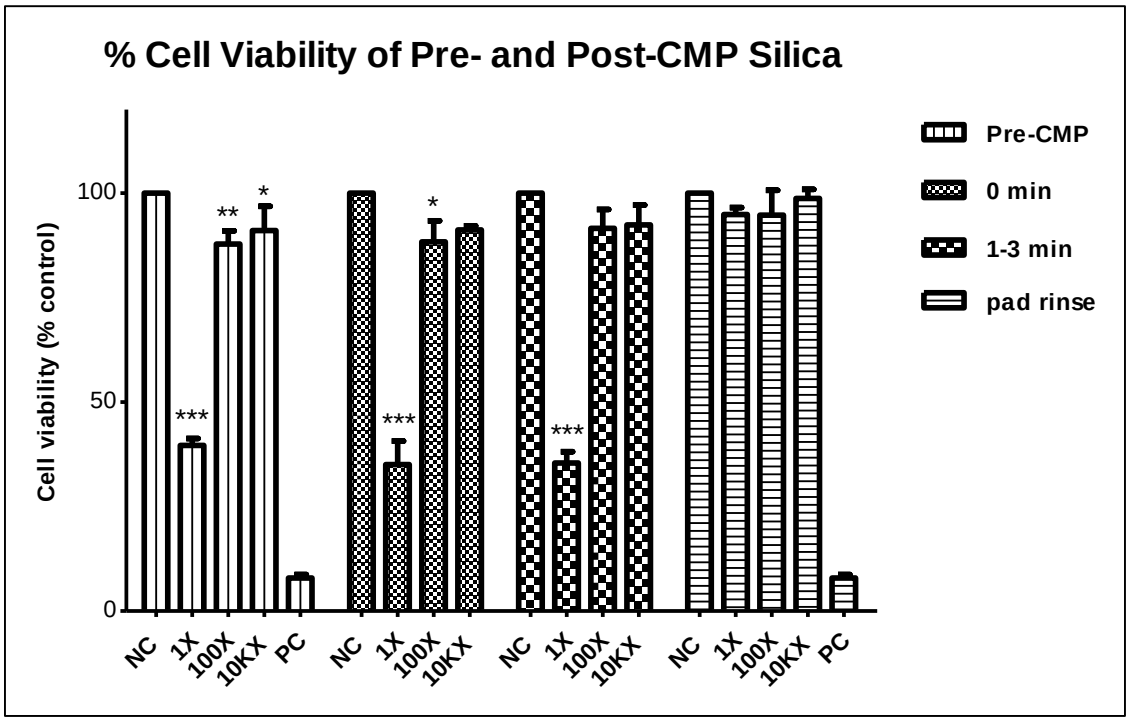

Figure 6.3. Cell Viability Analysis of A549 Cells Exposed to Pre- and Post-CMP Slurries

In Figure 6.3, NC stands for negative control (untreated cells); PC stands for positive control (lysis buffer); 1X- slurry used as is; 100X- slurry diluted 100 times with media; 10KX- slurry diluted 10, 000 times with media. One-way ANOVA was performed on the data using a significance level of 0.05 (95% confidence intervals); *** - highly significant.

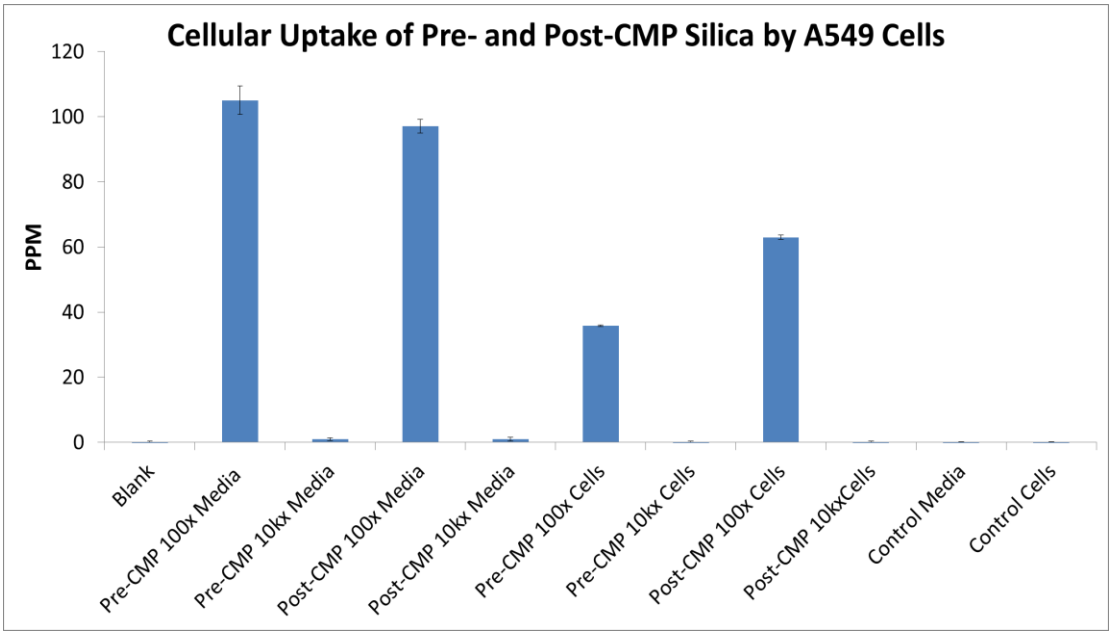

Figure 6.4. ICP-OES Analysis of Uptake of Pre- and Post-CMP Colloidal Silica Slurries by A549 Cells

Control media- fresh media; Control cells- cells not exposed to slurries; 100X- slurry diluted 100 times with media; 10KX- slurry diluted 10, 000 times with media.

VI.3.3 Uptake of pre- and post-CMP slurries

Cellular uptake was assessed by using ICP-OES. For cellular uptake studies, only the 100x and 10000x dilutions of pre- and post-CMP (at 3 time-point) slurries were studied. After exposing A549 cells to the pre- and post-CMP slurries, the cells were washed 10 times with PBS to wash away any NPs that are loosely bound to the cell membrane and/or floating in the media. Figure 6.4 shows the ICP-OES measurements after cell digestion for 3 hours at 90 ^{0}C in concentrated mixture of sulfuric and nitric acid, followed by 4x dilution to 4 mL sample size. It can be observed that the 100x dilution showed detectable levels of silicon in the spectra, while no silicon was observed at 10,000x dilution. The blank media

and cell controls also did not show any traces of background silicon. The concentration of silicon (from silica NPs) was found to be slightly higher in pre-CMP/polish slurry compared to post-CMP/polish slurry. On the other hand, the concentration of silicon was observed to be higher for cells exposed to post-CMP/polish slurry when compared to cells exposed to pre-CMP/polish slurry. It is interesting to note that even though MTT/cell viability studies did not show any difference in silica NP toxicity for pre- and post-CMP slurries, the cellular uptake studies indicated that post-CMP slurries have higher NP uptake concentration compared to pre-CMP slurries. This difference cellular uptake mechanism could be due to the differences in the zeta potential of pre-CMP slurry (~-36) and post-CMP slurry (~-24) after 3 minute of polish.

VI.4 Conclusion

It can be concluded that no significant changes in the physicochemical properties of colloidal silica NPs based slurries were observed before and after the CMP process, except for zeta-potential which decreased in the case of post-CMP slurries. The cellular toxicity analysis on A549 cells also did not show any significant difference between pre- and post-CMP slurries at the chosen time-points of polishing. It was also observed that minimal to no toxicity was exhibited when the slurries are diluted either 100x or 10000x. Lastly, the cellular uptake studies showed significant differences in pre- and post-CMP slurries when exposed to A549 cells. In future, we will investigate more complex and variable polishing conditions and time-points on the physicochemical properties of NPs in pre- and post-CMP slurry.

CHAPTER VII

NONINVASIVE EVALUATION OF CARDIAC REPOLARIZATION IN CD-1 MICE EXPOSED TO SWCNTS AND CERIA NANOPARTICLES VIA INTRATRACHEAL INSTLLATION

VII.1 Introduction

The unique physicochemical properties of carbon and metallic nanoparticles (NPs) such as small size, large surface area and the ability to be easily customized make them suitable candidates for various applications in fields such as the medical industry, semiconductor fabrication, transportation, aerospace, textile production, waste water treatment, agriculture, and many more under investigation[5]. According to the 2013 International Technology Roadmap for Semiconductors (ITRS), a number of engineered nanomaterials (ENs) in the form of NPs such as silica, ceria and alumina, nanotubes (multi-walled and single-walled carbon nanotubes), nanowires (gallium-arsenide nanowires), and thin sheets (graphene) are slated for introduction in front-end processing, interconnect, lithography, assembly and packaging from now through 2028[11]. However, the small size, large surface area and chemical reactivity of these nanostructures comprise a variety of essential environmental hazards.

Recent experimental studies demonstrated that just a moderate pulmonary exposure to carbon nanotubes may trigger oxidative vascular damage which, in turn, may significantly accelerate the formation of atherosclerosis and atherosclerotic plaques[13]. It was also reported that acute exposure to ceria nanoparticles via inhalation

may lead to cytotoxicity through oxidative stress response and ultimately lead to chronic inflammatory response with overloaded alveolar macrophages and neutrophils[14]. Although these findings conclusively demonstrated the importance of biochemical and immunological markers for identifying nanoparticle-induced oxidative stress and vascular damage, the association of such exposure with noninvasive electrophysiological factors is not understood. Even if monitoring of the cardiovascular system using electrophysiological measurements is one of the most robust biomedical tools, it is currently not adapted for applications in the environmental studies. The development of non-invasive electrographic predictors of toxic effects on the human cardiovascular system is of a critical importance for public health and warrants aggressive exploratory research. Moreover, various studies have reported that both carbon nanotubes (CNTs) and ceria nanoparticles have demonstrated both pro- and anti-oxidative stress responses, thus making CNTs and ceria nanoparticles ideal candidates to study nanoparticle-related cardiotoxicity. The objective of the work is to study the effect of CNTs and ceria NPs on cardiac response, monitored non-invasively, in mice subjected to exposure via intra-tracheal instillation.

We employ the **reserve of refractoriness** ($\boldsymbol{RoR}$**)** as a quantitative measure of stability for the acquired signals[82]. The analytically solvable, two-variable Chernyak-Starobin-Cohen (CSC)[83] model for electrical excitation of propagation in cardiac tissue allows one to compute the proximity of a given waveform to unstable regimes using only the QT and RR time intervals measured experimentally. The resulting measure of stability of propagating excitation known as the RoR, can be computed as discussed below. For

each propagating excitation, there exists a critical value of the recovery current v_r^{crit}. If the recovery current cannot decrease below this value before the next excitation is initiated, stable propagation is not possible, and this one-dimensional mathematical instability corresponds to complex disruptions in the electrical activity on the two-dimensional cardiac surface. The CSC model parameters may be found from fitting computed QT and RR intervals to the values obtained from measured ECG signals, allowing one to extract a prediction for v_r^{crit} as well as the actual minimum value attained by the recovery current, v_{min} (with $v_{min} < v_r^{crit}$ for stable propagation). The normalized difference between the critical value and the actual minimum constitutes the RoR. Previously, the RoR has been applied to data collected from humans[82]. In this study, we will focus our attention on otherwise healthy mice exposed to carbon nanotubes and ceria nanoparticles.

VII.1.1 CSC model to measure ROR

RoR is calculated from a pair of QT and RR interval measurements acquired form an ECG signal. The two-variable CSC model for propagation of electrical excitation pulses[83] is given by Eqs. (1).

$$\frac{\partial u}{\partial t} = \frac{\partial^2 u}{\partial t^2} - i(u, v)$$
$$\frac{\partial v}{\partial t} = \varepsilon(\zeta u + v_r - v)$$
$$i(u, v) = \begin{cases} \lambda u & (u < v) \\ u - 1 & (u \geq v) \end{cases} \qquad (1)$$

Here, u corresponds to dimensionless cellular transmembrane potential and v is the dimensionless recovery current. The singular limit of Eqs. (1) corresponds to rectangular pulses for which the variable u abruptly shifts between its maximum and minimum values, as depicted in figure 7.1. Within this limit, one may analytically obtain expressions for the dimensionless RR and QT intervals in terms of system parameters through a simple integration of Eqs.(1), obtaining:

$$QT = \frac{1}{\varepsilon}\ln\frac{\zeta + v_r - v_{min}}{\zeta + v_r - 1}$$

$$RR - QT = \frac{1}{\varepsilon}\ln\frac{1 - v_r}{v_{min} - v_r}$$

We work in a regime where $\zeta = 1.04$, $\lambda = 0.4$ may be fixed according to Idriss et al, 2012[82]. This leaves ε, v_{min} and v_r as fitting parameters. Applying an optimization procedure within the singular limit has demonstrated a stiffness in the parameter v_r, so we fix $v_r = 0.04$ for all mice. Additionally, it should be noted that a global shift in v_r acts as a compression or dilation of the overall scale in observed RoR values. The results of this analysis are essentially unchanged as v_r is varied over a range 0.01-0.05. With only two unknowns in the system Eqs. (2), ε and v_{min} may be obtained by solving Eqs. (2) for each pair of QT and RR values using a numerical root-finding procedure. The procedure of fitting is thus reduced to the solution of a two-variable algebraic system. To convert the dimensionless RR and QT predictions, we multiply by the ratio of membrane capacitance

to sodium conductance $\frac{c_m}{\sigma_{Na}} \approx$ 1ms, so that the dimensionless predictions are equivalent to measurements in milliseconds.

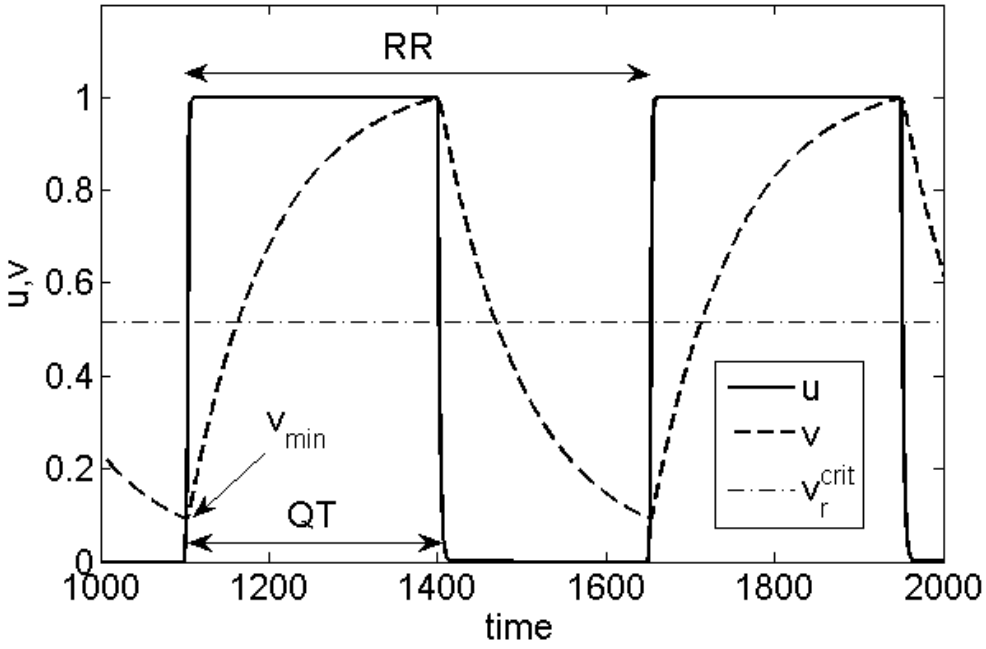

Figure 7.1. Simulated Electrical Excitations within the CSC Model in the Singular Limit

The variable u corresponds to membrane potential. As the pulses become more narrowly separated, the minimum value attained by the recovery current v rises. A critical value v_r^{crit} exists for each set of parameters such that $v_{min} > v_r^{crit}$ corresponds to propagation instabilities. The RoR uses QT and RR interval measurements to assess vulnerability by computing the normalized difference between v_r^{crit} and v_{min} using QT and RR intervals as inputs.

Armed with all system parameters, one may obtain the critical recovery current by applying the methods of Chernyak et al[83] to obtain the value of v_r for which wave propagation speed c is maximized,

$$v_r = \frac{\varepsilon(1-\zeta) + k_1^2(c) - \lambda}{\varepsilon + k_1^2(c) - \lambda} \cdot \frac{k_2(c)}{k_2(c) - k_1(c)}$$

$$k_1(c) = -\frac{c}{2} - \sqrt{\frac{c^2}{4} + \lambda}$$

$$k_2(c) = -\frac{c}{2} + \sqrt{\frac{c^2}{4} + 1}$$

The RoR is defined as the normalized difference between the actual minimum in recovery current v_{min} and this critical value v_r^{crit}.

VII.2 Methods and Materials

VII.2.1 Animals

A total of 30 female CD-1 mice 6-8 weeks of age (23.8±2g) were purchased from Charles River Laboratories (Raleigh, NC). All mice were fed Purina 5001 – standard rodent chow – and provided water ad libitum throughout the study, and were weighed daily on an Arbor 1605 electronic balance. Mice were maintained in the laboratory animal research unit of North Carolina Agricultural and Technical State University and used after the IACUC approval.

VII.2.2 Nanoparticles

VII.2.2.1 Preparation of SWCNTs dispersion. SWCNTs with 1-3 nm diameter and 1-2 um length were purchased from Nanoamor, TX. The nanotube dispersions were prepared by adding 4 mg (for low dosage) and 40 mg (for high doasage) of SWCNTs to 5 ml of PBS followed by addition 0.1% of pluronic F68 (purchased from Sigma Aldrich, MO), a nonionic surfactant, to make a final concentration of 800 µg/mL (low dosage) and 8000 µg/mL (high dosage). The dispersions was sonicated for 2 hours.

VII.2.2.2 Ceria nanoparticle dispersion. Electrostatically stabilized, highly dispersed ceria NPs used in this study were obtained from Cabot Microelectronics. The dispersion with pH of 3-4 was composed of 1% ceria NPs with a size ranging from 60 to100 nm. The dispersion was diluted with PBS to make final concentrations of 400 µg/mL (low dosage) and 4000 µg/mL (high dosage).

VII.2.3 Characterization

The nanoparticles were characterized for size by using a Carl Zeiss Libra 120 Plus transmission electron microscope (TEM) and for chemical composition by using a Horiba Xplora One Confocal Raman spectroscopy. The nanoparticles were further characterized by dynamic light scattering and zatapotential to measure particle size distribution (PSD) and surface charge, respectively, using a Malvern Instruments ZEN 3600 Zaetasizer Nano-ZX. Further, the surface area of ceria NPs was measured using a Nova Quantachrome 2200e BET surface area analyzer.

VII.2.4 ECG measurements

The instrument used for noninvasive ECG measurement in conscious small animals was ECGenie (Mouse Specific, Inc, MA) ECG recording platform (Figure 7.2). The ECGenie was installed on-site with technical support from Mouse Specifics. The software for data acquisition (LabChart7) and data analysis (Mouse) were installed on a Dell Latitude laptop with an Intel Core i7 processor. The equipment was tested and baseline parameter optimization was performed with an initial set of conscious mice.

All mice were ear tagged and weighed immediately upon arrival to the animal facility. It was found that one day is sufficient for acclimatization of mice to the ECGenie system to allow reliable data recording. The mice were randomly assigned to control (n = 5), low dosage (n = 5) or high dosage (n = 5) groups for SWCNT and ceria NP exposure with pre-exposure ECG signals recorded. After the pre-exposure measurement, lightly anaesthetized animals were exposed via intra-tracheal instillation to either SWCNTs dispersed in 50 µl phosphate buffered saline (PBS) or ceria NPs in model ceria CMP slurries. At one and three days following nanoparticle instillation, ECG recordings were performed in all groups of mice. An additional measurement was performed on the groups exposed to SWCNT at seven days post-exposure. After completion of ECG recordings all mice were euthanized with isoflorane followed by cardiac puncture to collect blood, lungs, trachea and heart for ex vivo analyses. Postmortem 0.5-1 ml blood samples were collected to evaluate blood lactate dehydrogenase (LDH) and differential cell counts to assess toxicity of exposure. Organs of the mice (trachea, lungs, heart) were harvested and stored at -80^{0}C for immunohistology and ultrastructural characterization.

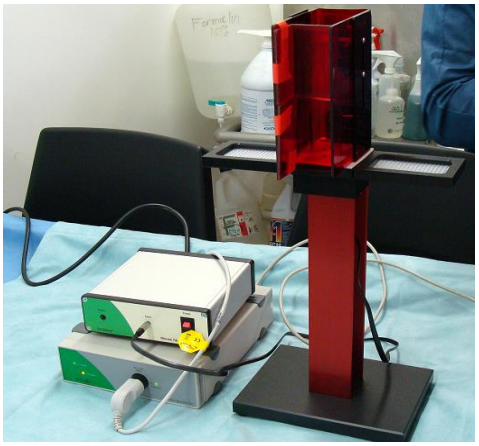

Figure 7.2. ECGenie System with its Electronics and a Chamber and Platform for ECG Measurements

VII.2.5 Acquisition of QT/RR intervals

Segments of signals containing at least six distinguishable waveforms were processed using ECGenie software, resulting in individual QT and RR measurements for each waveform. To obtain a single QT and RR pair for each measurement event, the numerous values for each measurement event were averaged. Within each measurement event, QT and RR values different by more than 2.7 standard deviations from the mean were classified as outliers and excluded from the subsequent analysis.

VII.2.6 RoR calculation

A pair of average QT/RR intervals for each mouse at each measurement event was used to fit the measured signal to the CSC model. Mathematical details of the model and the fitting procedure are discussed in the Appendix. One of the fitting parameters corresponds to the minimum value attained by the CSC recovery current, v_{min}. The critical

recovery current v_r^{crit} was computed from the remaining parameters, and the RoR follows from the normalized difference between these two quantities:

$$RoR = \frac{v_r^{crit} - v_{min}}{v_r^{crit}}. \quad (1)$$

MedCalc statistical software was used for the statistical comparisons presented below.

VII.3 Results

VII.3.1 Characterization of SWCNTs

The CNT dispersions were characterized using TEM and Confocal Raman Microscopy. Figure 7.3A shows transmission electron microscope (TEM) image which indicates a good dispersion of SWCNTs. Using Malvern Zetasizer the SWCNTs were also characterized for particle size and dispensability by using DLS and zeta potential measurements, respectively. Before dispersing the SWCNTs had a size of 2242 d.nm and a zeta potential of -49.8 in water which changed to 227 d.nm and -21.4 respectively, after dispersing in pluronic F68. The SWCNTs were also characterized in a Horiba Confocal Raman Microscope. Raman spectra of SWCNTs (Figure 7.3B) indicate the presence of radial breathing mode, D, G and G' bands, which verifies SWCNTs in the dispersion.

VII.3.2 Characterization of ceria nanoparticles

Nitrogen adsorption-desorption isotherms were collected for dried ceria NPs and surface area of 16.979 m^2/g was determined using extension of Langmuir Theory. Figure 7.3C shows TEM image of dried ceria NPs which indeed indicate that the particle size of the NPs was in the range of 60-100 nm confirming the size obtained from the manufacturer.

The ceria nanoparticles were characterized by DLS which indicated PSD of 145.3±2.6 d. nm when diluted 100x in water and zeta potential measurements, which indicated the surface charge to be 42.7±1.4. The ceria nanoparticles were further characterized using a Horiba Confocal Raman Microscope. Raman spectra of SWCNTs (Figure 7.3D) indicate the presence of Ce-O vibrational band at 450 cm^{-1}.

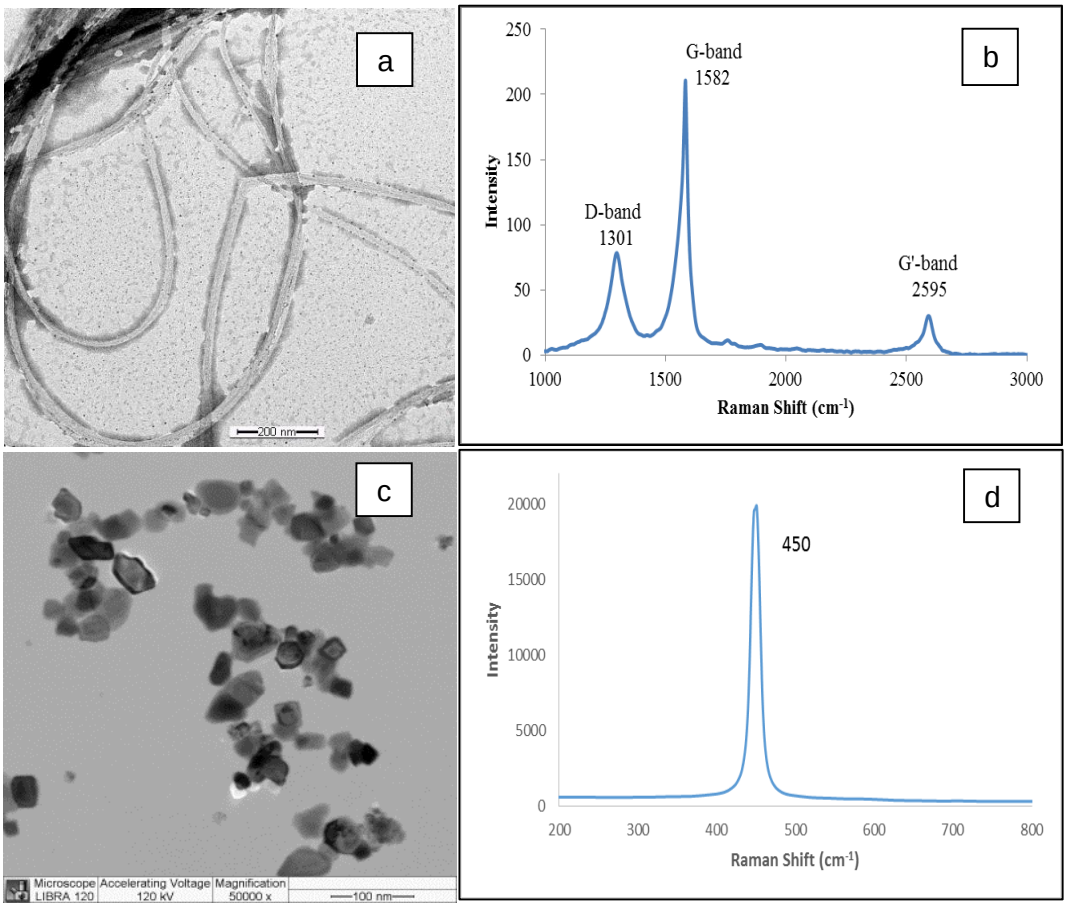

Figure 7.3. A) TEM Image of SWCNTs Dispersed in 1% Pluronic F68, B) Raman Spectrum of SWCNTs, C) TEM Image of Ceria NPs, and D) Raman Spectrum of Ceria NPs

VII.3.3 RoR measurements

The RoR was computed for each mouse at each measurement event on each day. The QT/RR interval averages and standard deviations over an entire day for the mice with median number of usable waveforms are shown in Table 7.1. The results for exposure to SWCNT demonstrate a much more significant effect in the high dosage mice compared to the low-dosage group, as depicted in the box plots (Figure 7.4) and table (Table 7.2) below. The mice treated with low dosage of SWCNT demonstrated positive trends whereas the mice treated with high dosage of SWCNT showed negative trends in RoR. Unlike SWCNTs negative *RoR* trends were observed for both low and high ceria dosages. The change in RoR in mice exposed to low dosage of ceria (Figure 7.5 and Table 7.3) was found to increase from -1.4% on Day 1 to -6.3% on Day 3 when compared to pre-exposed mice (Day 0) whereas it was found to decrease, from -4.29% on Day 1 to -2.65% on Day 3, in mice exposed to high dosage of ceria. However, statistical significance of these trends was still marginal ($P > 0.064$).

Table 7.1. RR and QT Averages with Standard Deviations for Mice in Each Group Corresponding to the Median Number of Processed Waveforms within Each Group

Group	Mouse	Day	Waveforms	RR (ms)	RR std. dev. (ms)	QT (ms)	QT std. dev. (ms)
SWCNT-C	1	3	229	83.5	7.11	41.5	8.16
SWCNT-L	8	3	384	84.4	5.46	41.4	8.06
SWCNT-H	12	7	267	76.0	3.41	39.4	6.44
CERIA-C	17	3	193	75.1	3.25	38.2	8.10
CERIA-L	22	3	242	76.7	3.31	39.9	6.14
CERIA-H	30	1	370	81.3	7.26	41.9	7.79

Table 7.2. Percentage Change in RoR for Carbon Nanotube Exposure from Day Zero for Low- and High-Dose Groups on Various Days shown with *p*-values

Group	RoR % change from Day 0	p-value
Day 1 Low	2.23	0.6044
Day 3 Low	3.89	0.3181
Day 7 Low	1.23	0.6915
Day 1 High	-7.29	0.0829
Day 3 High	-4.37	0.1159
Day 7 High	-5.29	0.0540

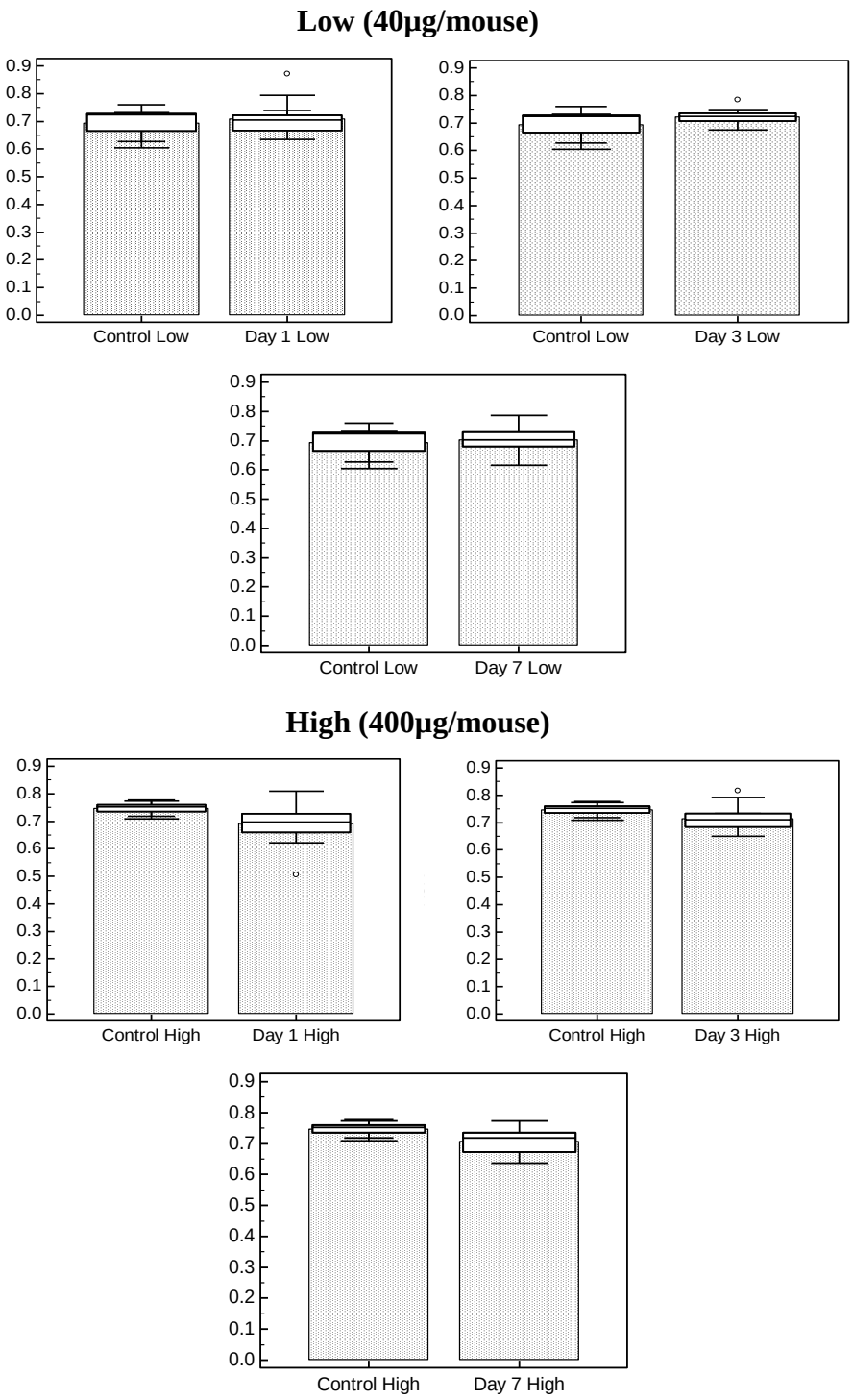

Figure 7.4. Box-plot Comparison of Control (Day 0) and Post-Exposure RoR Values for Mice Exposed to Carbon Nanotubes

Low (20µg/mouse)

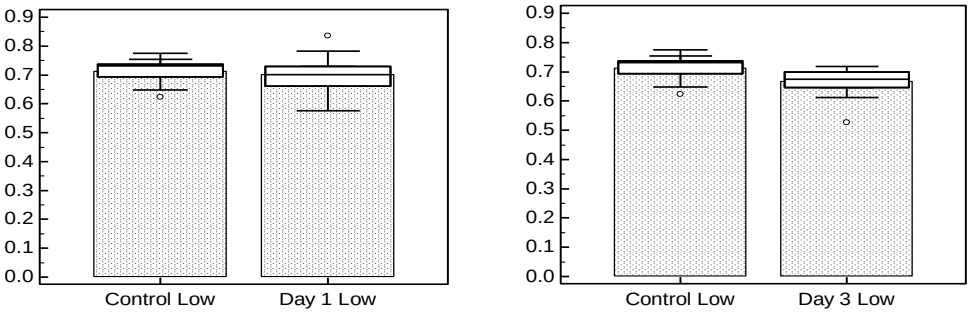

High (200µg/mouse)

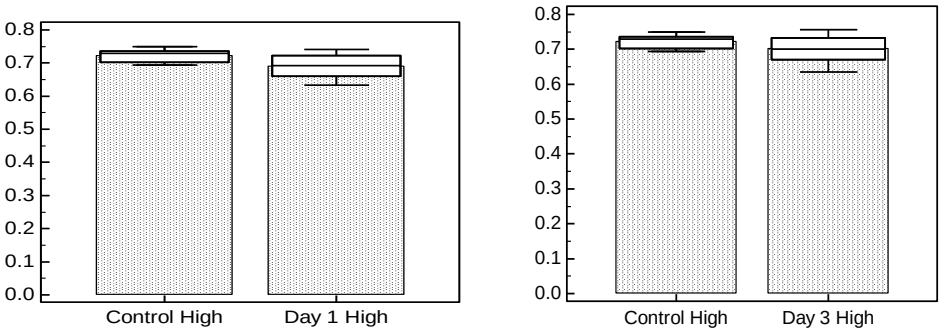

Figure 7.5. Box-plot Comparison of Control (Day 0) and Post-Exposure RoR Values for Mice Exposed to Ceria Nanoparticles

Table 7.3. Percentage Change in RoR for Exposure to Ceria Nanoparticle Exposure from Day Zero for Low- and High-Dose Groups on Various Days shown with *p*-values

Group	RoR % change from Day 0	p-value
Day 1 Low	-1.40%	0.7321
Day 3 Low	-6.30%	0.0642
Day 1 High	-4.29%	0.0740
Day 3 High	-2.65%	0.2666

VII.3.4 Tissue analysis

Figure 7.6a shows healthy (control) lung tissue which has a good spacing in the alveoli, bronchioles and alveolar ducts. Figures 7.6b and 7.6c show images of lung tissue in mice exposed to low and high dosages of SWCNTs, respectively. It can be observed that the space in the alveoli and the alveolar ducts are infiltrated with cells as a consequence of inflammatory response. This effect is significant (7.6c) in mice treated with high dosage of SWCNTs, and minimal (Figure 7.6b) in mice treated with low dosage of SWCNTs. Figures 6d and 6e show images of lung tissue of mice exposed to low and high dosages of ceria NPs, respectively. In this case the alveolar spacing decreases significantly even in mice exposed to low dosage of ceria NPs resulting in constriction of bronchiole (Figure 7.6d). The trend gets stronger indicating the deterioration of lung tissue, whereas mice treated with high dosage of ceria NPs expose large areas of collapsed bronchioles (Figure 7.6e) indicating severe damage to the lung tissue. In summary, even though none of the mice died over seven day observation period, we noticed a distinct lung tissue damage which was enhanced at higher dosages of nanoparticles. It should be also emphasized that a stronger dosage effect was found for ceria nanoparticles which was in a good agreement with observed dynamics of *RoR*.

VII.4 Discussion

With increasing usage of nanoparticles in modern industry, understanding the adverse effects of nanoparticles on cellular systems and organs is of extreme importance. SWCNTs and ceria nanoparticles are two varieties nanoparticles which have been extensively studied for use in various applications including manufacture of commercial

products and drug delivery. Therefore, it is important to study the effect of these nanoparticles on living systems. Although many studies have reported effects of nanoparticles on several cell types *in vitro* and several organs *in vivo,* there is minimal understanding about the effects of nanoparticles on heart and brain.

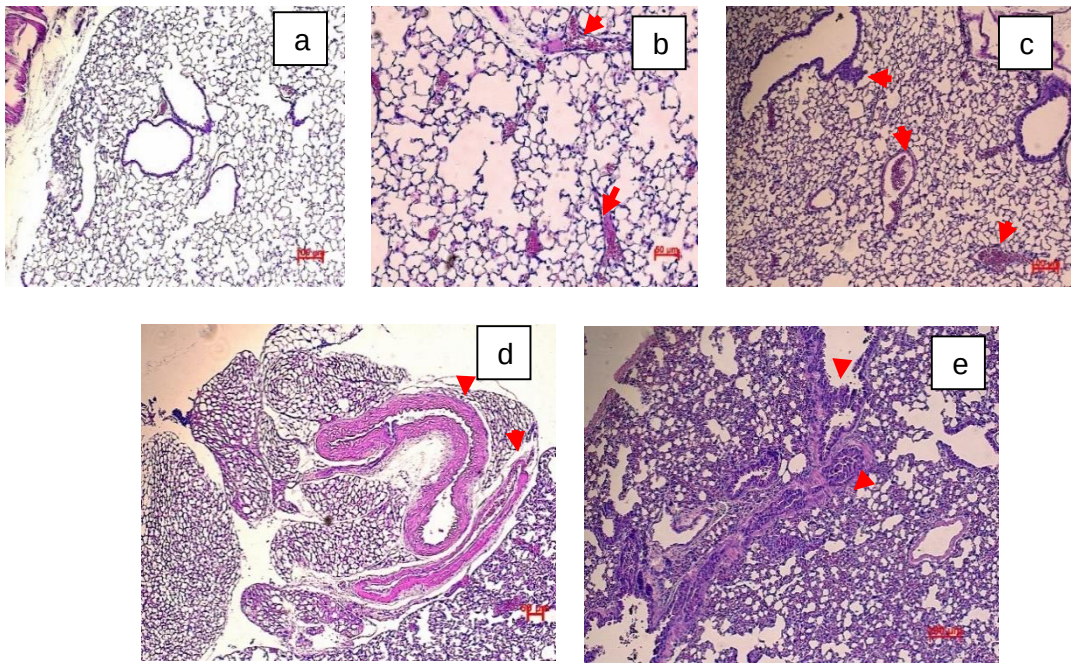

Figure 7.6. H&E Stains of Lung Tissues (a) Control, (b) Low Dosage SWCNTs, (c) High Dosage SWCNTs, (d) Low Dosage Ceria NPs, and (e) High Dosage Ceria NPs

In this study, we focus our efforts on understanding the effect of inhalational exposure of these nanoparticles to heart. Even though there are robust techniques to study, measure and evaluate the functioning of the heart, there is an urgent need to collect these measurements noninvasively. In this study, we employ a novel method that uses QT and RR intervals of an electrocardiogram, to predict cardiac cardiotoxicity in mice exposed to SWCNTs and ceria NPs.

Recent findings demonstrate that exposure to carbon and metallic nanoparticles can cause cytotoxic effects in vascular endothelial cells[84]. Yan et al reported that pulmonary exposure to SWCNTs may induce cardiovascular toxicity via indirect effects on vascular homeostasis[85]. It has been reported that instillation of SWCNTs with a diameter of 1-2 nm and length of up to 100 um in mice[86] and rats[87] could lead to the formation of lung granuloma. Recent reports provide evidence that exposure to ceria NPs causes adverse effects in various organs such including the lung, liver, spleen, kidney, brain and heart, and their related cellular systems[88]. Supporting the antioxidant nature of ceria nanoparticles, Pagliari et al reported that 24 hour exposure of ceria nanoparticles did not affect cell growth and function while protecting from H2O2-induced cytotoxicity for at least 7 days in cardiac progenitor cells[89]. However, another study by Poma et al demonstrate inflammatory response in CD-1 mice exposed to ceria NPs with no lethal toxic effects suggesting that ceria NPs are not particularly safe[90]. From all these findings, it is understood that that cardiovascular effects due to nanoparticle exposure occur through systemic inflammatory signaling cascades that are affected as a consequence of progression of atherosclerosis which in turn can lead to molecular responses in heart.

Our experimental findings based on the dynamics of RoR show that ceria nanoparticles induce more toxicity and tissue damage when compared to SWCNTs used in this study. The mice instilled with high and low dosage of ceria showed negative trends of RoR when compared to the pre-exposed RoR values collected for the same mice. With increasing time (from Day 1 to Day 3), the mice instilled with low dosage of ceria showed and increased percentage drop in RoR compared to pre-exposure measurements, which

infers increased cardiotoxicity. However, a reverse trend was observed in case of mice instilled with high dosage of ceria nanoparticles, i.e., cardiotoxicity decreased with time. In case of mice instilled with SWCNTs, the mice exposed to low dosage of CNTs showed positive trends of RoR. The resting heart rate RoR values were practically the same in case of control and exposed mice. However, the mice exposed with high dosage of SWCNTs showed a persistent negative trends in RoR from Day 1 to Day 7 with 7.29%, 4.39% and 5.39% change in RoR from Day 0 for Day 1, Day 3 and Day 7, respectively. From these results, it can be inferred that the high dosage (400 ug/mouse) of SWCNTs was found to show higher cardiotoxicity compared to that of the low dosage (40 ug/mouse) used in this study. Imunohistochemical analysis of the lung tissues also support this findings. It was found that there was more tissue damage in case of mice exposed to ceria NPs. The mice treated with low concentration of SWCNTs did not show significant damage, but the mice treated with the high dosage of the same SWCNTs showed tissue damage with less alveolar air space, infiltration of immune cells and formation of septa. The lung tissue damage was found to increase with concentration in case of both SWCNTs and ceria instilled CD-1 mice. However, similarly to the mice exposed to a high dosage, the low dosage of ceria also caused lung tissue damage with shortening of brochiolar space and infiltration of immune cells. However, the effects were comparatively severe in case of mice instilled with high dosage of ceria where collapse of bronchi was also observed.

Even though the RoR values showed trends indicative of cardiotoxicity due to SWCNTs and ceria nanoparticles, the *p*-values were marginal. Even marginal trends in the *RR* and *QT* intervals were absent, suggesting strongly that information relevant to cardiac

toxicity is absent from these isolated measurements. The RoR constitutes a legitimate measure of refractoriness which is statistically independent of the *RR* and *QT* intervals and highly sensitive to cardiac toxicity. Since toxic cardiac responses such as arrhythmias and ischemia should depend on levels of physiological load, it may be helpful to perform the measurements under dobutamine-induced cardiac stress. As explored in Hazari et al dobutamine causes the heart to respond as if the animals were exercising in a conventional "stress" test. When exposed to diesel exhaust, spontaneously hypertensive rats show a drop in heart-rate variability compared to otherwise healthy rats which becomes more significant when dobutamine is used to simulate a stress test. The RoR provides a concise metric complimentary to heart-rate variability which should also be sensitive to the effects of spontaneous hypertensivity in the presence of toxins. A direction for future research is to consider several classes of mice with varying states of predisposition to disease, all exposed to nanoparticles and subjected to a rigorous dobutamine stress test.

CHAPTER VIII

CONCLUSIONS AND FUTURE PERSPECTIVES

In conclusion, silica, ceria and alumina CMP slurries were comprehensively characterized for size, shape, crystallinity, chemical composition, surface area, surface charge and aggregation (PSD). It was observed that both colloidal and fumed silica NPs showed concentration dependent toxicity. Unlike in fumed silica NPs, colloidal silica nanoparticles showed time dependence toxicity. Fumed silica slurry nanoparticles was observed to have higher toxicity compared to the colloidal silica, though they latter is smaller in size. This could be attributed to either the method of synthesis of fumed silica NPs or the difference in shape of the two silica NPs. Acute toxicity was observed for exposure periods up to 12 hours in case of ceria slurry NPs whereas alumina slurry NPs showed no significant toxicity. Significant difference in the toxicity was observed in groups when exposed to dispersed NPs (slurry) and undispersed NPs (aggregated NPs), emphasizing that agglomeration state is an important factor in cellular toxicity. Apart from aggregation state, particle size, surface area and surface charge, have also affected toxicity of silica NPs to A549 cells. Oxidative stress analysis showed significant increase in production of intracellular ROS, indicating that silica nanoparticles cause cellular toxicity via oxidative stress. Even though they showed different toxicity profiles, all the NPs were observed to be internalized in the cells. Further, non-invasive evaluation of NP uptake using confocal Raman Spectroscopy provided evidence for the cellular uptake and

internalization with inhomogeneous distribution of ceria nanoparticles in A549 cells. Since ceria NPs were internalized in cells without showing significant toxicity it can be stated that uptake of NPs would not always lead to toxicity. The future work, could be targeted to understand specific mechanisms that are being altered during cell interaction with NPs and its implications. With interesting observations like the one with ceria, studying transformations of NPs could be another area for future interests.

Following *in vitro* studies, *in vivo* experiments were performed by exposing ceria NPs and SWCNTs in CD-1 mice via intratrachael instillation. The *in vivo* work was performed with an objective of developing a novel, non-invasive, longitudinal method employing *RoR* to evaluate cardiac health. *RoR* was found to be a better method in comparison to the traditional method of assessing cardiac health by evaluating QT and RR intervals in an electrocardiogram. Ceria NPs were found to show more damage than SWCNTs, in spite of low dosage of ceria NPs. Even though the RoR values showed trends indicative of cardiotoxicity due to SWCNTs and ceria nanoparticles, the *p*-values were marginal. Even marginal trends in the *RR* and *QT* intervals were absent, suggesting strongly that information relevant to cardiac toxicity is absent from these isolated measurements. The RoR provides a concise metric complimentary to heart-rate variability which should also be sensitive to the effects of spontaneous hypertensivity in the presence of toxins. From the *RoR* measurements, it can be noted that exposure of NPs to a primary organ (lung in our case) can lead to adverse effects in a secondary organ (heart). A direction for future research is to consider several classes of mice with varying states of predisposition to disease, all exposed to nanoparticles and subjected to dobutamine post-stress response.

REFERENCES

1. Donaldson, K.; Stone, V.; Tran, C. L.; Kreyling, W.; Borm, P. J. A., Nanotoxicology. *Occupational and Environmental Medicine* **2004,** *61* (9), 727-728.

2. Nel, A. X., T. Madler, L. Li, N., Toxic potential of materials at the nanolevel. *Science* **2006,** *311*.

3. Yokel, R. A.; Hussain, S.; Garantziotis, S.; Demokritou, P.; Castranova, V.; Cassee, F. R., The yin: an adverse health perspective of nanoceria: uptake, distribution, accumulation, and mechanisms of its toxicity. *Environmental Science: Nano* **2014,** *1* (5), 406-428.

4. Riviere, J. E., Pharmacokinetics of nanomaterials: an overview of carbon nanotubes, fullerenes and quantum dots. *Wiley Interdisciplinary Reviews: Nanomedicine and Nanobiotechnology* **2009,** *1* (1), 26-34.

5. Murty, B. S.; Shankar, P.; Raj, B.; Rath, B. B.; Murday, J., Applications of Nanomaterials. In *Textbook of Nanoscience and Nanotechnology*, Springer Berlin Heidelberg: 2013; pp 107-148.

6. Mandal, G.; Ganguly, T., Applications of nanomaterials in the different fields of photosciences. *Indian Journal of Physics* **2011,** *85* (8), 1229-1245; Alves, A.; Berutti, F.; Sánchez, F., Nanomaterials and Catalysis. In *Nanostructured Materials for Engineering Applications*, Bergmann, C.; de Andrade, M., Eds. Springer Berlin Heidelberg: 2011; pp 93-117.

7. Bell, A. T., The Impact of Nanoscience on Heterogeneous Catalysis. *Science* **2003,** *299* (5613), 1688-1691.

8. Saini, R.; Saini, S.; Sharma, S., Nanotechnology: the future medicine. *Journal of cutaneous and aesthetic surgery* **2010,** *3* (1), 32.

9. Energy Harvesting for Structural Health Monitoring Sensor Networks. *Journal of Infrastructure Systems* **2008,** *14* (1), 64-79.

10. Andre E. Nel, L. M., Fred Klaessig, Darrell Velegol, Vince Castranova, Tian Xia, Eric M. V. Hoek; Thompson, a. M., Understanding biophysicochemical interactions at the nano–bio interface. *nature materials* **2009,** *8*.

11. International Technology Roadmap for Semiconductors. 2013.

12. Speed, D.; Westerhoff, P.; Sierra-Alvarez, R.; Draper, R.; Pantano, P.; Aravamudhan, S.; Chen, K. L.; Hristovski, K.; Herckes, P.; Bi, X.; Yang, Y.; Zeng, C.; Otero-Gonzalez, L.; Mikoryak,

C.; Wilson, B. A.; Kosaraju, K.; Tarannum, M.; Crawford, S.; Yi, P.; Liu, X.; Babu, S. V.; Moinpour, M.; Ranville, J.; Montano, M.; Corredor, C.; Posner, J.; Shadman, F., Physical, chemical, and in vitro toxicological characterization of nanoparticles in chemical mechanical planarization suspensions used in the semiconductor industry: towards environmental health and safety assessments. *Environmental Science: Nano* **2015,** *2* (3), 227-244.

13. Li, Z.; Hulderman, T.; Salmen, R.; Chapman, R.; Leonard, S. S.; Young, S.-H.; Shvedova, A.; Luster, M. I.; Simeonova, P. P., Cardiovascular Effects of Pulmonary Exposure to Single-Wall Carbon Nanotubes. *Environmental Health Perspectives* **2007,** *115* (3), 377-382; Stenvinkel, P., Endothelial dysfunction and inflammation—is there a link? *Nephrology Dialysis Transplantation* **2001,** *16* (10), 1968-1971.

14. Srinivas, A.; Rao, P. J.; Selvam, G.; Murthy, P. B.; Reddy, P. N., Acute inhalation toxicity of cerium oxide nanoparticles in rats. *Toxicology Letters* **2011,** *205* (2), 105-115.

15. Zhang, Y.; Ali, S. F.; Dervishi, E.; Xu, Y.; Li, Z.; Casciano, D.; Biris, A. S., Cytotoxicity Effects of Graphene and Single-Wall Carbon Nanotubes in Neural Phaeochromocytoma-Derived PC12 Cells. *ACS Nano* **2010,** *4* (6), 3181-3186.

16. Park, Y.-H.; Bae, H.; Jang, Y.; Jeong, S.; Lee, H.; Ryu, W.-I.; Yoo, M.; Kim, Y.-R.; Kim, M.-K.; Lee, J.; Jeong, J.; Son, S., Effect of the size and surface charge of silica nanoparticles on cutaneous toxicity. *Molecular & Cellular Toxicology* **2013,** *9* (1), 67-74.

17. Kim, I.-Y.; Joachim, E.; Choi, H.; Kim, K., Toxicity of silica nanoparticles depends on size, dose, and cell type. *Nanomedicine: Nanotechnology, Biology and Medicine* **2015,** *11* (6), 1407-1416.

18. Rabolli, V.; Thomassen, L. C.; Uwambayinema, F.; Martens, J. A.; Lison, D., The cytotoxic activity of amorphous silica nanoparticles is mainly influenced by surface area and not by aggregation. *Toxicol Lett* **2011,** *206* (2), 197-203.

19. Liu, W.; Choi, H. S.; Zimmer, J. P.; Tanaka, E.; Frangioni, J. V.; Bawendi, M., Compact Cysteine-Coated CdSe(ZnCdS) Quantum Dots for in Vivo Applications. *Journal of the American Chemical Society* **2007,** *129* (47), 14530-14531.

20. Zhang, H.; Gilbert, B.; Huang, F.; Banfield, J. F., Water-driven structure transformation in nanoparticles at room temperature. *Nature* **2003,** *424* (6952), 1025-1029.

21. Magrez, A.; Kasas, S.; Salicio, V.; Pasquier, N.; Seo, J. W.; Celio, M.; Catsicas, S.; Schwaller, B.; Forró, L., Cellular Toxicity of Carbon-Based Nanomaterials. *Nano Letters* **2006,** *6* (6), 1121-1125.

22. Hoet, P.; Bruske-Hohlfeld, I.; Salata, O., Nanoparticles - known and unknown health risks. *Journal of Nanobiotechnology* **2004,** *2* (1), 12.

23. Oberdörster, G.; Oberdörster, E.; Oberdörster, J., Nanotoxicology: An Emerging Discipline Evolving from Studies of Ultrafine Particles. *Environmental Health Perspectives* **2005,**

113 (7), 823-839; Chen, Z.; Meng, H.; Xing, G.; Chen, C.; Zhao, Y.; Jia, G.; Wang, T.; Yuan, H.; Ye, C.; Zhao, F.; Chai, Z.; Zhu, C.; Fang, X.; Ma, B.; Wan, L., Acute toxicological effects of copper nanoparticles in vivo. *Toxicology Letters* **2006,** *163* (2), 109-120; Bhavsar, M. D.; Amiji, M. M., Gastrointestinal distribution and in vivo gene transfection studies with nanoparticles-in-microsphere oral system (NiMOS). *Journal of Controlled Release* **2007,** *119* (3), 339-348.

24. Nel, A.; Xia, T.; Mädler, L.; Li, N., Toxic Potential of Materials at the Nanolevel. *Science* **2006,** *311* (5761), 622-627.

25. Fruijtier-Pölloth, C., The toxicological mode of action and the safety of synthetic amorphous silica—A nanostructured material. *Toxicology* **2012,** *294* (2–3), 61-79.

26. He, X.; Nie, H.; Wang, K.; Tan, W.; Wu, X.; Zhang, P., In Vivo Study of Biodistribution and Urinary Excretion of Surface-Modified Silica Nanoparticles. *Analytical Chemistry* **2008,** *80* (24), 9597-9603.

27. Kreyling, W. G.; Semmler, M.; Erbe, F.; Mayer, P.; Takenaka, S.; Schulz, H.; Oberdörster, G.; Ziesenis, A., TRANSLOCATION OF ULTRAFINE INSOLUBLE IRIDIUM PARTICLES FROM LUNG EPITHELIUM TO EXTRAPULMONARY ORGANS IS SIZE DEPENDENT BUT VERY LOW. *Journal of Toxicology and Environmental Health, Part A* **2002,** *65* (20), 1513-1530.

28. Cho, M.; Cho, W.-S.; Choi, M.; Kim, S. J.; Han, B. S.; Kim, S. H.; Kim, H. O.; Sheen, Y. Y.; Jeong, J., The impact of size on tissue distribution and elimination by single intravenous injection of silica nanoparticles. *Toxicology Letters* **2009,** *189* (3), 177-183.

29. Oberdörster, G.; Sharp, Z.; Atudorei, V.; Elder, A.; Gelein, R.; Kreyling, W.; Cox, C., Translocation of Inhaled Ultrafine Particles to the Brain. *Inhalation toxicology* **2004,** *16* (6-7), 437-445.

30. Xia, T.; Kovochich, M.; Liong, M.; Mädler, L.; Gilbert, B.; Shi, H.; Yeh, J. I.; Zink, J. I.; Nel, A. E., Comparison of the Mechanism of Toxicity of Zinc Oxide and Cerium Oxide Nanoparticles Based on Dissolution and Oxidative Stress Properties. *ACS Nano* **2008,** *2* (10), 2121-2134.

31. Toxicity Testing in the 21st Century: A Vision and a Strategy (2007).

32. Lankoff, A.; Arabski, M.; Wegierek-Ciuk, A.; Kruszewski, M.; Lisowska, H.; Banasik-Nowak, A.; Rozga-Wijas, K.; Wojewodzka, M.; Slomkowski, S., Effect of surface modification of silica nanoparticles on toxicity and cellular uptake by human peripheral blood lymphocytes in vitro. *Nanotoxicology* **2013,** *7* (3), 235-250.

33. Brunner, T. J.; Wick, P.; Manser, P.; Spohn, P.; Grass, R. N.; Limbach, L. K.; Bruinink, A.; Stark, W. J., In vitro cytotoxicity of oxide nanoparticles: comparison to asbestos, silica, and the effect of particle solubility. *Environ Sci Technol* **2006,** *40* (14), 4374-81.

34. Pujalté, I.; Passagne, I.; Brouillaud, B.; Tréguer, M.; Durand, E.; Ohayon-Courtès, C.; L'Azou, B., Cytotoxicity and oxidative stress induced by different metallic nanoparticles on human kidney cells. *Particle and Fibre Toxicology* **2011,** *8*, 10-10; Passagne, I.; Morille, M.; Rousset, M.; Pujalté, I.; L'Azou, B., Implication of oxidative stress in size-dependent toxicity of silica nanoparticles in kidney cells. *Toxicology* **2012,** *299* (2–3), 112-124.

35. Oberdorster, G.; Sharp, Z.; Atudorei, V.; Elder, A.; Gelein, R.; Lunts, A.; Kreyling, W.; Cox, C., Extrapulmonary translocation of ultrafine carbon particles following whole-body inhalation exposure of rats. *J Toxicol Environ Health A* **2002,** *65* (20), 1531-43.

36. Mittal, S.; Pandey, A. K., Cerium Oxide Nanoparticles Induced Toxicity in Human Lung Cells: Role of ROS Mediated DNA Damage and Apoptosis. *BioMed Research International* **2014,** *2014*, 14.

37. Cho, W. S.; Choi, M.; Han, B. S.; Cho, M.; Oh, J.; Park, K.; Kim, S. J.; Kim, S. H.; Jeong, J., Inflammatory mediators induced by intratracheal instillation of ultrafine amorphous silica particles. *Toxicol Lett* **2007,** *175* (1-3), 24-33.

38. McCarthy, J.; Inkielewicz-Stępniak, I.; Corbalan, J. J.; Radomski, M. W., Mechanisms of Toxicity of Amorphous Silica Nanoparticles on Human Lung Submucosal Cells in Vitro: Protective Effects of Fisetin. *Chemical Research in Toxicology* **2012,** *25* (10), 2227-2235.

39. Lin, W.; Huang, Y.-w.; Zhou, X.-D.; Ma, Y., In vitro toxicity of silica nanoparticles in human lung cancer cells. *Toxicology and Applied Pharmacology* **2006,** *217* (3), 252-259.

40. Ghiazza, M.; Polimeni, M.; Fenoglio, I.; Gazzano, E.; Ghigo, D.; Fubini, B., Does vitreous silica contradict the toxicity of the crystalline silica paradigm? *Chem Res Toxicol* **2010,** *23* (3), 620-9.

41. Kumar, R.; Roy, I.; Ohulchanskky, T. Y.; Vathy, L. A.; Bergey, E. J.; Sajjad, M.; Prasad, P. N., In Vivo Biodistribution and Clearance Studies Using Multimodal Organically Modified Silica Nanoparticles. *ACS Nano* **2010,** *4* (2), 699-708; Selvan, S. T.; Tan, T. T. Y.; Yi, D. K.; Jana, N. R., Functional and Multifunctional Nanoparticles for Bioimaging and Biosensing. *Langmuir* **2010,** *26* (14), 11631-11641.

42. Xie, G.; Sun, J.; Zhong, G.; Shi, L.; Zhang, D., Biodistribution and toxicity of intravenously administered silica nanoparticles in mice. *Arch Toxicol* **2010,** *84* (3), 183-90.

43. Passagne, I.; Morille, M.; Rousset, M.; Pujalte, I.; L'Azou, B., Implication of oxidative stress in size-dependent toxicity of silica nanoparticles in kidney cells. *Toxicology* **2012,** *299* (2-3), 112-24.

44. Napierska, D.; Thomassen, L. C.; Rabolli, V.; Lison, D.; Gonzalez, L.; Kirsch-Volders, M.; Martens, J. A.; Hoet, P. H., Size-dependent cytotoxicity of monodisperse silica nanoparticles in human endothelial cells. *Small* **2009,** *5* (7), 846-53.

45. Zhang, H.; Dunphy, D. R.; Jiang, X.; Meng, H.; Sun, B.; Tarn, D.; Xue, M.; Wang, X.; Lin, S.; Ji, Z.; Li, R.; Garcia, F. L.; Yang, J.; Kirk, M. L.; Xia, T.; Zink, J. I.; Nel, A.; Brinker, C. J., Processing Pathway Dependence of Amorphous Silica Nanoparticle Toxicity: Colloidal vs Pyrolytic. *Journal of the American Chemical Society* **2012,** *134* (38), 15790-15804.
46. Pratsinis, S. E., Flame aerosol synthesis of ceramic powders. *Progress in Energy and Combustion Science* **1998,** *24* (3), 197-219.

47. Lin, W.; Huang, Y.-w.; Zhou, X.-D.; Ma, Y., Toxicity of Cerium Oxide Nanoparticles in Human Lung Cancer Cells. *International Journal of Toxicology* **2006,** *25* (6), 451-457.

48. Radziun, E.; Dudkiewicz Wilczynska, J.; Ksiazek, I.; Nowak, K.; Anuszewska, E. L.; Kunicki, A.; Olszyna, A.; Zabkowski, T., Assessment of the cytotoxicity of aluminium oxide nanoparticles on selected mammalian cells. *Toxicol In Vitro* **2011,** *25* (8), 1694-700.

49. Di Virgilio, A. L.; Reigosa, M.; Arnal, P. M.; Fernandez Lorenzo de Mele, M., Comparative study of the cytotoxic and genotoxic effects of titanium oxide and aluminium oxide nanoparticles in Chinese hamster ovary (CHO-K1) cells. *J Hazard Mater* **2010,** *177* (1-3), 711-8.
50. Al-Rawi, M.; Diabate, S.; Weiss, C., Uptake and intracellular localization of submicron and nano-sized SiO(2) particles in HeLa cells. *Arch Toxicol* **2011,** *85* (7), 813-26.

51. Lu, X.; Qian, J.; Zhou, H.; Gan, Q.; Tang, W.; Lu, J.; Yuan, Y.; Liu, C., In vitro cytotoxicity and induction of apoptosis by silica nanoparticles in human HepG2 hepatoma cells. *International Journal of Nanomedicine* **2011,** *6*, 1889-1901.

52. Lesniak, A.; Fenaroli, F.; Monopoli, M. P.; Åberg, C.; Dawson, K. A.; Salvati, A., Effects of the Presence or Absence of a Protein Corona on Silica Nanoparticle Uptake and Impact on Cells. *ACS Nano* **2012,** *6* (7), 5845-5857.

53. Estrela-Lopis, I.; Romero, G.; Rojas, E.; Moya, S.; Donath, E. In *Nanoparticle uptake and their co-localization with cell compartments–a confocal Raman microscopy study at single cell level*, Journal of Physics: Conference Series, IOP Publishing: 2011; p 012017.

54. Konczol, M.; Ebeling, S.; Goldenberg, E.; Treude, F.; Gminski, R.; Giere, R.; Grobety, B.; Rothen-Rutishauser, B.; Merfort, I.; Mersch-Sundermann, V., Cytotoxicity and genotoxicity of size-fractionated iron oxide (magnetite) in A549 human lung epithelial cells: role of ROS, JNK, and NF-kappaB. *Chem Res Toxicol* **2011,** *24* (9), 1460-75.

55. Sies, H., What is Oxidative Stress? In *Oxidative Stress and Vascular Disease*, Keaney, J., Jr., Ed. Springer US: 2000; Vol. 224, pp 1-8.

56. Ayres, J. G.; Borm, P.; Cassee, F. R.; Castranova, V.; Donaldson, K.; Ghio, A.; Harrison, R. M.; Hider, R.; Kelly, F.; Kooter, I. M.; Marano, F.; Maynard, R. L.; Mudway, I.; Nel, A.; Sioutas, C.; Smith, S.; Baeza-Squiban, A.; Cho, A.; Duggan, S.; Froines, J., Evaluating the toxicity of airborne particulate matter and nanoparticles by measuring oxidative stress potential--a workshop report and consensus statement. *Inhal Toxicol* **2008,** *20* (1), 75-99.

57. Buzea, C.; Pacheco, I. I.; Robbie, K., Nanomaterials and nanoparticles: Sources and toxicity. *Biointerphases* **2007,** *2* (4), MR17.

58. Donaldson, K.; Stone, V.; Borm, P. J.; Jimenez, L. A.; Gilmour, P. S.; Schins, R. P.; Knaapen, A. M.; Rahman, I.; Faux, S. P.; Brown, D. M.; MacNee, W., Oxidative stress and calcium signaling in the adverse effects of environmental particles (PM10). *Free Radic Biol Med* **2003,** *34* (11), 1369-82; Xia, T.; Kovochich, M.; Nel, A., The role of reactive oxygen species and oxidative stress in mediating particulate matter injury. *Clin Occup Environ Med* **2006,** *5* (4), 817-36.

59. Manke, A.; Wang, L.; Rojanasakul, Y., Mechanisms of Nanoparticle-Induced Oxidative Stress and Toxicity. *BioMed Research International* **2013,** *2013*, 15.

60. *Global Market For Nanoparticles In Electronic, Magnetic And Optoelectronic Applications Slated For High Growth Through 2012*; 2008.

61. Holden, P. A.; Klaessig, F.; Turco, R. F.; Priester, J. H.; Rico, C. M.; Avila-Arias, H.; Mortimer, M.; Pacpaco, K.; Gardea-Torresdey, J. L., Evaluation of Exposure Concentrations Used in Assessing Manufactured Nanomaterial Environmental Hazards: Are They Relevant? *Environmental Science & Technology* **2014,** *48* (18), 10541-10551.

62. Nel, A. E.; Madler, L.; Velegol, D.; Xia, T.; Hoek, E. M. V.; Somasundaran, P.; Klaessig, F.; Castranova, V.; Thompson, M., Understanding biophysicochemical interactions at the nano-bio interface. *Nat Mater* **2009,** *8* (7), 543-557.

63. Bakand, S.; Winder, C.; Khalil, C.; Hayes, A., Toxicity Assessment of Industrial Chemicals and Airborne Contaminants: Transition from In Vivo to In Vitro Test Methods: A Review. *Inhalation Toxicology* **2005,** *17* (13), 775-787.

64. Shepard, M. N.; Brenner, S., An Occupational Exposure Assessment for Engineered Nanoparticles Used in Semiconductor Fabrication. *Annals of Occupational Hygiene* **2013**.

65. Roth, G. A.; Neu-Baker, N. M.; Brenner, S. A., SEM analysis of particle size during conventional treatment of CMP process wastewater. *Science of The Total Environment* **2015,** *508* (0), 1-6.

66. Warheit, D. B.; McHugh, T. A.; Hartsky, M. A., Differential pulmonary responses in rats inhaling crystalline, colloidal or amorphous silica dusts. *Scandinavian Journal of Work, Environment & Health* **1995,** *21*, 19-21.

67. Oberdorster, G., Safety assessment for nanotechnology and nanomedicine: concepts of nanotoxicology. *J Intern Med* **2010,** *267* (1), 89-105.

68. Mu, Q.; Hondow, N. S.; Krzeminski, L.; Brown, A. P.; Jeuken, L. J.; Routledge, M. N., Mechanism of cellular uptake of genotoxic silica nanoparticles. *Part Fibre Toxicol* **2012,** *9*, 29.

69. de Planque, M. R. R.; Aghdaei, S.; Roose, T.; Morgan, H., Electrophysiological Characterization of Membrane Disruption by Nanoparticles. *ACS Nano* **2011,** *5* (5), 3599-3606.

70. Zhang, T.; Stilwell, J. L.; Gerion, D.; Ding, L.; Elboudwarej, O.; Cooke, P. A.; Gray, J. W.; Alivisatos, A. P.; Chen, F. F., Cellular Effect of High Doses of Silica-Coated Quantum Dot Profiled with High Throughput Gene Expression Analysis and High Content Cellomics Measurements. *Nano Letters* **2006,** *6* (4), 800-808; Lim, Y.; Kim, J. H.; Kim, K. A.; Chang, H. S.; Park, Y. M.; Ahn, B. Y.; Phee, Y. G., Silica-induced apoptosis in vitro and in vivo. *Toxicology Letters* **1999,** *108* (2–3), 335-339; Chang, J. S.; Chang, K. L.; Hwang, D. F.; Kong, Z. L., In vitro cytotoxicitiy of silica nanoparticles at high concentrations strongly depends on the metabolic activity type of the cell line. *Environ Sci Technol* **2007,** *41* (6), 2064-8.

71. Nowack, B.; Bucheli, T. D., Occurrence, behavior and effects of nanoparticles in the environment. *Environmental Pollution* **2007,** *150* (1), 5-22.

72. Reed, K.; Cormack, A.; Kulkarni, A.; Mayton, M.; Sayle, D.; Klaessig, F.; Stadler, B., Exploring the properties and applications of nanoceria: is there still plenty of room at the bottom? *Environmental Science: Nano* **2014,** *1* (5), 390-405.

73. Xu, C.; Qu, X., Cerium oxide nanoparticle: a remarkably versatile rare earth nanomaterial for biological applications. *NPG Asia Mater* **2014,** *6*, e90.

74. Singh, S.; Kumar, A.; Karakoti, A.; Seal, S.; Self, W. T., Unveiling the mechanism of uptake and sub-cellular distribution of cerium oxide nanoparticles. *Molecular BioSystems* **2010,** *6* (10), 1813-1820.

75. Celardo, I.; Pedersen, J. Z.; Traversa, E.; Ghibelli, L., Pharmacological potential of cerium oxide nanoparticles. *Nanoscale* **2011,** *3* (4), 1411-1420.

76. Pirmohamed, T.; Dowding, J. M.; Singh, S.; Wasserman, B.; Heckert, E.; Karakoti, A. S.; King, J. E. S.; Seal, S.; Self, W. T., Nanoceria exhibit redox state-dependent catalase mimetic activity. *Chemical Communications* **2010,** *46* (16), 2736-2738.

77. Patrick, W. J.; Guthrie, W. L.; Standley, C. L.; Schiable, P. M., Application of Chemical Mechanical Polishing to the Fabrication of VLSI Circuit Interconnections. *Journal of The Electrochemical Society* **1991,** *138* (6), 1778-1784.

78. Zantye, P. B.; Kumar, A.; Sikder, A. K., Chemical mechanical planarization for microelectronics applications. *Materials Science and Engineering: R: Reports* **2004,** *45* (3–6), 89-220.

79. Singh, R.; Lee, S.; Choi, K.; Basim, G.; Choi, W.; Moudgil, B.; Chen, Z., Fundamentals of dielectric and metal chemical mechanical planarization (CMP) slurry design. *MRS Bull* **2002,** *27* (10), 752-760.

80. Iler, R. K., *The chemistry of silica: solubility, polymerization, colloid and surface pro perties, and biochemistry*. Wiley: 1979.

81. Kosaraju, K.; Tarannum, M.; Crawford, S.; Garde, K.; Aravamudhan, S., Examining the Cellular Uptake and Toxicity of Engineered Nanomaterials. *ECS Transactions* **2014,** *61* (36), 15-21.

82. Idriss, S. F.; Krassowska Neu, W.; Varadarajan, V.; Antonijevic, T.; Gilani, S. S.; Starobin, J. M. In *Feasibility of non-invasive determination of the stability of propagation reserve in patients*, Computing in Cardiology (CinC), 2012, 9-12 Sept. 2012; 2012; pp 353-356.
83. Chernyak, Y. B.; Starobin, J. M.; Cohen, R. J., Class of Exactly Solvable Models of Excitable Media. *Physical Review Letters* **1998,** *80* (25), 5675-5678.

84. Andrea, G.; Guo, B.; Rama, S. K.; John, C. R.; Kennedy, I. M.; Abdul, I. B., Induction of Inflammation in Vascular Endothelial Cells by Metal Oxide Nanoparticles: Effect of Particle Composition. *Environmental Health Perspectives* **2007,** *115* (3), 403-409.

85. Yan, J.; Lin, Z.; Lin, B.; Yang, H.; Zhang, W.; Tian, L.; Liu, H.; Zhang, H.; Liu, X.; Xi, Z., Respiratory exposure to single-walled carbon nanotubes induced changes in vascular homeostasis and the expression of peripheral blood related genes in a rat model. *Toxicology Research* **2015,** *4* (5), 1225-1237.

86. Lam, C.-W.; James, J. T.; McCluskey, R.; Hunter, R. L., Pulmonary Toxicity of Single-Wall Carbon Nanotubes in Mice 7 and 90 Days After Intratracheal Instillation. *Toxicological Sciences* **2004,** *77* (1), 126-134.

87. Warheit, D. B.; Laurence, B. R.; Reed, K. L.; Roach, D. H.; Reynolds, G. A. M.; Webb, T. R., Comparative Pulmonary Toxicity Assessment of Single-wall Carbon Nanotubes in Rats. *Toxicological Sciences* **2004,** *77* (1), 117-125.

88. Geraets, L.; Oomen, A. G.; Schroeter, J. D.; Coleman, V. A.; Cassee, F. R., Tissue Distribution of Inhaled Micro- and Nano-sized Cerium Oxide Particles in Rats: Results from a 28-day Exposure Study. *Toxicological Sciences* **2012**.

89. Pagliari, F.; Mandoli, C.; Forte, G.; Magnani, E.; Pagliari, S.; Nardone, G.; Licoccia, S.; Minieri, M.; Di Nardo, P.; Traversa, E., Cerium Oxide Nanoparticles Protect Cardiac Progenitor Cells from Oxidative Stress. *ACS Nano* **2012,** *6* (5), 3767-3775.

90. Poma, A.; Ragnelli, A. M.; de Lapuente, J.; Ramos, D.; Borras, M.; Aimola, P.; Di Gioacchino, M.; Santucci, S.; De Marzi, L., In Vivo Inflammatory Effects of Ceria Nanoparticles on CD-1 Mouse: Evaluation by Hematological, Histological, and TEM Analysis. *Journal of Immunology Research* **2014,** *2014*, 14.